SIGNALING PATHWAYS IN CELL MODELS OF FABRY DISEASE NEPHROPATHY

by

Anatália Labilloy

M.D., Universidade Federal do Piauí, Brazil, 2010

M.P.H., University of Pittsburgh, 2013

Submitted to the Graduate Faculty of the

Graduate School of Public Health in partial fulfillment

of the requirements for the degree of

Doctor of Philosophy

University of Pittsburgh

2015

UNIVERSITY OF PITTSBURGH

GRADUATE SCHOOL OF PUBLIC HEALTH

This dissertation was presented

by

Anatália Labilloy

It was defended on

May 15, 2015

and approved by

Dissertation Advisor:
Ora A. Weisz, Ph.D.
Professor, Departments of Medicine and Cell Biology
School of Medicine, University of Pittsburgh

David N. Finegold, M.D.
Professor, Departments of Pediatrics, Medicine and Human Genetics
School of Medicine and Graduate School of Public Health
University of Pittsburgh

Zsolt Urban, Ph.D.
Associate Professor, Department of Human Genetics
Graduate School of Public Health, University of Pittsburgh

Kirill Kiselyov, Ph.D.
Associate Professor, Department of Biological Sciences
Dietrich School of Arts and Sciences, University of Pittsburgh

Robert E. Ferrell, Ph.D.
Professor and Associate Dean Faculty Affairs, Human Genetics
Graduate School of Public Health, University of Pittsburgh

Ora A. Weisz, Ph.D.

SIGNALING PATHWAYS IN CELL MODELS OF FABRY DISEASE

NEPHROPATHY

Anatália Labilloy, Ph.D

University of Pittsburgh, 2015

ABSTRACT

Chronic Kidney Disease is a leading cause of morbidity, impaired quality of life and premature death in patients with Fabry disease, being of major public health significance. Glycosphingolipids that accumulate in Fabry disease due to alpha-galactosidase A (α-gal A) deficiency in the lysosomes localize to membrane microdomains, which play crucial roles in protein clustering, membrane trafficking, and especially cell signaling. The mechanisms by which increased levels of these glycosphingolipids and consequent changes in microdomain dynamics and lysosomal dysfunction all result in cellular and organ injury are not well understood. To effectively study Fabry disease disease mechanisms at the cellular level, I first established and characterized an epithelial kidney cell model of Fabry disease in Madin-Darby canine kidney (MDCK) cells using small interfering RNA (siRNA). I then examined plasma membrane protein dynamics of a model raft-associated protein, GFP-GPI, in this model system. Number and Brightness Analysis in live cells showed a significant increase in the oligomeric size of antibody-induced clusters in α-gal A silenced cells compared to control cells. To explore possible consequences of these findings in signaling pathways that are relevant to human disease, I generated human kidney cell models of Fabry disease in immortalized podocytes and tubule epithelial cells (HK-2) applying the genome editing technique of Clustered, Regularly Interspaced, Short Palindromic Repeats and associated endonuclease 9 from *S. pyogenes*

(CRISPR/Cas9). I compared the abundance and phosphorylation of relevant signaling proteins in Fabry disease and control immortalized human podocytes using a high-throughput phosphorylation microarray. Fabry disease podocytes showed significant changes in total protein abundance and/or phosphorylation in 59 proteins. Pathway analysis predicted differential signaling of several canonical pathways in Fabry disease podocytes. These studies provided for the first time an understanding of raft protein dynamics and signaling in kidney cells deficient for α-gal A, potentially opening new avenues for biomarker discovery and drug development for Fabry disease nephropathy.

Keywords: Fabry disease, glycosphingolipids, lipid rafts, alpha-galactosidase A, signaling, nephropathy

TABLE OF CONTENTS

LIST OF TABLES

LIST OF FIGURES

LIST OF SUPPLEMENTARY FIGURES

PREFACE

I would like to show my deepest appreciation to all faculty, staff and students of the Department of Human Genetics, School of Public Health and Renal-Electrolyte Division, School of Medicine. I learned so much from all of you. I would like to take this opportunity to express my sincere gratitude to my advisor Dr. Ora Weisz, for serving as a role model of woman in science, along with Dr. Finegold, for being my role model in patient care, and for all the support they gave me through this journey. I also would like to give special thanks to the other members of my dissertation committee Dr. Zsolt Urban, Dr. Kirill Kiselyov and Dr. Bob Ferrell for the fruitful discussions and helpful advice.

My sincere thank you to all collaborators that made this work possible, especially Dr. Robert Youker for his expertise in Number & Brightness Analysis, Dr. Arohan Subramanya and Dr. Ankita Roy, for having introduced me to a "CRISPR world" and Dr. Jatinder Sigh for the discussions in bioinformatics and statistics. I also thank Shire Plc. for an educational grant that has supported my stipends.

Many thanks to my colleagues at Dr. Weisz's lab: the "honorary member" Ester Miranda for her assistance and Jennifer Bruns, Dr. Polly Mattila, Venkatesan Raghavan, Youssef Rbaibi and former lab members Dr. Di Mo and Dr. Christina Szalinski for their friendship and support and for sharing their broad technical expertise with me.

1.0   INTRODUCTION

1.1   PUBLIC HEALTH SIGNIFICANCE

Chronic kidney disease (CKD), defined as decreased glomerular filtration rate and/or significant loss of albumin in the urine, represents a heterogeneous group of conditions with overlapping clinical features and usually poor health outcomes [1]. CKD has a rising prevalence, affecting over 26 million individuals in the US alone, with an annual cost of over 17 billions USD per year, which encompasses almost one quarter of the total Medicare budget [2].

Due to the public health impact of CKD, Healthy People 2020 (HP2020), a national public health program set by the United States Department of Health and Human Services to improve the health of all individuals in the US, includes as one of its goals to "reduce new cases of CKD and its complications, disability, death and economic costs" [3].

The majority of males and a significant proportion of female patients with Fabry disease, an X-linked inherited disorder, develop progressive loss of kidney function, which represents a major cause of decreased quality of life and premature death in these patients [4, 5]. In addition to CKD, other life-threatening clinical manifestations of Fabry disease such as stroke and heart failure also contribute to significant burden, with public health implications.

Diagnosis for Fabry disease has been recently incorporated into national newborn screening programs of several countries and is being performed as pilot studies in several states

1

of the USA [6-10]. Newborn screening programs have been one of the most successful public health initiatives to improve health outcomes and to prevent significant morbidity and early mortality of individuals through early diagnosis and intervention of serious conditions [11].

The only clinically available therapy for Fabry disease at the moment in the US is enzyme replacement therapy (ERT) by intravenous administration of agalsidase beta, which has an estimated yearly cost of over 210,000 USD per patient [12]. Unfortunately, ERT has not shown to be effective in preventing loss of kidney function in Fabry disease patients, especially for those who start therapy at later stages of CKD [13].

A better comprehension of the pathophysiology of Mendelian genetic conditions such as Fabry disease, as well as complex disorders that share some of the disease mechanisms, can foster biomarker discovery and drug development, which can potentially improve quality and effectiveness of care provided to these patients. Translational research, in this sense, allows for "research [ing] for new insights and innovative solutions to health problems", which is considered one of the 10 Essential Public Health Services according to the National Public Health Performance Standards (NPHPS) of the Centers of Disease Control and Prevention (CDC) [14].

1.2   FABRY DISEASE

Fabry disease is a X-linked progressive multisystem lysosomal storage disease (LSD) caused by absence or dysfunction of the hydrolase alpha-galactosidase A (α-gal A), encoded by the gene *GLA*. Intra-lysosomal deficiency of α-gal A leads to progressive buildup of its substrates, mainly globotriaosylceramide (Gb3), in a variety of cell types and tissues, leading to organ

2

dysfunction with increased morbidity and early death. Fabry disease occurs in individuals of both genders, and classically presents with renal, cardiovascular, neurological, gastroenterological, ocular, auditory and dermatological findings, among others [15].

Drs. William Anderson (England) [16] and Johann Fabry (Germany) [17] independently described from a clinical perspective the first patients with the condition in 1898. The following timeline provides a historical perspective of major contributions to the understanding of disease pathogenesis and advancements in development of disease-specific therapy in Fabry disease.
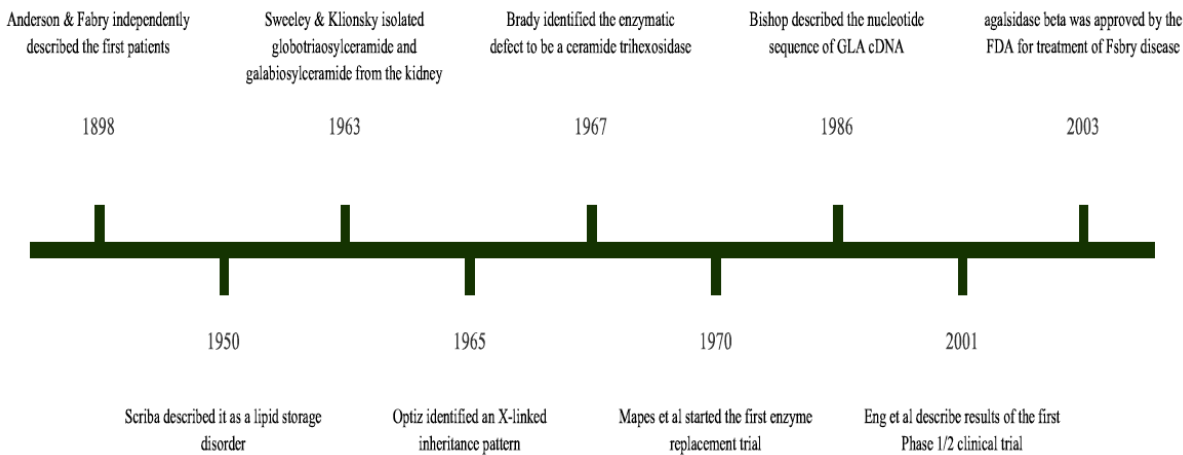
Figure 1. Timeline of Fabry disease.

Fabry disease is pan-ethnic and fairly under-diagnosed, with unknown prevalence in the general population. Several population-wide screenings in specific countries yielded prevalence from 1:476,000 in Australia [18] to 1:77,500 in the Czech Republic [19]. Targeted screening focusing on specific high-risk patient subpopulations such as adult patients with unknown cause of renal failure [20-24], stroke [25] or hypertrophic cardiomyopathy [26] have been successful in identifying individuals with the condition.

More recently, newborn screening initiatives have attempted to better estimate the incidence of the disease, which showed a varied but much greater than expected incidence, such

as 1:2,913 in the state of Missouri [9], 1:7,057 in Japan [6] 1:1,250 in Taiwan [7] and 1:3,100 in Italy [8]. These newborn screenings for the condition revealed a greater than expected number of patients predicted to have variants of the disease predicted to present later in life, raising some ethical concerns regarding neonatal diagnosis of adult-onset diseases.

1.2.1   Alpha-galactosidase A

Alpha-galactosidase A (EC 3.2.1.22), also known as melibiase or alpha-D-galactosidase galactohydrolase, is a homodimeric glycoprotein that hydrolyzes Gb3 into lactosylceramide as well as catalyzes melibiose into galactose and glucose. Other substrates for α-gal A include glycolipids, glycoproteins, and oligosaccharides, including the blood antigens B, B1, Pk and P1. Upon substrate binding, the lysosomal hydrolase cleaves terminal alpha-galactosyl residues producing a free α-anomeric galactose through two successive hits on the same carbon and requires Mg^{2+} and NAD^+ as co-factors [27]. The biochemical properties of α-gal A of Fabry disease patients differ from those of healthy individuals, with significantly lower Km and Vmax for mutant α-gal A compared to the wild type enzyme [28].

The crystal structure of the α-gal A can be seen in Figure 2. The protein has a length of 429 amino acids, with nucleophile and proton donor active site located at residues 170 and 231, respectively, and substrate binding at residues 203 to 207. The enzyme belongs to the glycosyl hydrolase 27 family (GH27) and is synthesized in the endoplasmic reticulum as a precursor 50.5 KDa glycoprotein, processed into a mature 46 KDa form and post-translationally modified in the Golgi for by addition of mannose-6-phosphate (M6P) and three N-linked glycans (N139, N192 and N215) [29, 30]. The enzyme is then targeted to the pre-lysosomal/endosomal compartments through interaction with mannose-6-phosphate receptors,. A portion of the

synthesized α-gal A is secreted through exocytosis, and can then re-enter the cells through surface M6P receptors and be delivered to the lysosomes.
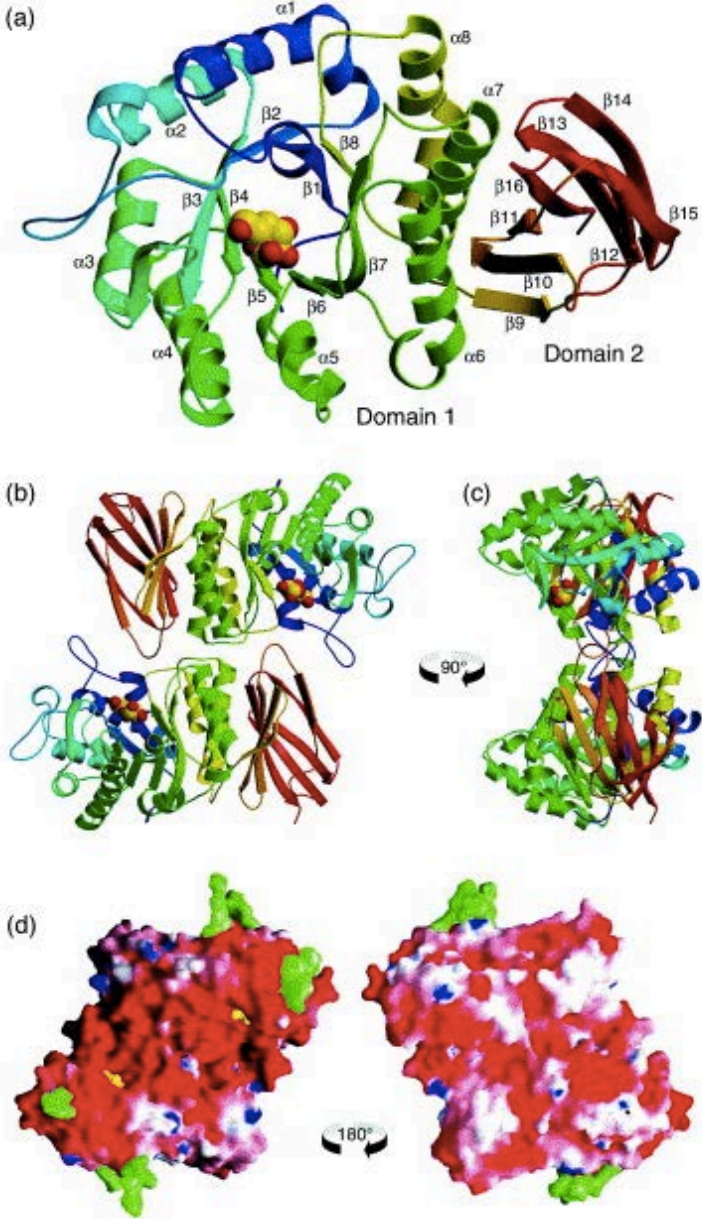
Figure 2: The crystal structure of α-gal A.

Panel a represents the monomeric form of α-gal A, with N-terminus in blue and C terminus in red. Domain 1 contains the active site. Panels b and c show the dimeric form of α-gal A, and panel d shows two views of the molecular surface.
Reproduced with permission from [27].

Alpha-galactosidase A has an isozyme, alpha-galactosidase B, which presents similar physicochemical features but different charges and substrate affinities. Alpha-galactosidase B is an α-N-acetylgalactosaminidase and is the biochemical defect of Schindler and Kanzaki diseases. [31, 32]

1.2.2   Globotriaosylceramide

Gb3, also termed ceramide trihexoside (CTH), galactosyl-α1-4-galactosyl-β1-4-glucosylceramide, P' antigen or CD77, is a glycosphingolipid synthesized from lactosylceramide through action of the enzyme α-1,4-galactosyltransferase Gb3 synthase in the Golgi apparatus. This enzyme is ubiquitously expressed in humans, with highest expression in the kidney and the heart. [33] After its synthesis in the Golgi, Gb3 reaches the outer leaflet of the plasma membrane via vesicle-mediated transport, being incorporated mainly in lipid rafts [34, 35]. Besides bound to membranes, Gb3 can also be found associated to LDL in the plasma. [36]

Increases in Gb3 are not specific for Fabry disease and are observed in other inherited conditions, such as in Zelglweger syndrome, a peroxisome biogenesis disorder, [37] and in individuals with a Pk blood phenotype [38]. Gb3 also accumulates in acquired conditions such as Burkitt lymphoma and in patients with other solid tumors such as breast cancer [39]. The apolipoprotein E knockout mice also presents elevated levels of Gb3 [40].

In addition, increases in Gb3 are seen as a physiological response to lipopolysaccharide exposure during the acute phase response in the liver [41, 42]. Gb3 has been implicated in gp120 binding during HIV-1 infection in lymphocytes [43] and is the preferred receptor for

Shiga toxin 1, verotoxin 1 [44] and for uropathogenic E. coli R45 binding [45]. Gb3 also anchors the molecular chaperone Hsp70 to the plasma membrane, facilitating its role in translocation of unfolded proteins across membranes [46, 47]. Desselle et al [48] have demonstrated that the use of monoclonal antibody against Gb3 inhibits endothelial cell proliferation, angiogenesis and tumor growth and invasiveness.

A growing body of evidence shows that globotryaosylsphingosine, the deacylated form of Gb3 (lyso-Gb3), may play an important role in the pathogenesis of Fabry disease. [49, 50] Lyso-Gb3 presents an inhibitory effect over native and recombinant α-gal A, as it tightly associates with the enzyme but it is degraded at a rate 50 times slower than for Gb3. [51] Clinically, patients with higher lyso-Gb3 levels are more likely to present classic disease phenotype and its levels could potentially be a more reliable biomarker of poor outcome to Enzyme replacement therapy (ERT). [52, 53] In addition, *in vitro* studies demonstrated that lyso-Gb3 sensitizes peripheral nociceptive neurons by enhancing voltage-dependent Ca^{2+} currents. [54] In podocytes, lyso-Gb3 increases expression of TGF-β1 and of CD74 [55].

1.2.3 Genetics

Alpha-galactosidase A is encoded by *GLA*, a 12 kb gene mapped to Xq22.1, composed of seven exons ranging in length from 92 to 291 nucleotides. The first exon contains a 60 nucleotide 5'-UTR and the nucleotide sequence for a signal peptide of 31 residues [56]. Nucleotides encoding for the substrate-binding motif are present in exon 3. The 5' flanking region also contains several regulatory elements such as TATA-like sequences, CCAAT box sequences and the GC box consensus sequence for the zinc finger transcription factor Sp1. The gene also contains recognition motifs for enhancer binding sites such as AP1, OCTA and c-fos and lacks a 3'

untranslated sequence. [56] Interestingly, some polymorphisms in GLA 5'UTR affect GLA expression in a cell-type specific manner, which might have implications in the phenotypic variability seen in these patients. [57]

GLA mutations that cause Fabry disease affect synthesis, processing, stability, lysosomal targeting or substrate binding or activity of α-gal A, resulting in enzyme deficiency at the lysosome. [58] To date, a total of 632 different mutations have been publicly described for Fabry disease, the majority of them being missense. Table 1 shows a frequency distribution of these mutations according to HGMD. [59]

Table 1: Types and frequencies of GLA gene mutations.

Mutation type	Number of mutations
Missense	431
Small deletions	94
Splicing	34
Small insertions	32
Gross deletions	22
Small indels	9
Complex rearrangements	6
Gross insertions/duplications	2
Regulatory	1

Adapted from HGMD [59].

As most mutations are private, genotype-phenotype correlations are difficult to estimate; however, pathogenic mutations predicted to cause complete loss of function of the protein are expected to cause more severe disease phenotype. [60]

1.2.4 Clinical Phenotype and Natural History

Fabry disease is a highly heterogeneous condition, with a usual progressive appearance of signs and symptoms in childhood and early adulthood. Early reports classify Fabry disease as an X-linked recessive condition, in which females are asymptomatic carriers. However, observations of several clinicians that female relatives also presented symptoms compatible with the disease led to a more thorough investigation of this population. Natural history studies have then shown that females may present full spectrum of the disease, although usually with a delayed presentation when compared to their male counterparts. [61, 62] Skewed X-chromosome inactivation has been proposed as the main mechanism for the observation of symptomatic females in Fabry disease. [63] While the precise mechanism for possible skewed X-chromosome inactivation in Fabry disease remains unknown, several factors in general can lead to skewed X-chromosome inactivation such as imprinted X inactivation, stochastic events or a positive selection with survival or proliferation advantage for the mutated X-chromosome during early development. [63, 64]

Patients with classic disease phenotype present signs and symptoms of the disease in the first decade of life, with a mean age of onset of 6 years for boys and 9 years for girls. Commonly, the disease first manifests as chronic or episodic neuropathic pain, triggered or exacerbated by changes in temperature, stress or physical exercise as well as non-specific recurrent gastrointestinal symptoms such as abdominal pain or distension, nausea and changes in bowel habits [65]. Other signs and symptoms that are common in childhood include fatigue, dyshidrosis and angiokeratomas.

Chronic kidney disease is an important cause of increased morbidity and mortality in Fabry disease. The majority of male patients present significant decline in kidney function

overtime, which is also seen in 39% of females. [5] Albuminuria and overt proteinuria can be seen in children and adolescent of both genders, which can culminate in end-stage renal disease with need for renal replacement therapy. In kidney pathology, glomerulosclerosis and interstitial fibrosis may be present early in life and even before clinical kidney disease can be detected, along with signs of podocyte injury such as segmental effacement of foot-processes [66, 67].

Fabry registry data points to a life expectancy of 58.2 years for males and 75.4 years for females with FD, compared to 76 and 80.9, respectively, in the US general population [68]. Cardiovascular disease is the most common cause of death among Fabry disease patients [68]. Other major cardiac events such as myocardial infarction and heart failure can also occur in the 4th or 5th decade of life [69]. Other cardiac findings include concentric left ventricular hypertrophy with early diastolic dysfunction, which may progress to systolic dysfunction and left ventricular outflow obstruction, arrhythmias and valvulopathies. Progressive heart fibrosis is seen, being first detected in the mid-myocardial layers and potentially evolving to transmural fibrosis with disease progression [70, 71].

Cerebrovascular involvement is also a major cause of death among Fabry disease patients, most commonly manifested by transient ischemic attacks and stroke. Other manifestations include dizziness and headaches. Progressive pathological changes to the micro- and macrovasculature, with thickening of the media and arterial remodeling are seen in both males and females [72]. The most commonly observed sign of CNS disease seen in MRI is the presence of white matter lesions, which progress with age and are thought to be caused by a combination of microvascular and neuronal involvements. Vertebrobasilar dolichoectasia and higher signal intensity of the pulvinar thalamic nuclei (i.e. the pulvinar sign) can also be seen [73].

Currently, three disease severity scoring systems have been validated for FD patients: MSSI (and its modified FOS-MSSI) [74, 75], DS3 [76] and FIPI [77], the latter also conferring some prognostic value. The phenotypic variability seen in this patient population hinders disease course prediction. Lukas et al. [78] proposed a comprehensive molecular analysis for phenotype prediction. This algorithm combines functional characterization of GLA mutations, lyso-Gb3 measurements, and α-gal A biochemical and crystallographic analysis as well as responsiveness to the pharmacological chaperone 1-deoxygalactonojirimycin (DGJ), being able to predict classic/severe vs. mild disease.

1.2.5   Diagnosis

Fabry disease is under-diagnosed and often misdiagnosed, especially due to the absence of a pathognomonic finding and the multitude of clinical findings that often overlap with other conditions [79].

Diagnostic testing upon clinical suspicion can be performed by either measurement of α-gal A enzyme activity and/or molecular testing. For males, demonstration of low α-gal A enzyme activity in leukocytes or cultured fibroblasts (less than 5 percent of mean reference value) is sufficient for the diagnosis, and sequence analysis of GLA gene can be confirmatory. Female Fabry disease patients can have normal enzyme activity levels, thus sequence analysis of the *GLA* gene is considered the test of choice for this population [80]. Nevertheless, Pasqualim et al. recently proposed a novel approach for screening females with positive family history and strong clinical suspicion using α-gal A enzyme activity in plasma and leukocytes at a different cutoff than of males [81].

Deletion/duplication analysis can be performed in patients that lack PCR amplification of a certain exon and for patients with strong clinical suspicion and negative sequence analysis [82].

For patients with an uncertain diagnosis, such as the presence of a variant of uncertain significant in the *GLA* gene, biopsy of a target organ (i.e. kidney, heart) demonstrating of ultra-structural changes compatible with the disease in the absence of drugs that induce lysosomal lipidosis is diagnostic [83, 84].

For male patients, α-gal A enzyme activity in leukocytes often correlates with phenotype, as patients with non-detectable enzyme activity usually present with classic or severe disease phenotype whereas patients with residual activity may develop later-onset disease [85].

Fabry disease should be considered as a differential diagnosis of conditions such as multiple sclerosis [86], cryptogenic transient ischemic attack or stroke [87], sensory peripheral neuropathies or neuropathic pain [88, 89], some auto-immune conditions such as rheumatoid arthritis and systemic lupus erythematous [90], Crohn's disease [91], familial lymphedema [92], familial Mediterranean fever [93] and in patients with vortex keratopathy associated with conjunctival and retinal vascular tortuosity [94] among others.

1.2.6 Management

Several consensuses and clinical practice guidelines have been published in the past decade for both diagnosis and clinical management of Fabry disease for different countries [95-99]. Two enzyme replacement therapy (ERT) options are currently available in most countries: agalsidase alfa (Replagal®, Shire) and agalsidase beta (Fabrazyme®, Genzyme). In the United States,

agalsidase beta is the only FDA approved drug available clinically and other treatment options are currently under investigation.

Long-term longitudinal studies show a variable clinical response to ERT. In addition, ERT does not completely prevent the occurrence of severe clinical events, such as stroke, end-stage renal disease and sudden death [100]. Decline in renal function usually persists despite long term ERT, just at a slightly decreased rate. However, GFR decline is slower for patients with low renal involvement at baseline than for patients that have greater renal involvement when they start ERT [13]. For patients without proteinuria at baseline, long-term ERT might be associated with a slight increase in eGFR.

Other commonly used symptomatic therapies include: angiotensin receptor blockers/angiotensin converting enzyme inhibitors for proteinuria; gabapentin, carbamazepine or diphenylhydantoin for acroparesthesias as well as anti-arrhythmic, beta-blockers and calcium channel blockers for hypertrophophic cardiomyopathy.

1.2.7 Disease models

The first animal model of the disease was generated by Ohshima et al. [101] The *Gla* knockout (KO) mice show complete absence of α-gal A and histopathological evidence of Gb3 accumulation, however these *Gla* KO mice fail to reproduce classic phenotype of Fabry disease, especially the nephropathy, a major clinical manifestation of the disease [102]. A transgenic mouse model expressing a human mutant α-gal A with an R301Q substitution, thought to cause a "cardiac variant" of the disease, was also generated. However, these mice also appeared to be healthy [103], even when crossbred with the *Gla* KO mice, but are used for testing biochemical efficacy of chaperone therapy *in vivo* [104].

More recently, another Fabry disease mouse model has been generated by crossbreeding *Gla* KO mice with transgenic mice that express Gb3 synthase [105]. These mice show a greater accumulation of Gb3 when compared with the *Gla* KO mice. More importantly, these mice show signs of glomerular and tubular proteinuria and progressive increase in BUN with age, indicating impaired kidney function. However, these mice still fail to fully reproduce all aspects of Fabry nephropathy seen in patients, as they show no histological signs of glomerulosclerosis or podocyte foot process effacement [105].

Several cell models have also been generated for Fabry disease. Inagaki et al. described the first attempt of a cell model of Fabry disease using SV40 immortalized umbilical venous human endothelial cells. Treatment with chloroquine induced 70-80 percent reduction in α-gal A enzyme activity, with only 5 percent reduction in β-glucosidase, β-hexosaminidase and β-glucuronidase [106]. Shu et al. isolated and characterized primary cultures of aortic endothelial cells from wild-type and *Gla* KO mice [107]. In a like manner, Shen et al. established a more physiologically relevant microvascular endothelial cell model from skin biopsy specimens obtained from Fabry disease patients and healthy controls [108]. Recently, cardiomyocytes were derived from induced pluripotent stem cells (iPSC) from Fabry disease patients [109]. Kawagoe et al. had also generated iPSC from Fabry disease patients, but these cells failed to differentiate into neuronal cells or cardiomyocytes [110].

For the purpose of modeling the renal disease *in vitro*, Thomaidis et al. generated the first kidney cell models of the disease in HK-2 and human primary tubular epithelial cells using transient and stable RNA interference approaches. They reported accumulation of Gb3/CD77 and ultrastructural changes compatible with Fabry disease, and observed a decreased viability in these human renal epithelial cells silenced for α-gal A [111]. Using a similar approach of stable

shRNA α-gal A silencing, Liebau et al. first generated a human podocyte cell model of Fabry disease [112]. However, at best, this approach was able to reduce mRNA levels of α-gal A by 73%. Notwithstanding, these cells showed some degree of Gb3 accumulation by thin layer chromatography and in changes in the phosphorylation pattern of AKT and mTOR [112].

1.3   LYSOSOMES

Lysosomes are heterogeneous membrane-bound organelles that are ubiquitous in all eukaryotic cells, and play a critical role in the degradation and recycling of intra- and extracellular material. They were first incidentally discovered by De Duve in 1955, in an attempt to clarify the action of insulin on the liver and received their name from the Greek 'digestive body' [113] Their catabolic action is performed by hydrolases present in the lumen; they receive their extracellular or membrane-bond cargos through the endocytic pathway, and intracellular components through autophagy [114]. Their acidic pH of 4.5-5 is maintained by the action of the membrane complex vacuolar-type H+-ATPase [115].

The human lysosome gene database (hLGDB) describes 435 proteins as belonging to the lysosomal system, which comprises resident proteins such as catalytic enzymes, structural proteins, transporters and receptors as well as proteins that temporarily associate with lysosomes such as members of the mechanistic target of rapamycin complex (mTORC) and of the major histocompatibility complex (MHC) [116] Lysosomal associated proteins 1 and 2 (LAMP1 and LAMP2) are the most abundant membrane bound proteins found in the lysosome.

Most newly synthesized lysosomal hydrolases leave the endoplasmic reticulum and are sorted from the *trans* Golgi network (TGN) to the lysosome under the guidance of a mannose-6-

phosphate (M6P) tag, facilitating M6P receptor mediated, chathrin-dependent vesicular delivery to late endosomes. The acidic nature of this compartment induces dissociation of the hydrolases from the M6P receptor, where they start their catalytic function, allowing M6PR to be recycled back to the TGN. [117] Most lysosomal membrane proteins are highly glycosylated to protect against the highly acidic environment and digestion by luminal proteases. Transient lysosome membrane proteins may contain short motifs in their cytosolic tails that targets them to the lysosome. Several lysosomal proteins do not have a definite function established yet. [118, 119] A schematic representation of the lysosome with its main groups of components and its major intracellular functions can be found in Figure 3.
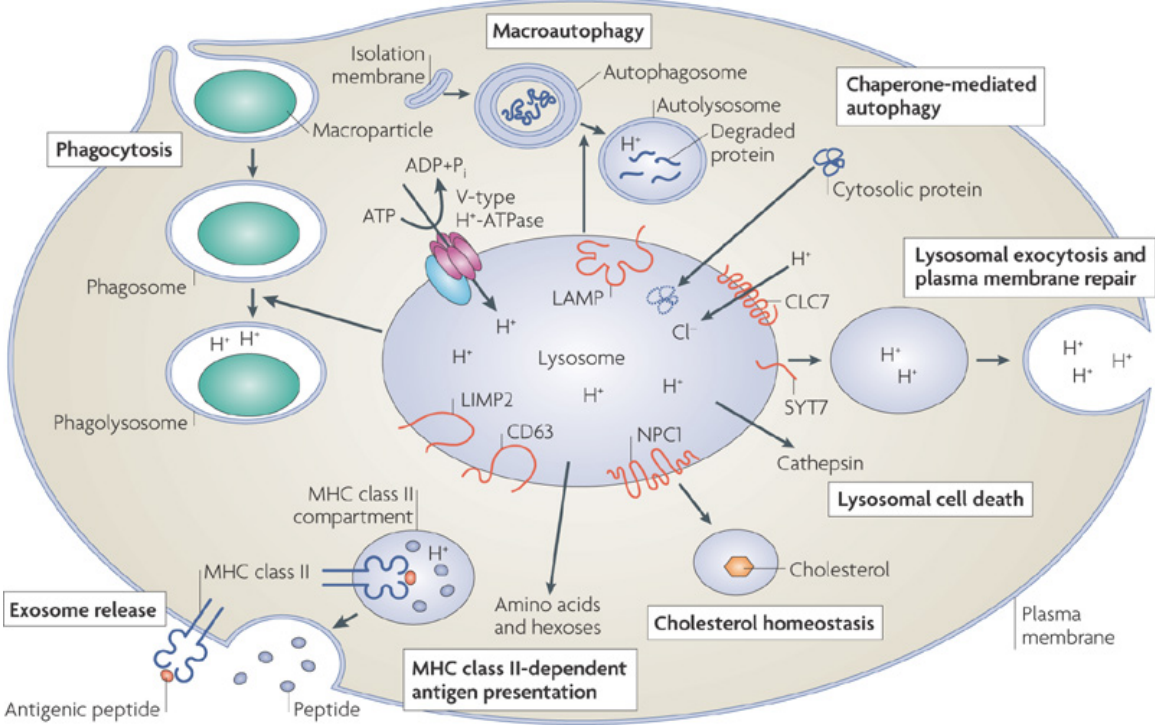
Figure 3: Main lysosomal components and function.

Reproduced with permission from [120].

16

In the past years, lysosomes have changed from being considered a static degradation organelles to be seen as a dynamic compartment, which actively senses and responds to intra- and extracellular stimuli and involved in an intricate interconnection to major cellular functions, such as intracellular signaling, autophagy, phago- and exocytosis, plasma membrane repair and cell homeostasis [121].

The recent discovery of the action of members of the microphthalmia/transcription factor E (MiT/TFE) subfamily in coordinating transcription of lysosomal components has significantly expanded the knowledge on lysosomal biogenesis and function. TFEB, a basic Helix-Loop-Helix leucine zipper transcriptional factor and member of this subfamily, modulates expression of genes known to participate in lysosomal organization, biogenesis and function, including hydrolases, membrane proteins and members of the vacuolar H+ ATPase complex, vesicle-mediated transport and secretion as well as membrane lipid and ATP metabolic processes. TFEB interacts with the Coordinated Lysosomal Expression and Regulation (CLEAR) consensus sequence, a shared unique palindromic 10 bp motif GTCACGTGAC located within 200 bp from the transcription start site of these genes, inducing transcription. Physiological or pathological lysosomal accumulation of undegraded molecules activates TFEB-mediated expression of CLEAR network components [122].

Lysosomes serve as the cell's center for sensing nutrients and maintaining energy homeostasis. They also accommodate to changes in the intra- and extracellular environment by changes in their size, number and intracellular distribution [123]. For instance, early nutrient starvation (first 4 h) induces lysosomal fusion into autophagosomes, increasing their size and decreasing their number, which are restored after 12 h of starvation [124]. Nutrient sensing takes place through the action of the mammalian target of rapamycin (mTOR) and associated

proteins, which are part of the multi-protein complexes mTORC1 and mTORC2. Under basal conditions of adequate nutrient availability and lysosomal function, mTOR phosphorylates TFEB, which causes the latter to associate to 14-3-3 proteins and be retained in the cytoplasm. Upon starvation-induced autophagy or lysosomal dysfunction, mTOR is inhibited, thus does not phosphorylate TFEB, which is then able to translocate to the nucleus and induce expression of genes involved in lysosomal biogenesis [125].

1.3.1   Other Lysosome Storage Disorders

To date, over 50 disorders have been categorized as Lysosomal Storage Disorders (LSDs), each of them resulting from deficient activity of a specific enzyme or due to abnormalities in proteins crucial for lysosomal function. Their combined prevalence is 1:5,000 to 1:6100 births [114, 126], with the most common lysosomal disorder being Gaucher disease, which is caused by deficiency of glucocerebrosidase [127].

Some conditions of this group are more prevalent in the Ashkenazi Jewish population, such as Gaucher disease type I, Tay-Sachs disease, Mucolipidosis type IV and Niemann Pick type A, presenting a much greater carrier frequency compared to the general population. Currently, both the American College of Medical Genetics (ACMG) and the American College of Obstetricians and Gynecologists (ACOG) recommend carrier testing for those conditions in the Ashkenazi Jewish population [128].

In terms of shared disease pathogenesis among LSDs, mostly, the accumulation of a substrate or also lack of a final product can be responsible for the phenotype observed in individuals with some of these disorders, which occur for the majority of these conditions due to deficiency of a hydrolase or activator or defect in a lysosomal transmembrane protein or

transporter. Intralysosomal accumulation of undegraded material is typically confined to those cells, tissues and organs with a higher turnover of the substrate. Even though the main substrate that accumulates substantially differs among LSDs, this group of conditions usually shares some biochemical and clinical features [121]. A commonly shared clinical finding among these conditions is developmental impairment. One of the most known classifications for LSDs occurs as a function of their stored materials. This classification system includes: mucopolysaccharidoses, sphingolipidoses, oligosaccharidoses and glycoproteinoses and glycogenoses [129]. Sphingolipidoses, which include Fabry disease, are the most common class of LSDs. Glycosphingolipid catabolism and associated sphingolipidoses are represented in Figure 4.
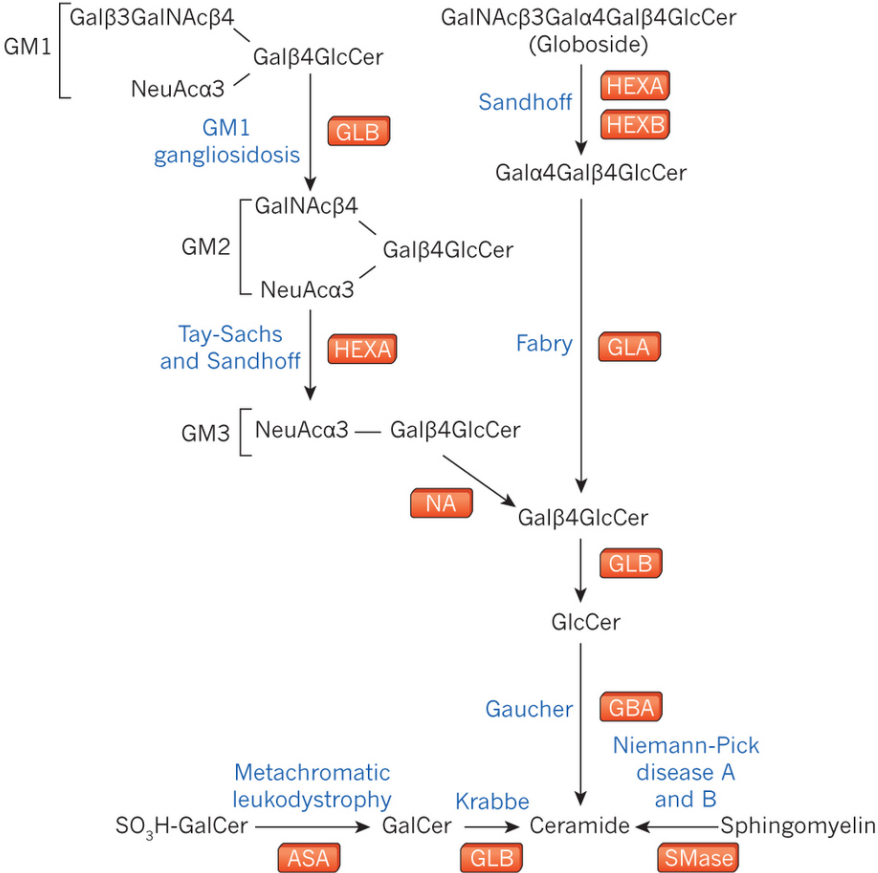
Figure 4: Glycosphingolipid catabolism and corresponding sphingolipidosis.

Enzymes are shown in red and diseases resulting from defects on those enzymes are shown in blue. ASA, arylsulphatase A; GBA, β-glucocerebrosidase; GLA, α-galactosidase; GLB, β-galactosidase; HEXA, β-hexosaminidase A; HEXB, β-hexosaminidase B; NA, neuraminidase; SMase, acid sphingomyelinase.
Reproduced with permission from [130].

Some cationic amphiphilic drugs with a weakly basic amine can precipitate and accumulate within acidic subcellular compartments, inducing lysosomal storage and dysfunction simulating an inherited phospholipidosis. More than 50 drugs in this category have been demonstrated to induce lysosomal storage *in vitro* and/or *in vivo*. They include antiarrhythmic medications such as amiodarone and disobutamide, antipsychotics such as promazine and chlorpromazine, antimalarials such as chloroquine and the antibiotic gentamicin [131, 132]. Drug-induced phospholipidosis can mimic Fabry disease [133, 134], and treatment with some of these drugs can cause lysosomal enzyme deficiency [106]. Thus, the use of cationic amphiphilic drugs should be avoided in patients with lysosomal storage disorders.

1.4   LIPID RAFTS

Lipid rafts are highly organized, diverse and dynamic microdomains of the plasma membrane and of biosynthetic and endocytic compartments that are enriched in cholesterol and sphingolipids and have a characteristic resident and transient protein composition [135]. Protein partitioning into lipid rafts is conferred by lipid modifications, such as glycosylphosphatidylinositol (GPI) lipid anchors and acylation, or by binding of N-glycans to raft-associated lectins [136, 137]. Proteins with affinity for these domains associate with rafts upon assembly in the Golgi complex and traffic in rafts to the plasma membrane.

Raft-associated cargoes are endocytosed from the plasma membrane in a clathrin-independent manner through dynamin-dependent and -independent routes [138, 139]. Biophysical properties of GSLs allow them to modulate membrane curvature, conferring to these microdomains unique features for endocytosis [140]. From endosomes, lipid raft components can either recycle back to the plasma membrane, return to the Golgi, or traffic to lysosomes for degradation [141, 142]. Recycling of raft-associated proteins occurs at a lower rate than of proteins that traffic through a clathrin-dependent pathway, and changes in lipid composition of rafts induce changes in this recycling rate [143, 144].

Lipid rafts also serve as stable or transient platforms for signaling components to enable or inhibit signal transduction [145]. Some proteins localize almost exclusively to rafts, whereas others associate or dissociate from these domains upon ligand binding. [146] Residence time of some receptors with relatively weak affinity to rafts can also be increased by formation of oligomers induced by ligand binding [147]. Activated receptors can also recruit proteins that crosslink adjacent rafts, resulting in raft coalescence and clustering, or form protein complexes within the rafts to trigger specific downstream signaling events [148]. Recent functional proteomic studies have begun to elucidate the quality, temporality and compartmentalization of some of these dynamic events as well as the networks of interactions and cellular processes triggered by activation of raft-mediated signaling using a systems biology approach [149, 150]. Several signaling pathways are directly and indirectly modulated by events that take place in membrane microdomains, and their lipid composition is critical for their function.

Changes in lipid rafts contribute to the pathogenesis of several human diseases including atherosclerosis [151], Alzheimer's disease [152], and inflammatory bowel disease [153]. Impaired lipid trafficking and changes in raft composition have also been described for LSDs,

21

including Niemann-Pick type C [154], type I Gaucher disease [155], and Sandhoff [156] and Sanfilippo syndromes [157]. However, very little is known regarding raft-associated trafficking or signaling in Fabry disease. Similar to other LSDs, trafficking of exogenously added BODIPY LacCer, a raft-associated glycolipid probe, is defective in Fabry disease, as the lipid accumulates in lysosomes instead of either routing to the Golgi apparatus or recycling to the plasma membrane as in control fibroblasts [158]. Additionally, dipeptidylpeptidase IV (DPPIV) accumulates intracellularly in Fabry disease patient fibroblasts rather than localizing to the plasma membrane [159].

1.5   PODOCYTE IN HEALTH AND DISEASE

Podocytes, also known as glomerular visceral epithelial cells, are highly specialized post-mitotic cells that along with endothelial cells and the glomerular basement membrane form the glomerular filtration barrier, which, as the name suggests, has the function of retaining essential macromolecules while allowing waste to be excreted into through urine. Urinary albumin excretion of up to 30 mg/g of creatinine [160] or of 150 mg of total protein over a 24 hour period [161] are considered physiological. Microalbuminuria and overt proteinuria are the first laboratory findings of an impaired glomerular filtration barrier. Both unique morphological and electric aspects as well as the crosstalk among those three components are important for proper glomerular function.

Podocytes are comprised of three distinct morphological segments: cell body, major processes and foot processes [162]. In terms of polarization, the apical membrane domain of the podocyte faces the urinary space and contains anionic proteins such as podocalyxin and

GLEPP-1. The basal domain anchors the podocyte to the underlying glomerular basement membrane and houses integrins and dystroglycans as well as podocin [163]. The slit diaphragm, a modified adherens junction that connects intergiditating foot processes of neighboring podocytes, is the main component of the glomerular filtration barrier responsible for preventing plasma proteins from leaking into the urinary space [164]. This junctional domain houses a variety of resident and transient signaling proteins that connect the outer with the intracellular space and are crucial for podocyte function [165]. Perturbations in signaling originating at any of the membrane domains or actin-associated proteins can lead to glomerular dysfunction.

Dynamic changes to the actin cytoskeleton triggered by intra- or extracellular signaling lead to modulation of podocyte morphology and function. Podocyte foot processes have a unique actin cytoskeleton distribution where actin can be found as contractile longitudinal bundle filaments as well as branched filaments in the subcortical region, where these filaments can be easily connected to and signal from proteins in the slit diaphragm [166]. Figure 5 shows a representation of previously reported signaling cascades between slit diaphragm proteins and the podocyte cytoskeleton. Regulatory mechanisms and key molecules to play a role in the interaction between slit diaphragm and the actin cytoskeleton is an area of active research [167-169].
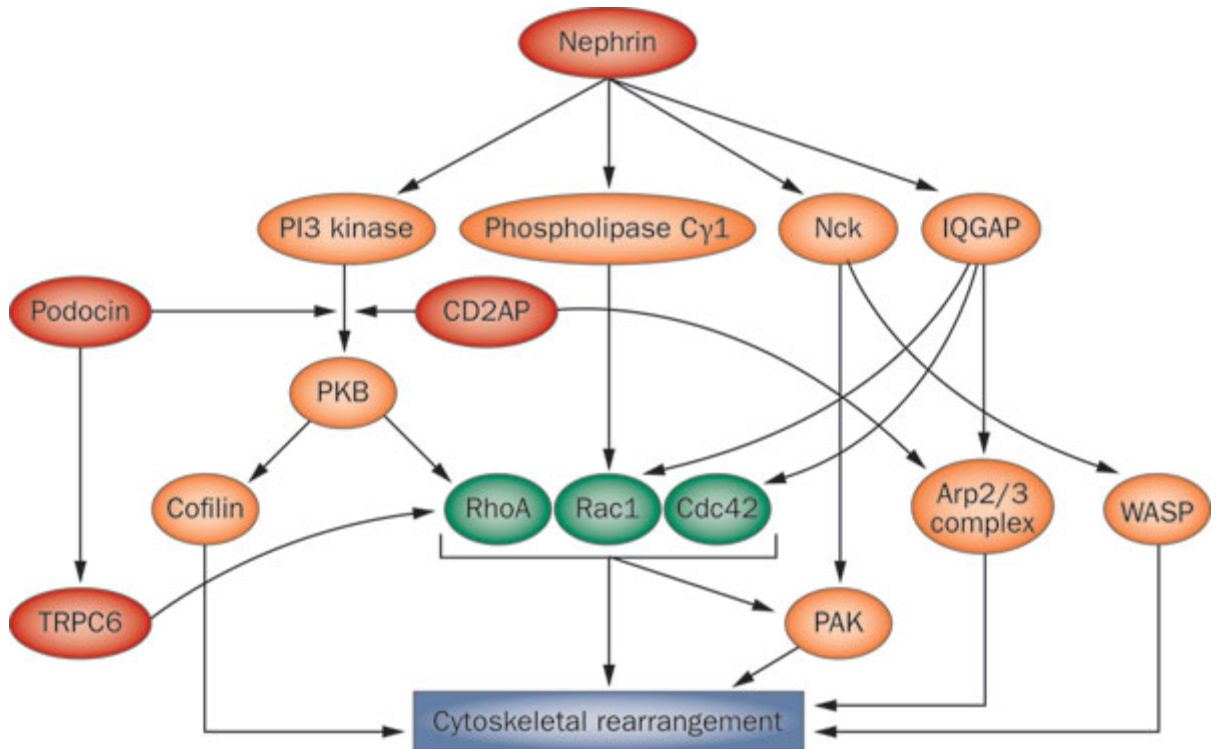
Figure 5: Slit diaphragm proteins and their signaling to the podocyte cytoskeleton.

Diaphragm proteins are seen in red and their downstream effectors with small GTPases in green and connecting signaling proteins in orange, and how they regulate podocyte cytoskeleton dynamics.
Figure reproduced with permission from [170].

Foot process effacement is a phenotypical result of podocyte injury characterized by retraction and flattening of the foot processes due to derangements in the podocyte actin cytoskeleton. Although not a strict prerequisite for its occurrence, foot process effacement and slit diaphragm dysfunction are both implicated in the pathogenesis of proteinuria in a variety of glomerular diseases [171].

1.6   STUDY APPROACH AND METHODOLOGY

The studies proposed herein were designed to elucidate and further characterize the effect of α-Gal A and subsequent glycosphingolipid buildup on the trafficking, stability, and signaling of physiologically relevant proteins in kidney cells. Results of this work provide important information about the role of lipid raft structure and function as well as signaling in the maintenance of renal cell function in the pathophysiology of Fabry nephropathy. A better understanding of the effect of α-gal A deficiency on the localization and function of model proteins whose trafficking is well characterized under non-disease states can help unravel the pathogenesis of other renal signaling disorders. In addition, understanding the role of lipid raft sphingolipid composition in renal cell function may lead to new therapeutic approaches to treat Fabry disease nephropathy.

Specific Aim 1: To dissect the consequences of α-gal A silencing and subsequent Gb3 accumulation on lipid raft mediated cellular events **(Chapter 2).**

Rationale: Changes in lipid composition of membrane microdomains have been implicated in the pathophysiology of a variety of human diseases, including other LSDs. Fabry disease fibroblasts show altered lactosylceramide trafficking [156] and cell models of the disease show increased levels of Gb3 at the plasma membrane [111]. Maalouf et al. have suggested an impaired trafficking of the membrane protein DPP-IV in Fabry disease patient fibroblasts [159], but no previous study has been performed in polarized cells. To better elucidate this relationship, I silenced the *GLA* gene in Madin-Darby Canine kidney (MDCK) tubular epithelial

cells using small interfering RNA against α-gal A. I performed RT-PCR and qRT-PCR to confirm reduction of α-gal A mRNA levels. I characterized these cells for substrate accumulation using indirect immunofluorescence against Gb3/CD77 and for ultra-structural changes compatible with Fabry disease by transmission electron microscopy. I also measured lysosomal size of LAMP-2 positive vesicles in both control and α-gal A silenced MDCK cells in confocal microscopy image stacks. ZO-I was used as a marker for tight junctions, and I also performed immunofluorescence staining for EEA1 and giantin, markers of early endosomes and the *trans* Golgi network respectively, to assess morphology and distribution of these intracellular compartments upon α-gal A silencing. Using this model, I characterized the effects of α-gal A deficiency in trafficking of model raft and non-raft associated model proteins. I also applied N&B analysis to examine clustering of a model raft-associated protein in living cells.

1a. How is trafficking of raft-associated proteins compromised in α-gal A deficient cells? **(Chapter 2)**.

Several lipid modifications confer protein affinity for lipid rafts, including GPI-anchor addition, double palmitoylation, and sterol linkages [172]. Raft association of some proteins can also be conferred by interaction of their extracellular regions with specific raft components; for example, EGFR binding to GM3 ganglioside inhibits the kinase activity of the receptor and its auto-phosphorylation, translating to changes in signal transduction [173]. Trafficking of raft-associated proteins is perturbed by changes in glycosphingolipid amount and organization at the plasma membrane [174], but little is known about polarized raft-associated trafficking in Fabry disease. To this end, I characterized the effects of α-gal A silencing on trafficking of model raft-associated and raft-independent proteins in MDCK cells. I heterologously expressed the apical proteins HA, DPPIV and p75-GFP, and immunostained the endogenous basolateral proteins

26

Na$^+$/K$^+$ ATPase, E-cadherin and caveolin-1 and performed confocal microscopy to assess changes in the steady state distribution of these well-characterized raft dependent or independent proteins.

1b. Are there changes in lipid raft structure or dynamics (including protein oligomerization) in the context of Gb3 accumulation? **(Chapter 2).**

Clustering of GPI-anchored proteins has been demonstrated to be essential for their targeting to the apical surface, and disruption of raft structure impairs sorting [175, 176]. Additionally, clustering of proteins in and between lipid rafts modulates downstream signaling [177]. I used Number and Brightness (N&B) Analysis to assess clustering of lipid raft-associated proteins in control living cells and cells silenced for α-gal A. N&B analysis of fluorescence confocal images provides a quantitative assessment of the size as well as spatial and temporal organization of oligomeric protein complexes at the plasma membrane of living cells. In this technique, movement of very low levels of a fluorescent protein through a small confocal volume creates fluorescence fluctuations that are used to obtain the number and brightness of particles in the observation volume. Comparison of the particle brightness with the brightness of free GFP (or other relevant fluorophore) provides an estimate of the oligomeric status of the protein of interest. I induced low expression of the model raft-associated protein GFP-GPI and compared its oligomeric size at the plasma membrane of living control and in α-gal A silenced MDCK cells. Molecular brightness was normalized to that for cytoplasmatic EGFP (brightness = 1) and for a tandem GFP-GFP construct (brightness = 2) measured by N&B. I also performed N&B analysis upon antibody induced clustering. For that set of experiments, control MDCK cells and cells silenced for α-gal A expressing low levels of GFP-GPI were pre-incubated with anti-GFP antibody and cluster size was measured upon both conditions.

Specific Aim 2: To assess differences in modulation of signaling pathways in human kidney cells deficient for α-gal A. (**Chapter 3**).

Rationale: In several disease states, changes in phosphorylation status of key proteins by action of upstream kinases or phosphatases result in aberrant activation or suppression of signaling. Strikingly, the intracellular events triggered by increased levels of glycosphingolipids as well as the molecular mechanisms by which this accumulation results in cellular and kidney dysfunction in Fabry disease remain largely unknown. To this end, I induced stable α-gal A deficiency in human kidney cell lines by disrupting the *GLA* gene at the genome level using CRISPR/Cas9. I characterized these cells phenotypically for α-gal A enzyme deficiency and substrate accumulation. I then performed a phosphorylation antibody array composed of hundreds of signaling proteins and looked for differences in the phosphorylation and total protein abundance between Fabry disease and control podocytes.

2a. Generate a model of Fabry disease in human kidney cells (**Chapter 3**).

As disease mechanisms and signaling pathways may vary from species to species, to dissect signaling differences in α-gal A deficiency that are relevant to human kidney disease, I have generated human immortalized podocyte and HK-2 cell lines edited for Fabry disease at the *GLA* gene using the genome editing technique of clustered, regularly interspaced, short palindromic repeats and associated endonuclease 9 from *S. pyogenes* (CRISPR/Cas9). CRISPR/Cas9 enables targeted genomic modifications from cells in culture to whole organisms. These programmable nucleases can generate double-strand breaks (DSBs) in targeted regions of the genome, which are repaired usually by the error-prone non-homologous end joining (NHEJ) machinery, resulting in indels and frameshifting, leading to gene disruption. [178] I used a surrogate reporter plasmid to enrich for cell populations that were genome edited. This plasmid

28

contains a RFP cassette, which is constitutively expressed, the target sequence in the genome and an out-of-frame hygromycin-GFP cassette. Plasmid modification at the target sequence introduces indels, shifting the frame and allowing for hygromycin-GFP expression. Cells can then be sorted using fluorescence-activated cell sorting (FACS) for RFP/GFP cells or hygromycin treatment. First, I enriched cell populations of podocytes and HK-2 cells through FACS and grew individual cell colonies. I then performed a T7 Endonuclease I assay to examine cells for genome editing. In this assay, PCR amplicons that include the region of interest are denatured through heat and self- or heterohybridized to generate homo- or heteroduplexes. Hybridization products are then treated with T7 endonuclease I enzyme, which recognizes and cleaves mismatched DNA or quaternary Holliday DNA junctions, generating a cleaved product that can be visualized through agarose gel electrophoresis. Podocytes underwent a second round of CRISPR/Cas9 treatment, targeting an additional region in the *GLA* gene, with enrichment using hygromycin. For characterization of these cells regarding the Fabry disease phenotype, I measured enzyme activity of α-gal A and of alpha-mannosidase as an internal control through a fluorometric assay using specific 4-MU substrate. I also examined at Gb3 levels by indirect immunofluorescence.

2b. Which signaling pathways might be differentially activated in α-gal A deficiency? (**Chapter 4**)

Podocyte function and survival are tightly regulated by a variety of signaling pathways and gene networks; disruption of this signaling homeostasis by underlying pathological processes result in foot process effacement, changes in cell-matrix adhesion or apoptosis [179]. To explore different pathways that could have distinct patterns of activation under conditions of α-gal A deficiency, I performed a high-throughput protein phosphorylation profiling in control and α-gal

A deficient human podocytes using an antibody microarray. This array is probed with 1318 well-characterized antibodies against both phosphorylated and non-phosphorylated forms of 366 proteins of interest, allowing simultaneous analysis of phosphorylation pattern and total abundance of proteins involved in over 65 signaling pathways. I estimated the fold change in intensity for each epitope tested comparing Fabry disease to control podocytes and performed gene enrichment and clustering analyses as well as pathway analysis using DAVID Bioinformatics Resources.

1.7   SPECIFIC AIMS

Progressive cardiovascular, cerebrovascular, and renal involvements are major causes of morbidity and premature death in patients with Fabry disease, a lysosomal storage disorder caused by deficiency of α-galactosidase A (α-gal A) that results in accumulation of the neutral glycosphingolipid Gb3. Recent screening studies in adult populations point to Fabry disease as an important and potentially treatable differential diagnosis in patients with cryptogenic ischemic stroke, left ventricular hypertrophy and end-stage renal disease of undetermined etiology. How increased levels of Gb3 result in cellular and organ dysfunction is unknown. Gb3 localizes to lipid raft domains, which function in membrane trafficking and signal transduction. **I hypothesized that accumulation of Gb3 in kidney and other cells results in changes in lipid raft organization and function, with implications for disease pathogenesis.** I tested my hypothesis in the following aims:

Aim 1: To dissect the consequences of Gb3 accumulation on raft-mediated trafficking in renal epithelial cells silenced for α-gal A. I hypothesized that the Gb3 build-up seen in Fabry disease disrupts trafficking of raft-associated proteins, with implications for the pathogenesis of the disease. I used biochemical and morphological assays to assess differences in protein distribution and polarized trafficking of physiologically relevant raft-associated proteins in renal epithelial cells silenced for α-gal A. I also evaluated changes in clustering and oligomerization of raft-associated proteins using Number and Brightness (N&B) analysis. These studies shed a light in the potential effects of lipid raft disruption related to glycosphingolipid accumulation in kidney cells.

Aim 2: To assess differences in modulation of signaling pathways in renal cells deficient for α-gal A. Lipid rafts act as signaling platforms for GPI-anchored and acylated proteins. I

hypothesized that the increase in levels of Gb3 upon α-gal A deficiency induces changes in signal transduction. I genome edited human kidney cell lines at the *GLA* gene using CRISPR/Cas9 and assessed cells for α-gal A enzyme deficiency and Gb3 accumulation. I then examined differences in phosphorylation patterns of key signaling proteins in a high-throughput protein phosphorylation profiling assay in human immortalized podocytes edited fro Fabry disease. I performed gene enrichment and clustering analysis, as well as pathway analysis of candidate proteins. Together, these studies provided for the first time a comprehensive analysis of how alterations in a raft-associated lipid might perturb cell function to cause kidney disease.

2.0   ALTERED DYNAMICS OF A MODEL LIPID RAFT ASSOCIATED PROTEIN IN A KIDNEY CELL MODEL OF FABRY DISEASE

2.1   ABSTRACT

Accumulation of globotriaosylceramide (Gb3) and other neutral glycosphingolipids with galactosyl residues is the hallmark of Fabry disease, a lysosomal storage disorder caused by deficiency of the enzyme alpha-galactosidase A (α-gal A). These lipids are incorporated into the plasma membrane and intracellular membranes, with a preference for lipid rafts. Disruption of raft mediated cell processes is implicated in the pathogenesis of several human diseases, but little is known about the effects of the accumulation of glycosphingolipids on raft dynamics in the context of Fabry disease. Using siRNA technology, we have generated a polarized renal epithelial cell model of Fabry disease in Madin-Darby canine kidney cells. These cells present increased levels of Gb3 and enlarged lysosomes, and progressively accumulate zebra bodies.

The polarized delivery of both raft-associated and raft-independent proteins was unaffected by α-gal A knockdown, suggesting that accumulation of Gb3 does not disrupt biosynthetic trafficking pathways. To assess the effect of α -gal A silencing on lipid raft dynamics, we employed number and brightness (N&B) analysis to measure the oligomeric status and mobility of the model glycosylphosphatidylinositol (GPI)-anchored protein GFP-GPI. We observed a significant increase in the oligomeric size of antibody-induced clusters of GFP-GPI at the plasma membrane of α-gal A silenced cells compared with control cells. Our results suggest that the interaction of GFP-GPI with lipid rafts may be altered in the presence of accumulated Gb3. The implications of our results with respect to the pathogenesis of Fabry disease are discussed.

Keywords: Fabry disease, lipid rafts, GPI-anchored proteins, number and brightness analysis, kidney, polarized sorting

2.2   INTRODUCTION

Fabry disease is a lysosomal storage disorder (LSD) caused by deficient activity of the lysosomal hydrolase α -galactosidase A (α-gal A) (EC 3.2.1.22), encoded by the gene GLA [79, 180]. The presence of dysfunctional α -gal A or its absence leads to progressive accumulation of neutral glycosphingolipids with α -D-galactosyl residues, mainly globotriaosylceramide (Gb3), in a variety of cell types, and results in multi-system disease [15].

The kidney is one of the most affected organs in Fabry disease and end-stage renal disease is a significant cause of morbidity in these patients [181]. While advanced stages of chronic renal disease usually develop in middle adulthood in males, the first histological signs of kidney involvement are seen as early as *in utero* [182, 183]. Additionally, pediatric patients

may present early signs of nephropathy such as microalbuminuria, overt proteinuria, and hyperfiltration [184]. Histopathologic analyses of kidney biopsies of Fabry disease patients show Gb3 inclusions in most renal segments and cell types [185]. As Fabry nephropathy progresses, mesangial expansion, interstitial fibrosis, tubular atrophy, and glomerulosclerosis are often observed [186].

Recombinant Enzyme Replacement Therapy (ERT) for Fabry disease has been clinically available since 2001 and its administration improves overall clinical status and quality of life of Fabry patients [187-189]. However, ERT regimens only slightly retard the progression of chronic kidney disease, and a steady decline in glomerular filtration rate is still observed in Fabry disease patients receiving long-term ERT [190-192]. While our understanding of the molecular mechanisms and clinical progression of the disease has exponentially increased over the past several years, the pathogenic link between glycosphingolipid accumulation and renal cellular dysfunction that culminates in kidney failure remains unclear. A better appreciation of how these are connected may contribute to identification of novel drug targets for optimized therapy for the disease.

After its synthesis from lactosylceramide in the Golgi apparatus, Gb3 reaches the outer leaflet of the plasma membrane via vesicle-mediated transport [33, 34]. Like other glycosphingolipids, Gb3 resides preferentially in specialized membrane domains termed lipid rafts [35]. Lipid rafts constitute tightly packed dynamic assemblies of the plasma membrane and of biosynthetic and endocytic compartments that are enriched in sphingolipids and/or cholesterol [135]. Differential protein partitioning into these rafts can be conferred by lipid modifications such as glycosylphosphatidylinositol (GPI) lipid anchors, acylation, and palmitoylation, or by binding of N-glycans to raft-associated lectins [137, 193] Raft domains

35

orchestrate the distribution and diffusion of a variety of proteins and lipids to enable or prevent lipid-lipid, protein-lipid, and protein-protein interactions [194].

Lipid rafts play important roles in post-Golgi membrane trafficking, intra- and inter-cellular signaling, and cell adhesion [145, 195, 196]. A primary function of these domains is to serve as scaffolds that enable the formation of higher order protein associations required for proper sorting and signal transduction. In polarized epithelial cells, a subset of newly synthesized proteins requires association with lipid rafts in the *trans*-Golgi network for efficient delivery to the apical plasma membrane [197]. Clustering of these raft-associated proteins into high molecular weight complexes is essential for their proper polarized delivery [198-200]. Similarly, oligomerization and higher order clustering of proteins is also important for the formation of signaling synapses in membrane microdomains in response to physiological stimuli [201].

Perturbations in lipid raft composition or dynamics contribute to the pathogenesis of several human diseases including atherosclerosis [151] and Alzheimer's disease [152]. Furthermore, changes in raft composition have been described for some lysosomal storage disorders such as Niemann-Pick type C [154], Gaucher disease type I [202], Sandhoff disease [156], Sanfilippo disease [157], neuronal ceroid lypofuscinosis [203], and Krabbe disease [204]. Whether lipid raft structure is altered in Fabry disease is not known, however recent studies have suggested that trafficking of the glycosphingolipid lactosylceramide and of the apical glycoprotein dipeptidylpeptidase IV are perturbed in fibroblasts of Fabry disease patients compared to control fibroblasts [158, 159].

Changes in the lipid composition of lipid rafts may alter the stoichiometry of their protein components, with possible functional effects [205]. A recent advance in our ability to

study spatial and temporal dynamics of proteins in living cells is the establishment of fluorescence fluctuation technique of Number and Brightness (N&B) analysis. In this method, quantitation of temporal fluctuations in the emission intensity of fluorescent molecules is used to calculate the oligomerization of fluorescently-tagged proteins expressed at low levels [206-209].

Here we have established and characterized a polarized cell model of Fabry disease in the canine kidney cell line MDCK (for Madin-Darby canine kidney). Cells silenced for α-gal A had increased levels of Gb3 and developed ultrastructural changes consistent with those observed in histopathological analyses of Fabry disease patient samples. Accumulation of Gb3 in intracellular compartments and at the cell surface did not alter the targeted delivery of either raft-associated or raft-independent proteins to the apical and basolateral membranes. To investigate lipid raft dynamics, we examined the effect of α-gal A depletion on the clustering of a model raft-associated GPI-anchored protein (GFP-GPI). N&B analysis in living cells revealed an increased oligomeric size of GFP-GPI at the plasma membrane of α-gal A silenced cells upon antibody-induced clustering compared with control cells. We speculate that accumulation of Gb3 in Fabry disease may lead to changes in protein-protein and protein-lipid interactions in lipid rafts.

2.3   MATERIALS AND METHODS

2.3.1   Cell culture

MDCK cells were cultured in MEM with 10% heat-inactivated fetal bovine serum. Growth media was replaced every 48 h. Cells at 70-90% confluence were detached using TrypLE select (Life Technologies), transfected as described below, and seeded on 0.4 μm Transwell® permeable supports (Corning Life Sciences) for up to six days prior to experiments.

2.3.2   SiRNA-mediated knockdown

An siRNA oligonucleotide targeting the following sequence 5'-GATAGATCTGCTGAAATT-3' was designed for transient silencing of the canine α-gal A using Dharmacon siDESIGN center (http://www.thermoscientificbio.com/design-center/). SiRNA against firefly luciferase (Dharmacon) targeting the sequence 5'-GAATATTGTTGCACGATTT-3' was used as a control. MDCK cells were transfected with either α-gal A or control siRNA using Lipofectamine™ 2000 transfection reagent (Life Technologies) and Opti-MEM® I Reduced Serum Media (Life Technologies). Briefly, 260 pmol of either α-gal A or control siRNA were incubated with 10 μL of lipofectamine and 500 μL of Opti-MEM for 30 min at ambient temperature. An aliquot (125 μL) of the transfection mix and 5×10^5 subconfluent MDCK cells suspended in 333 μL of MEM with serum were seeded in 12-well plates or on Transwell® permeable supports. Growth media was replaced within 8 h of transfection and every other day. Experiments were typically performed after 3 to 4 days. For longer knockdown periods, siRNA transfections were repeated every 3-4 days.

2.3.3 PCR analysis of knockdown efficiency

Isolation of total RNA was performed using the RNAqueous® kit (Ambion) according to the manufacturer's recommendations. Purified total RNA underwent reverse transcription by incubation with Moloney murine leukemia virus reverse transcriptase (Ambion) at 42°C for 1 h. PCR of canine alpha-galactosidase was performed using the Phusion® High-Fidelity PCR kit (New England BioLabs, Inc.), with the following sense and antisense primers: 5'-TGTGCAACGTTGACTGCCAAGAAG-3' and 5'- TCCTGCAGGTTTACCATAGCCACA-3'. As a control, canine β-actin was also amplified (sense and antisense primers 5'-CTGCTGGAAGGTGGACAG-3'; and 5'-ACCTTCAACTCCATCATGAAG-3'). Reactions were run under the following parameters: 30 sec at 98°C, 5 cycles at [98°C for 10 sec, 72°C for 30 sec, 65°C for 30 sec (reducing temperature by 1°C each cycle), 72°C for 30 sec], followed by 27 cycles at [98°C for 10 sec, 56°C for 30 sec, 72°C for 30 sec], and a final cycle of 72°C for 10 min. For real-time quantitative reverse transcription-PCR (qRT-PCR), 40 ng of RNA was loaded per experimental well. The following primers targeting canine mRNA products were used: α-gal A sense and antisense: 5'-ACCGGCTTAGAAAGGAAGACA-3' and 5'-TTTACCATAGCCACAGCCCA-3'; β-actin sense and antisense: 5'-GATCAAGATCATCGCACCCC-3' and 5'-ACAGTCCGCCTAGAAGCATT-3. Six-point standard curves were generated for each primer using progressive 1:2 dilutions of cDNA. Maxima SYBR (Thermo Scientific) was added to each experimental well containing sample and primers. qRT-PCR was performed on the 7300 Real Time System (Applied Biosystems). Reactions were run using the following parameters: 2 min at 50°C, 10 min at 95°C, and 40 cycles at 95°C for 15 sec followed by 60°C for 1 min. All samples were run in triplicate and normalized to β-actin controls.

2.3.4   Recombinant adenoviruses and adenoviral infection

Generation of replication-defective recombinant adenovirus encoding influenza hemagglutinin (HA) has been previously described [210]. Adenovirus encoding GFP-GPI was generated as described in [210]. Adenovirus stocks encoding dipeptidylpeptidase IV (DPPIV), and p75-GFP were generous gifts from A. Musch (Albert Einstein College of Medicine, New York, NY) and E. Rodriguez-Boulan (Weill Cornell Medical College, New York, NY), respectively. Sixteen to eighteen hours prior to experiments, MDCK cells grown on permeable supports were rinsed in Ca^{2+}-free PBS containing 1 mM $MgCl_2$ (PBS-Mg) and the indicated replication-defective adenoviruses (encoding HA, DPPIV, GFP-GPI, or p75-GFP) and the tetracycline transactivator (necessary for expression of some constructs) were added in PBS-Mg to the apical chamber at a multiplicity of infection of 25 to 75. PBS-Mg (500 μL) was added to the basolateral chamber and cells were incubated at $37^{\circ}C$ with 5% CO_2 for 1 h. Cells were then rinsed with PBS-Mg and incubated overnight in growth media.

2.3.5   Indirect immunofluorescence and confocal microscopy

MDCK cells cultured on permeable supports were fixed for 15 min in 4% paraformaldehyde, 100 mM sodium cacodylate, pH 7.4 warmed to $37^{\circ}C$. Cells were then quenched in PBS containing 20 mM glycine and 75 mM NH_4Cl for 5 min and permeabilized with 0.1% TritonX-100 in quench solution for 8 min with gentle shaking. After blocking in 1% BSA and 0.1% saponin in PBS for 30 min at ambient temperature, cells were incubated in primary antibody for 1 h. Rat IgM Anti-CD77 mAb (clone 38-13, Abcam), which recognizes Gb3, was used at a dilution of 1:20. Rabbit anti-giantin (from A Linstedt, Carnegie Mellon University, Pittsburgh,

PA) was diluted at 1:400. Mouse mAb to LAMP-2 (AC17; from E. Rodriguez-Boulan) was diluted at 1:2,000. Mouse mAb against the early endosomal antigen EEA1 (Affinity Bioreagents) was used at 1:200. Rat mAb against HA (clone 3F10; Roche Applied Biosystems) was used at 1:500. Rat anti-ZO-I (hybridoma R40.76 supernatant) was used neat. Monoclonal anti-DPPIV antibody was a gift from Ann Hubbard (Johns Hopkins School of Medicine, Baltimore, MD) and was used at 1:500. Rabbit polyclonal Ab against caveolin-1 (Cell Signaling Technology) was used at 1:300. Mouse mAb against Na^+/K^+ ATPase (Abcam) was used at 1:400. Mouse mAb against E-cadherin (BD Biosciences) was used at 1:400. After incubation with primary antibodies of interest, cells were washed four times for 5 min each in PBS containing 0.5% BSA and 0.05% saponin and incubated in secondary antibody for 30 min. Alexa-Fluor (Invitrogen Molecular Probes) and Cy3 (Jackson ImmunoResearch Inc.) secondary antibodies were used at a dilution of 1:500 and 1:200, respectively. Primary and secondary antibodies were diluted in PBS containing 0.5% BSA and 0.05% saponin. Filters were washed four times for 5 min each and mounted using ProLong antifade gold with DAPI (Life Technologies). For surface staining, MDCK cells seeded on permeable supports were washed five times with HEPES/MES-buffered MEM, pH 7.0 (binding medium) for 3 min on ice. After blocking with HEPES-buffered MEM, 0.6% BSA, pH 7.4 for 15 min on ice, cells were incubated with rat IgM anti-CD77 mAb (diluted at 1:20) in binding medium on ice for 10 min. Cy3 goat anti-rat IgM secondary antibody was used at concentration of 1:200 diluted in binding medium on ice in anti-CD77 treated cells. Cells were washed five times with binding medium following incubation with both primary and secondary antibodies and then fixed and quenched as described above before, mounting using ProLong antifade gold with DAPI. Where stated, SYTOX Green Nucleic Acid Stain was used to visualize nuclei. Images were captured on an

Olympus Fluoview FV1000 laser-scanning confocal microscope and processed using ImageJ (National Institutes of Health, Bethesda, MD), Metamorph imaging system (Universal Imaging Corp, Brandywine, PA) and Adobe Photoshop® CS6. Statistical background subtraction of the images was performed using Metamorph Imaging system (Universal Imaging Corp, Brandywine, PA).

2.3.6 Electron microscopy

Monolayers of MDCK cells seeded on permeable supports were fixed in solution of 2.5% glutaraldehyde and 4% paraformaldehyde in PBS for 30 min and post-fixed in 1% Osmium tetroxide overnight. Samples were dehydrated in graded series of ethanol solutions and embedded in EPON according to standard procedures. Ultra-thin sections were stained with uranyl acetate and lead citrate and examined using a JEOL electron microscope.

2.3.7 N&B measurements

Cells transfected with control or α-gal A siRNA for three to seven days were transfected with 0.2 μg of DNA plasmid encoding GFP fused to the GPI-anchor of 5' nucleotidase (GFP-GPI; provided by G. Ihrke; Uniformed Services University of the Health Sciences, Bethesda, MD) using Lipofectamine 2000 for 16-20 h. The oligomeric status of both GFP-tagged proteins in the absence or presence of 50 μg/mL rabbit anti-GFP antibody (Invitrogen) was determined by number and brightness (N&B) analysis as previously described [211]. Briefly, a set of 100 confocal images for control or α-gal A silenced cells were acquired on a Leica TCS system equipped with a 63X/1.2 NA water objective with 488-nm laser line and 500-570 nm emission

42

filter. Images were collected at 200 Hz using a hybrid detector set in the photon counting mode. Measurements were performed at 37°C and the average molecular brightness (B) and number of particles (N) per pixel were calculated using the SimFCS software ([206]; Laboratory of Fluorescence Dynamics, University of California, Irvine). N and B are defined as:

$$N = \frac{\langle k \rangle^2}{\sigma^2}$$

(Eq. 1)

$$B = \frac{\langle k \rangle}{N} = \frac{\sigma^2}{\langle k \rangle}$$

(Eq. 2)

The variable k represents the signal intensity and σ is the variance of the signal. The molecular brightness of either control or α-gal A silenced cells was divided by the average brightness of monomeric GFP measured in the cytosol to obtain the normalized brightness. To measure expression levels of heterologously expressed proteins in the cells analyzed by N&B analysis, the average intensity of fluorescence of a solution containing 30 nM of purified EGFP (Biovision) as well as the average intensity of fluorescence of cells expressing GFP-GPI were measured under the same experimental settings and quantitated using SimFCS. Approximate concentration of GFP-GPI in each cell was determined by dividing the measured value of intensity of fluorescence for GFP-GPI in that cell divided by the intensity of fluorescence for the EGFP solution multiplied by 30 nM. For calculation purposes, we considered autofluorescence to be negligible under the experimental conditions assessed.

2.4   RESULTS

2.4.1   SiRNA mediated silencing of α-gal A efficiently reduces of α-gal A mRNA in kidney epithelial cells

Despite their lack of α-gal A activity, knockout α-gal A mice do not fully reproduce the human clinical phenotype of Fabry disease [101]. As alternative approaches, cell models have been useful tools for understanding disease cellular pathogenesis, for identifying biomarkers of disease progression, and for developing and testing novel diagnostic and therapeutic avenues [111, 112, 212, 213]. To generate a renal epithelial cell model of Fabry disease, we transfected MDCK cells with siRNA oligonucleotides targeting α-gal A or a control oligonucleotide. Because commercially available antibodies against human α-gal A failed to recognize the canine enzyme, we measured knockdown efficiency using RT-PCR. As shown in figure 6A, we observed a significant reduction in α-gal A mRNA in MDCK cells treated with α-gal A siRNA compared to control siRNA, without significant differences in β-actin mRNA levels. We could maintain this level of α-gal A knockdown for at least four days with a single transfection and up to six weeks by repeating the transfection every three to four days (data not shown). Efficient knockdown was further confirmed by quantitative RT-PCR, which showed an average of 88% reduction in α-gal A mRNA in α-gal A siRNA transfected cells (figure 61B).
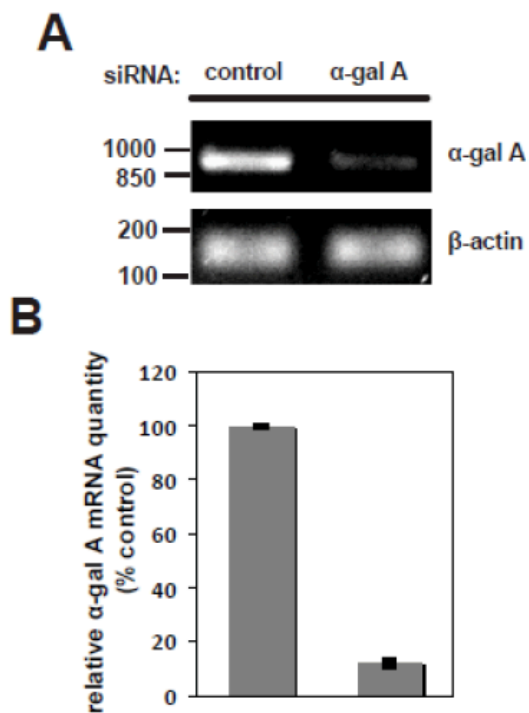
Figure 6: Efficient siRNA-mediated silencing of a-gal A in MDCK cells.

MDCK cells were transfected with control siRNA or siRNA targeted against α-gal A. After three days or seven days with repeated transfection, cells were solubilized and mRNA was extracted. (A) The efficiency of knockdown was quantified by RT-PCR, and a representative gel is shown. The migration of DNA ladder standards is shown on the left. The predicted PCR product for α-gal A is 898 bp. β-actin was used as a PCR control (expected product size 160 bp). (B) Quantitation of knockdown efficiency by qRT-PCR, performed as described in Methods. The mean +/- range of two independent experiments is plotted.

2.4.2   Accumulation of Gb3 in MDCK cells silenced for α-gal A

Gb3 is the main substrate of α-gal A and accumulates in a variety of cell types in Fabry disease

patients [214]. To investigate the consequences of α-gal A silencing on cellular Gb3 levels, we

compared the intensity and pattern of Gb3 staining in polarized MDCK cells three days after

transfection with α-gal A or control siRNA. Cells were fixed and processed for indirect

immunofluorescence using a monoclonal antibody against Gb3 (Anti-CD77). As shown in

45

Figure 7, we observed a marked increase in anti-CD77 staining in MDCK cells transfected for three days with α-gal A siRNA compared with control siRNA. The majority of the staining was present in intracellular compartments likely to correspond to lysosomes. Increased levels of Gb3 were also observed at the plasma membrane of non-permeabilized MDCK cells silenced for α-gal A (Figure 7, bottom). Cell surface Gb3 is also known to be elevated in Fabry disease and measurement of this pool has been recently proposed as a means to monitor the response to ERT [111].
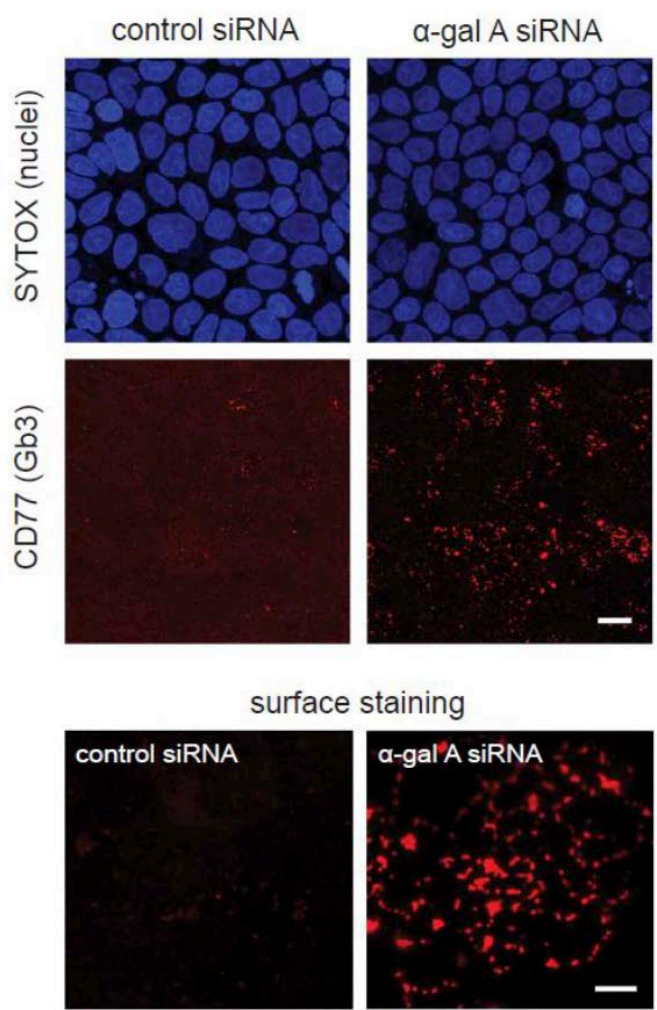
Figure 7: α -gal A siRNA silencing increases cellular levels of Gb3.

(Top) Filter-grown MDCK cells transfected with control (left panel) and α-gal A siRNA (right panel) for seven days were processed for indirect immunofluorescence using anti-CD77 antibody to detect Gb3 Gb3 and imaged by epifluorescence microscopy. SYTOX Green Nucleic Acid Stain was used to

visualize nuclei. Scale bar: 10 µm (Bottom) Surface staining of CD77/Gb3 in non-permeabilized MDCK control cells (left) and α-gal A siRNA silenced cells (right). Maximum projections of five optical sections taken at the apical surface are shown. Scale bar: 5 µm.

2.4.3 Ultrastructural changes upon α-gal A silencing in MDCK cells

Fabry disease patient fibroblasts have enlarged lysosomes that decrease in size upon disease-targeted therapy [215]. We therefore examined whether α-gal A silencing altered lysosome size in MDCK cells. We performed confocal microscopy of MDCK cells transfected with control or α-gal A siRNA and immunostained for the lysosome marker LAMP-2. By visual inspection there appeared to be an increase in the size of LAMP-2 positive compartments in α-gal A silenced cells compared with cells treated with control siRNA (Figure 8A). To quantify this difference, the average area of individual LAMP-2 positive compartments in confocal image stacks was determined using ImageJ software. While there was variability in individual lysosome sizes, on average, the lysosomal area in α-gal A silenced cells was 233 % greater per field than that measured in control cells (Figure 8B). In contrast, the morphology of early endosomes and the Golgi complex were unaffected (supplementary figure 1).

Light and electron microscopy of biopsied tissues of patients with Fabry disease reveals cell-type dependent ultra-structural changes that are characteristic of lipid deposition seen in LSDs [186]. In cell types with a greater degree of lipid deposition, the accumulation of intracellular inclusions formed of concentric or parallel arrays of lipid aggregates, also called "zebra bodies", is evident by electron microscopy [216]. To investigate renal epithelial cell ultrastructure upon α-gal A silencing, we fixed MDCK cells six days after siRNA transfection and processed the samples for transmission electron microscopy (Figure 8C). Osmiophilic myelin-like structures similar to the zebra bodies observed in affected tissues of patients with

Fabry disease were observed in α-gal A silenced cells and absent in cells transfected with control siRNA. These structures increased in number after six weeks of repeated α-gal A siRNA transfection (Figure 8C). These results confirm that siRNA-mediated silencing of α-gal A MDCK cells reproduces the Gb3 deposition pattern and ultrastructural changes observed in Fabry disease patient cells. Therefore, this model can be used to study cellular processes that when perturbed could potentially contribute to the disease mechanism in α-gal A deficiency.
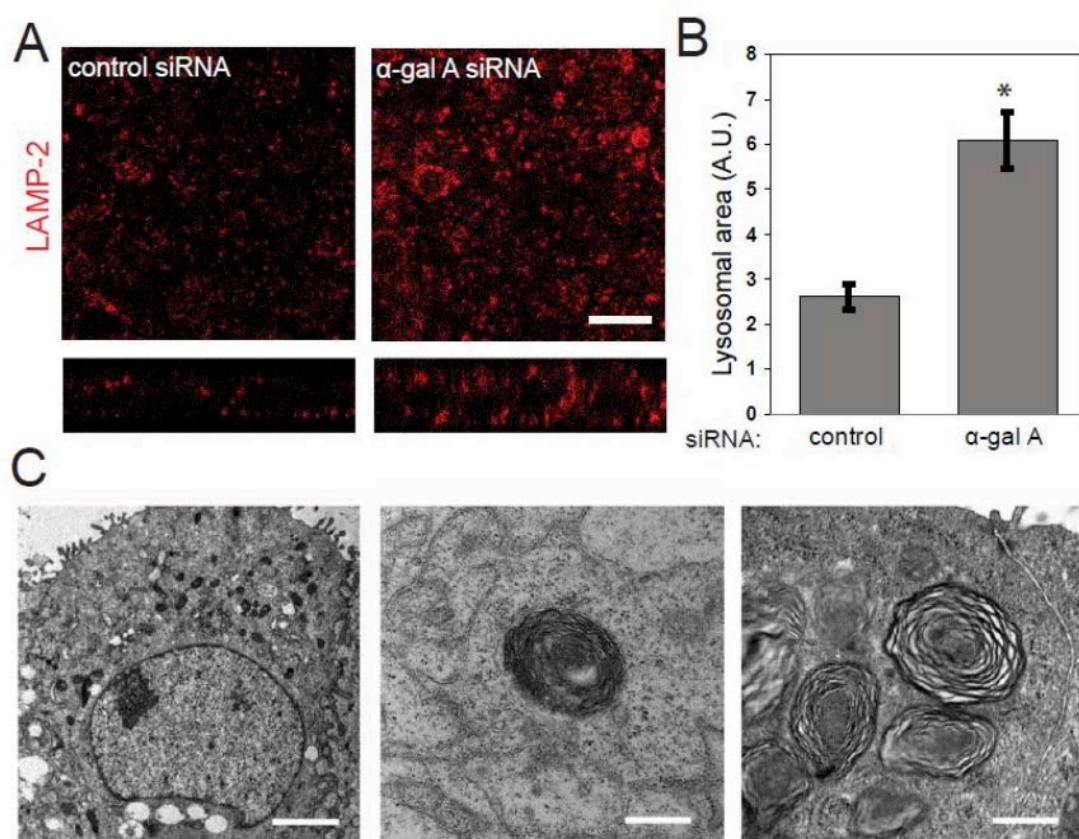
Figure 8: α-gal A siRNA silencing causes accumulation of zebra bodies and increased lysosome size.

(A) Indirect immunofluorescence of the late endosome/lysosome marker LAMP-2 in control (left panel) and α-gal A silenced (right panel) MDCK cells. SYTOX Green Nucleic Acid Stain was used to visualize nuclei. Scale bar: 10 µm (B) The average area of individual LAMP-2 positive compartments in control and α-gal A silenced cells was quantified using ImageJ. The graph shows data from 20 fields in three independent experiments. *t-test $p < 0.001$. (C) Transmission electron micrographs of MDCK cells treated with α-gal A siRNA for six days (left and middle panels) or six weeks (right panel). Transversely-stacked, osmiophilic myelin-like membranes also known as "zebra bodies" (arrow heads) are evident within six days of transfection and are more prevalent after six weeks of repeated transfections. Scale bar: left: 2 μm, middle and right: 500 nm.

2.4.4 Polarized sorting of raft-associated and raft-independent proteins is unaffected by α-gal A silencing

Association with lipid rafts is essential for efficient biosynthetic delivery of a subset of newly synthesized apically-destined proteins [217]. To test whether accumulation of Gb3 alters apical delivery pathways, we examined the steady state distribution of apical cargoes in α-gal A silenced polarized MDCK cells grown on permeable supports. As shown in Figure 9A, staining of the tight junction protein ZO-1 was unaffected by α-gal A knockdown. Moreover, we found no difference in the steady state distribution of the raft-associated protein HA (Figure 9B) or the raft-independent protein p75-GFP (Figure 9C) in α-gal A silenced cells. A previous study reported changes in the subcellular localization of DPPIV in fibroblasts cultured from Fabry patients [159]. However, we found no effect of α-gal A silencing on DPPIV distribution (Figure 9D). Additionally, we observed no differences in the steady state distribution of the basolaterally targeted proteins E-cadherin and Na+/K+ ATPase, as well as the raft-associated protein caveolin-1 in MDCK cells silenced for α-gal A and in control cells (Supplementary Figure 2). Thus, Gb3 accumulation in α-gal A-depleted cells is apparently insufficient to alter apical sorting in our model system.
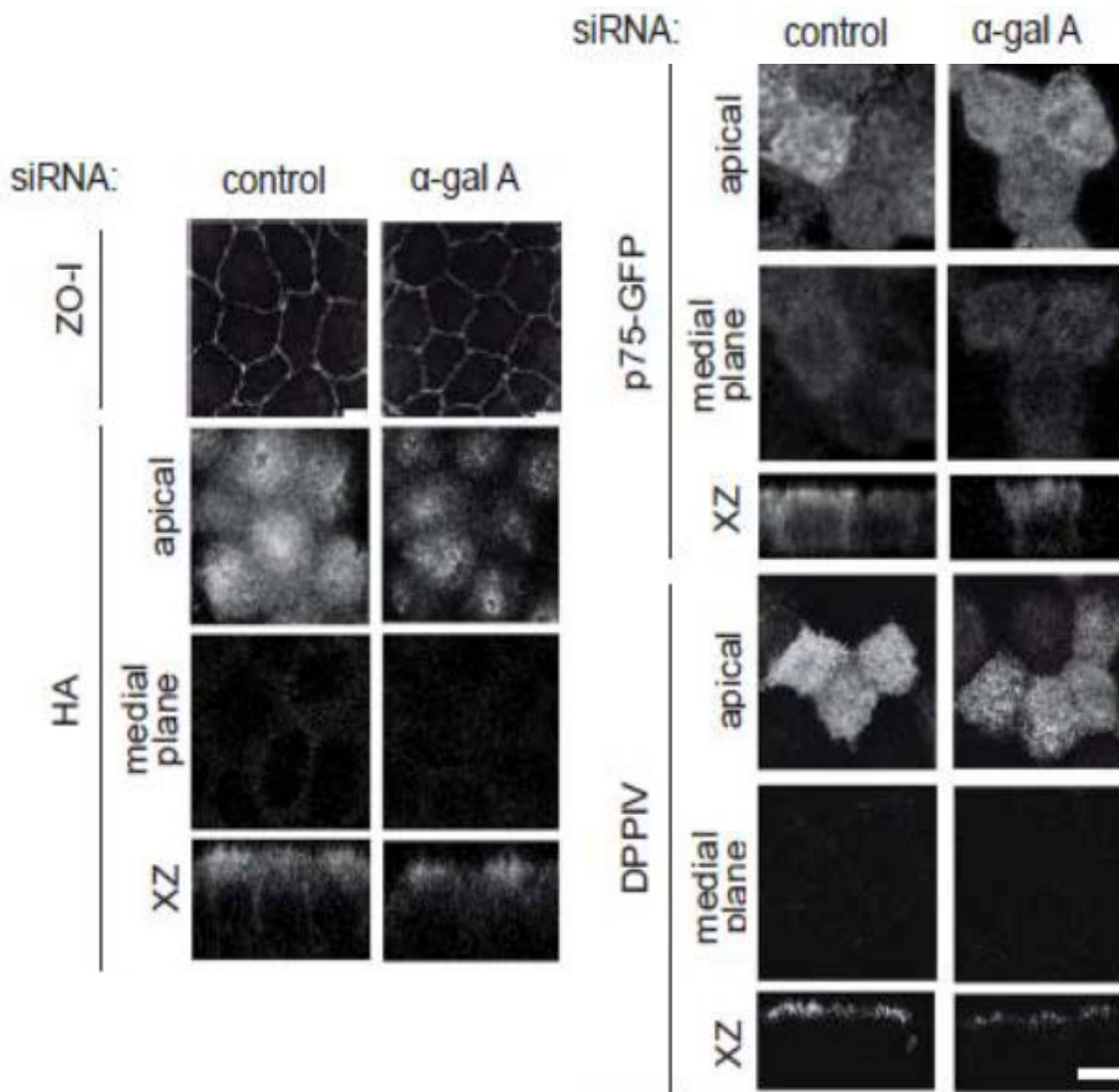
Figure 9: Steady state distribution of raft-associated and raft-independent apical cargoes is not affected by α-gal A siRNA silencing.

(A) Indirect immunofluorescence staining of ZO-I (tight junction marker) in control and α-gal A silenced MDCK cells confirms that tight junctions are intact. Control and α-gal A siRNA treated polarized MDCK cells were infected with replication-defective adenoviruses encoding **(B)** the raft-associated protein HA; **(C)** the raft-independent neurotrophin receptor p75 (tagged with GFP); or **(D)** the glycoprotein dipeptidylpeptidase IV (DPPIV). Cells were fixed, processed for immunofluorescence, and imaged by confocal microscopy. Images taken at the level of the apical surface and at a medial plane are shown for each protein, and xz reconstructions are below. Scale bar: 5 µm.

2.4.5 Dynamics of a model raft-associated protein upon α-gal A silencing in MDCK cells

Recent studies have demonstrated that the steady-state cellular distribution of lactosylceramide differs in fibroblasts of Fabry disease patients when compared to control fibroblasts, suggesting perturbed lipid raft trafficking in Fabry disease [158]. However, the effects of Gb3 accumulation on lipid raft dynamics and any consequences to the pathogenesis of Fabry disease remain unknown. We postulated that α-gal A silencing and subsequent accumulation of neutral glycosphingolipids at the plasma membrane would impact how proteins interact with lipid rafts and potentially induce changes in oligomerization of raft-associated proteins. As a proof of principle we chose to study the oligomeric status of GFP-GPI in our MDCK model of Fabry disease. GPI-anchored proteins are well-characterized raft-associated proteins and serve as models to study cell processes that occur in lipid rafts [218]. GFP-GPI is efficiently recruited to lipid rafts, and alteration of raft composition is known to change the oligomeric state of GFP-GPI, thus making it a useful probe for monitoring lipid raft microdomains [219].

Using N&B analysis, we measured the self-assembly of GFP-GPI at the plasma membrane of MDCK cells transfected with α-gal A and control siRNA. In N&B analysis, a series of confocal images of cells expressing the fluorescent protein of interest are acquired and the average intensity and the variance of the fluorescence signal per pixel are measured. The molecular brightness is then calculated as the ratio of the signal variance to intensity (see schematic in Figure 10A). For example, considering samples with the same average in intensity of fluorescence, tetramers would have a four-fold greater brightness compared to monomers since the signal variance of the many dim monomers is much smaller compared to the variance of several bright oligomers as they move in and out of the confocal volume. In both control and α-gal A siRNA treated cells, the majority of the GFP-GPI fluorescence was uniformly

distributed at the cell surface, with some intracellular staining as has been previously reported [220] (Figure 10B). The expression level of GFP-GPI in our experiments ranged from 0.2 to 1.4 μM, which is similar to the endogenous expression range observed for membrane tyrosine kinase receptors and associated downstream signaling molecules [221]. The brightness measured under these conditions corresponded to the total values across the area of interest because no identifiable puncta could be gated for analysis (see Supplementary Figure 3). The average molecular brightness for GFP-GPI at the plasma membrane was 2.21 and 2.24 for control and α-gal A silenced cells, respectively (Figure 10C, dashed line). These data are in good agreement with previous studies showing that under non-stimulated conditions GPI-anchored proteins are highly mobile and form transient homodimers at the plasma membrane [222]. Upon activation or ligand binding, GPI-anchored proteins form stable homodimers and higher order clusters composed of GPI-anchored proteins and other raft-associated proteins [223, 224]. Experimentally, clustering of GPI-anchored proteins can be induced by addition of antibodies, and leads to activation of downstream signaling pathways [225]. Addition of anti-GFP antibody for ten minutes caused rapid and visible coalescence of GFP-GPI into large patches at the cell surface (Figure 10B). Quantitation of the average brightness in these patches revealed an increase in clustering of GFP-GPI that was significantly greater in α-gal A silenced cells (5.08 ± 0.45; median ± SEM) compared to control cells (2.74 ± 0.24; median ± SEM; $p<0.005$; Figure 10C). Inclusion of brightness values across the region of interest (i.e., not limited to the patches) in these samples did not change the observation that α-gal A depletion leads to larger cluster size but would lead to an underestimation of the brightness in the patches (Supplementary Figure 3).

In order to determine if the change in oligomeric stability seen for GFP-GPI extended to non-raft membrane proteins, we next measured the molecular brightness of a lumenally GFP-tagged version of endolyn (GFP-endolyn), an apically destined sialomucin that traffics in a raft independent matter [226]. The average molecular brightnesses for GFP-endolyn at the plasma membrane were 1.65 and 1.27 in control and α-gal A silenced cells, respectively (figure 5E, dashed lines). Similar to GFP-GPI, addition of anti-GFP antibody caused the rapid accumulation of clusters of protein at the cell surface (Figure 10D). In control cells the GFP-endolyn clusters ranged in size from ~2-4 protein molecules per cluster with a median cluster size of 2.88. While GFP-endolyn in α-gal A silenced cells exhibited a much broader range of cluster sizes (~2-8 molecules, median 2.96; Figure 10E), cluster size in control and knockdown cells was not statistically significantly different. Together, our results suggest that there is greater stabilization of GFP-GPI oligomers in rafts of α-gal A silenced cells upon antibody-induced clustering and that this effect does not extend globally to all plasma membrane proteins.
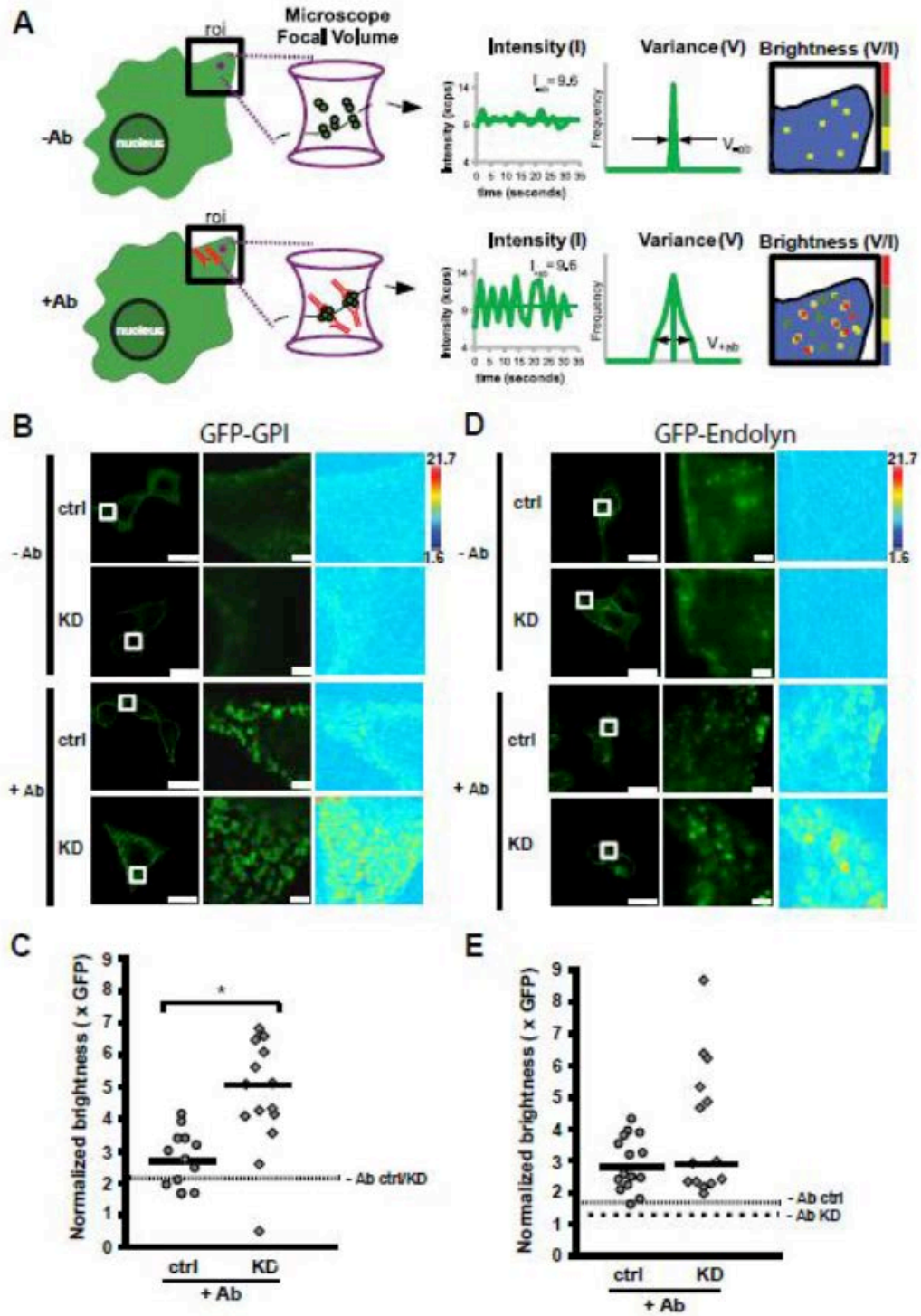
Figure 10: α-gal A silencing alters antibody induced-clustering of a lipid raft associated protein.

Schematic of the theory of number and brightness (N&B) analysis. Left: depiction of cell surface expression of GFP-GPI protein in the absence (-Ab), or presence (+Ab) of anti-GFP antibody (red). The magenta circle in the region of interest (roi) represents the focal volume of the microscope. The magenta hourglass is an expanded view of the focal volume with a representation of GFP-GPI clusters (membrane not shown for clarity) diffusing in the -Ab or +Ab conditions. Center: In this example, the total concentration in the roi before and after Ab addition is similar, giving rise to the same average fluorescence intensity (k). When antibody is added to induce clustering, the same average fluorescence intensity is now redistributed into a few oligomeric species within the focal volume, which causes a dramatic increase in the signal variance (σ) as the large oligomers diffuse through the focal volume. The ratio of variance to intensity is termed molecular brightness (brightness) and provides information on the oligomeric status of a protein when compared to the monomeric fluorescent probe. Right: Depiction of brightness map for the roi in the -Ab and +Ab conditions with cool and warm colors representing less and more clustering, respectively. **(B)** Control or α-gal A silenced (KD) cells expressing GFP-GPI in the absence or presence of anti-GFP antibody. Left panels: Fluorescence images showing control and or α-gal A silenced cells before (-Ab), or 10 min after addition of anti-GFP antibody (+Ab); scale bar: 20 μm. Middle panels: higher magnification of the boxed region where N&B measurements were acquired; scale bar: 2 μm. Right panels: map of molecular brightness for the inset regions shown in the fluorescence images; heat map scale bar = normalized molecular brightness per pixel (e.g. 2 = 2 GFP molecules per cluster). **(C)** Scatter plot of normalized molecular brightness values for control and or α-gal A silenced cells (n=13 and n=15, respectively, from two experiments). The dotted line represents the average normalized molecular brightness (~2.2) for control and α-gal A silenced cells in the absence of antibody. *p < 0.005 by unpaired t-test. **(D)** Control or α-gal A silenced (KD) cells expressing GFP-endolyn in the absence or presence of anti-GFP antibody. Image layouts same as in panel B. **(E)** Scatter plot of normalized molecular brightness values for GFP-endolyn in control or α-gal A silenced cells (n=16 and n=14, respectively, from two experiments). The fine dotted line represents the average normalized molecular brightness for control and the coarse dotted line for α-gal A silenced cells in the absence of antibody (1.65 and 1.27, respectively).

2.5   DISCUSSION

The cellular phenotype of Fabry disease is not well understood. In particular, how the accumulation of the raft-associated lipid Gb3 might alter the dynamics and efficiency of lipid raft dependent processes has never been examined. As lipid raft formation and composition have been widely studied in MDCK cells for several years [196], we decided to generate a cell model to study raft-dependent processes using this well-characterized kidney tubular epithelial cell line. We effectively knocked down α-gal A mRNA levels by nearly 90% using an siRNA approach. MDCK cells silenced for α-gal A had elevated levels of Gb3, enlarged lysosomes,

and progressively accumulated zebra bodies, consistent with the cellular phenotype of Fabry disease in humans.

In nonpolarized cells, lipid rafts are estimated to cover 30-40% of the plasma membrane, and are even more prevalent in the apical membrane of polarized cells [227]. Oligomerization of raft-associated proteins either by ligand binding or antibody crosslinking is known to increase their affinity for lipid rafts and their stabilization in these microdomains [228]. Additionally, oligomerization of raft components causes lipid rafts to coalesce and form larger domains [198]. Our results indicate that the alterations in lipid raft composition observed in Fabry disease induce changes in lipid raft dynamics that may occur upon activation/oligomerization of raft-associated proteins. We speculate that this could impact raft-mediated signal transduction in Fabry disease.

Using N&B analysis, we spatially mapped the dynamics of a GPI-anchored protein in our cell model of Fabry disease. This imaging approach allows us to measure the size of oligomeric complexes in live intact cells at physiologically relevant expression levels. Strikingly, we found that the average oligomeric size for the ligated GPI-anchored protein was ~two-fold higher in α-gal A silenced cells compared to cells transfected with control siRNA. We observed ~2.5-7 molecules of GFP-GPI per oligomer upon antibody addition. This range is consistent with single molecule studies of the GPI-anchored receptor CD59 that identified clustering of 3-9 molecules of CD59 per oligomer upon gold-induced crosslinking and activation of the receptor [220]. In contrast, the clustering of a lipid raft independent protein was not significantly affected in α-gal A silenced cells suggesting that the observed change in oligomeric stability was specific to raft proteins. Measurements in live cells are critical given

recent studies demonstrating that remodeling of G protein coupled receptors and GPI-anchored protein complexes can occur on the millisecond to second timescale [229-231].

What are the implications of our results with respect to Fabry disease? High-resolution studies of CD59 have identified transient stalling, or immobilization, as a key requirement for the recruitment of downstream signaling effectors, such as Lyn kinase and PLCγ2, to activate intracellular calcium signaling [220, 232]. The increased oligomer size we observed of a model GPI-anchored protein upon α-gal A depletion might represent "stalled" oligomers due to alteration in lipid-lipid interactions or protein-lipid interactions. Thus, we predict that signaling from raft-associated complexes may be altered in Fabry disease. In this regard, one signaling pathway that will require future exploration in the context of α-gal A silencing is that mediated by TGF-β. TGF-β signals through three different receptor isoforms that traffic via both raft-dependent and raft-independent pathways [233]. The binding ratio of monomeric TGF-β to heterotetrameric complexes of these receptors differs upon membrane compartmentalization, resulting in activation of different downstream effectors [234]. Human podocytes loaded with lyso-Gb3, the deacylated form of Gb3, showed increased expression of TGF-β1, which mediates an increase in the expression of the extracellular matrix components fibronectin and collagen type IV [235]. This dysregulation of TGF-β signaling was proposed as a contributor to development of glomerular injury in Fabry disease. The cell model that we have developed combined with N&B analysis will be a powerful tool to dissect the alterations that occur in lipid raft and cellular signaling in Fabry disease.

3.0 GENERATION OF FABRY DISEASE HUMAN KIDNEY CELL LINES USING CRISPR/CAS9 GENOME EDIITING

3.1 INTRODUCTION

The use of experimental models in translational research, including naturally occurring and transgenic animals, has provided novel insights for a variety of Mendelian and complex disorders. Disease models serve as key tools for enabling a better understanding of disease pathophysiology, identification of diagnostic and prognostic biomarkers and drug discovery. With the exponential advances in genome technologies and computational approaches, several model biological species have their genome fully sequenced and at least partially annotated, allowing for more comprehensive studies of comparative gene function [236]. Mice are the most commonly used model organism in biomedical research and share 85% of similarity in their gene coding regions with humans [237]. These animals can be easily maintained under controlled, standardized environment, minimizing confounding factors. They also share several aspects of their anatomy, physiology and metabolism with humans but with an accelerated lifespan, allowing for cost-effective translation to understand human biology. However, some mouse models fail to reproduce full spectrum of the disease, rendering them unsuited for the study of certain conditions, such as Fabry disease [101].

The use of human cell models in translational research has been of particular benefit when studying cell-type and species-specific disease phenotypes and has the additional advantage of allowing high throughput profiling and screening. The discovery and characterization of post-transcriptional gene silencing techniques have allowed their applications for targeted gene function studies and disease modeling in human cells. RNA interference (RNAi), for instance, is a highly evolutionary conserved system that provides protection against double-stranded RNA (dsRNA) viruses and transposons as part of a primitive immune response, first described in *Caenorhabditis elegans* [238]. These dsRNAs are cleaved into small interfering RNA (siRNA) and incorporated into a multiprotein-RNA complex termed RNA-induced silencing complex (RISC). Activated RISC-siRNA complex then recognizes complementary mRNA, triggering sequence-specific cleavage, destabilization or translational repression of the targeted mRNA and thus gene silencing [239]. Synthetic small siRNA molecules can be designed to target mRNA of a gene of choice and delivered into the cells for RISC loading, allowing for targeted gene silencing. While effective decrease in abundance of the targeted protein can be achieved in many instances, this system only allows for a transient silencing, as the majority of synthetic siRNA is degraded within 48 h [240], making this technique challenging to study the knockdown of proteins with low turnover/prolonged half-life. An alternative is the use of vector based short hairpin RNA (shRNA), which allows for stable expression and greater knockdown efficiency, but at the cost of potential off-target effects since genomic integration preferably takes place in coding or promoter regions of the genome [239, 241].

Morpholinos have also surged as a technique for mRNA targeted post-transcriptional gene silencing. These antisense oligomers bind to complementary mRNA, blocking their

translation or affecting pre-mRNA splicing. Due to their structure, Morpholinos are particularly resistant to endonuclease digestion; they contain 25 synthetic subunits comprised of a nucleic acid base and a morpholine ring, linked through a non-ionic phosphorodiamidate, being able to pair with complementary endogenous nucleic acid sequences with high affinity and specificity [242]. An important consideration that differentiates Morpholinos of their RNAi counterparts is that they prevent translation instead of inducing mRNA degradation, thus the location of the target site within the gene is important for proper action; Morpholinos targeting the 5'-UTR or beginning of first exon are predicted to have a higher efficiency for gene silencing [243]. A growing body of evidence has shown that off-target effects can be quite significant with the use of the use of mopholinos in the generation of disease models or in genetic screening studies in zebrafish, reinforcing the importance for proper monitoring of these effects and validation of results generated using this approach [244].

Despite the enormous progress achieved by applying post-transcriptional gene silencing in modeling diseases at the cellular level, these techniques present some important limitations. For instance, incomplete blockage of gene expression of a particular gene might fail to decrease protein expression to achieve total abundance that is low enough to induce a phenotype. These factors have led researchers to search for strategies that directly manipulate the genome instead for stable and more pathophysiologically relevant models [245]. Artificial chimeric proteins comprised of DNA binding modules and endonuclease catalytic domains have been engineered to modify the genome by the introduction of targeted double-stranded breaks (DSBs) at specific genomic loci. DSBs trigger the action of the cell's DNA repair machinery, of which non-homologous end joining (NHEJ) or homology-directed repair (HDR) are the most common [246]. In an attempt to correct the DSB in the absence of a template DNA, error-prone NHEJ

induces small frame-shifting insertions or deletions, which result in gene disruption. The first class of these programmable nucleases, zinc-finger nucleases (ZFN), consists of a FokI nuclease domain and zinc-finger modules designed to bind specific DNA sequences [247]. TALENs (transcription activator-like effector nucleases), another class of programmable nucleases, also contain a FokI nuclease domain but instead they are fused to a transcription activator-like effector (TALE). ZFN can induce both deletions and insertions, while TALENS preferentially induce deletions [248]. However, both techniques are quite costly and can also have off target effects that are particularly difficult to predict during the design phase.

More recently, a technology that employs RNA-guided endonucleases for targeted genome editing by repurposing the naturally occurring system of **C**lustered **R**egularly **I**nterspaced **S**hort **P**alindromic **R**epeats (CRISPR) DNA loci and their **C**RISPR-**as**sociated (Cas) gene 9 (CRISPR/Cas9) has revolutionized the field of engineered nucleases. CRISPR DNA loci and their Cas genes provide groups of prokaryotes with adaptive immunity against viruses and other foreign genetic elements. These systems function by stable integration of short sequences from invading exogenic elements into CRISPR loci located in the genome of these prokaryotic cells as "protospacers", then inducing expression of short CRISPR RNA (crRNA) complementary to the spacers. These loci are then transcribed into siRNAs that guide targeted degradation of these invading nucleic acids [249]. CRISPR-Cas systems are classified into three main types (I-III) and 11 subtypes (I-A to F, II-A to C, and III-A to B) according to their specific loci and Cas gene organization and content. Cas targeting requires the presence of a specific protospacer-adjacent motif (PAM) at the 3'-end, which for Cas9 is in the form of NGG. Type II CRISPR systems has been recently repurposed to induce targeted genome modifications in other organisms, including mammals [250, 251].

These type II CRISPR systems rely on the action of a single multi-functional protein, Cas9, for genome editing. In an unbound state, Cas9 is found in an auto-inhibited conformation. [252] Its function is then guided by binding of a dual-RNA scaffolding complex, consisting of a crRNA and a transactivating crRNA (tracrRNA), which have been reengineered into a chimeric single-guide RNA (sgRNA) that bears a 20-nucleotide target sequence. [253] Upon activation triggered by effective sgRNA directing and target binding, Cas9 acts as both a helicase to unwind the DNA duplex and as a dual nuclease, cleaving the DNA at both strands upon target recognition. [254] Effective directing and activation of Cas9 results in DSBs in a target genomic DNA sequence that complements the guide sequence in the sgRNA, which usually occurs 3 base pairs upstream of the PAM sequence. [255] A representation of this system and main mechanisms of action is shown in Figure 11.
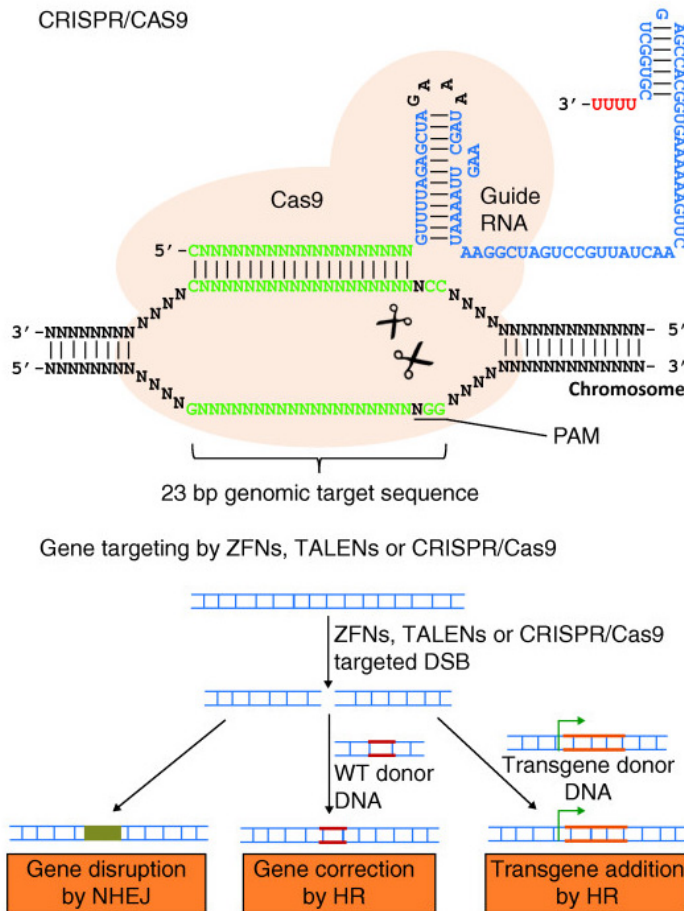
Figure 11: Schematic of CRISPR/Cas 9 and main applications of gene editing by engineered nucleases. Modified from [256].

I applied the CRISPR/Cas9 technique to disrupt *GLA* gene function in immortalized human podocytes and in human proximal epithelial cells. *GLA* gene abnormalities in humans cause Fabry disease, an X-linked lysosomal storage disorder characterized by alpha-galactosidase A (α-gal A) deficiency and accumulation of its substrates, mainly globotriaosylceramide (Gb3). To date, the Human Gene Mutation Database (http://www.hgmd.cf.ac.uk) describes over 600 mutations in the human *GLA* gene that cause Fabry disease. These mutations affect the synthesis, folding, stability, substrate binding or action of alpha-galactosidase A, all culminating in low or absent enzyme activity in the lysosome. [257] Small deletions in both of the exons we targeted have been shown to cause the

classic phenotype of Fabry disease in patients. [258] This disease often complicates with nephropathy, which can culminate in complete loss of kidney function [259]. Progressive podocyte and tubular epithelial cell dysfunction are major components of Fabry disease nephropathy [260, 261]. Pathologically, this nephropathy is characterized by renal cell inclusions, focal segmental glomerulosclerosis, followed by progressive tubulointerstitial disease and decline in kidney function. [262] The renal response to enzyme replacement therapy is suboptimal, and the progression of nephropathy, including worsening of foot process effacement, can occur despite long-term treatment [263]. Little is known about the disease mechanisms leading to renal cell injury and death, and as Fabry disease mice do not show the classic signs of the kidney dysfunction seen in patients with the condition, cell-type specific human models of the disease are critical.

With the assistance of an RFP/Hygromycin-GFP surrogate reporter plasmid, I was able to successfully achieve concurrent editing of two different coding regions of the *GLA* gene, generating kidney cell line knockouts for *in vitro* studies. As expected, *GLA* knockout cells exhibited the Fabry disease biochemical phenotype, characterized by reduced α-gal A enzyme activity and increased Gb3. These kidney cell lines may serve as tools for better understanding the pathogenesis of Fabry nephropathy as well as for drug discovery.

3.2 MATERIALS AND METHODS

3.2.1 Culture of kidney cell lines

Human proximal tubule cells HK-2 [264] were cultured in DMEM/F-12 medium (Gibco) supplemented with 10% heat-inactivated FBS (30 min at 56°C), 20mM HEPES buffer, 2mM L-glutamine, 1% (v/v) Insulin-Transferin-Selenium (Gibco), 5 μL of and 0.4 μg/mL of hydrocortisone, 5 μL of triiodothyronine 20 μg/ml in NaOH, 1% (v/v) Pen/Strep (10,000 units/mL, Gibco). Immortalized human podocytes were a gift of Dr. Jean Daniel Sraer, INSERM, France to Kunimasa Yan Kyorin University School of Medicine, Japan, and were provided by Dr. Agnieszka Swiatecka-Urban, Children's Hospital of Pittsburgh. Isolation and characterization of this SV40 large T antigen immortalized cell line is described in [265]. Cells were cultured in DMEM/F-12 medium (Gibco) supplemented with 10% heat-inactivated FBS (30 min at 56°C), 2mM L-glutamine, 1% (v/v) Insulin-Transferrin-Selenium (1mg/mL, 0.55 mg/mL and 0.67 μg/mL respectively, Gibco), and 1% (v/v) Pen/Strep (10,000 units/mL, Gibco). Podocytes were used for CRIPSR/Cas9 experiments between passages 13 and 17 from the originally immortalized cells. Cells were maintained at 37°C and 5% CO_2 in a humidified incubator, passaged at 1:10 when they reached 80% confluence and frozen in FBS containing 10% DMSO at -80°C or in liquid nitrogen for longer-term storage.

3.2.2 Oligonucleotide Design

Target sequences against the first, third, and last exons of *GLA* (i.e. exons 1, 3 and 7) were selected using bioinformatics tools. The first sgRNA used was against exon 7 and was selected

from a database of predicted sequences listed by Mali et al [250]. The sgRNA against exon 1 was designed using the CRISPR Design Tool of Zhang and colleagues (http://crispr.mit.edu). Other sgRNAs were designed using the E-CRISP design tool under medium stringency parameters [266]. The experiments described herein were performed with guides 1 (against exon 7, R2) and 4 (against exon 1, R1). For the pX330 CRISPR/Cas9 vector (see below), sgRNA R1 and R2 oligonucleotide sequences were checked to confirm the absence of BbsI enzyme sites (i.e. GAAGAC or GTCTTC) using BLAST (NCBI). To clone the target sequences into the pX330 backbone after digestion with BbsI, CACCG was added to the beginning of the 5' region of the forward oligonucleotide, and AAAC was added to the beginning of the 5' region of the reverse oligonucleotide, with a C following the target sequence at the 3' end, excluding the PAM sequence. Standard desalted oligos were purchased from Integrated DNA Technologies. Primer sets flanking the target regions of the *GLA* gene were designed using NCBI Primer Designing Tool under default settings, blasting against the *Homo sapiens* reference genome database (refer to Table 2 for primer sequences). Preference was given to product sizes between 600 and 1200 to allow for better separation and visualization of T7 Endonuclease 1 (T7E1) digestion products on a 2% agarose gel.

Table 2: Oligonucleotides and primers used in this study.

3.2.2.1 Region	Plasmid	3.2.2.2 Sequence 5'- 3'	
3.2.2.3 R1 (exon 1)	3.2.2.4 pX330	3.2.2.5 F: CACCGATAAATTTCCGCGGGTAACC	
		3.2.2.6 R: AAACGGTTACCCGCGGAAATTTATC	
	3.2.2.7 pHRS	3.2.2.8 F: AATTCTCCAGGTTACCCGCGGAAATTTATAGGAG	
		3.2.2.9 R: GATCCTCCTATAAATTTCCGCGGGTAACCTGGAG	
	3.2.2.10 PCR	3.2.2.11 F: ACGGCTATAGCGAGACGGTA	
		R: GGGTCTGAATAGAACCGGGC	
3.2.2.12 R2 (exon 7)	3.2.2.13 pX330	3.2.2.14 F: CACCGTGTGGGAACGACCTCTCTC	
		3.2.2.15 R: AAACGAGAGAGGTCGTTCCCACACC	
	3.2.2.16 pHRS	3.2.2.17 F: AATTCTGTGTGGGAACGACCTCTCTCAGGAGGAG	
		3.2.2.18 R: GATCCTCCTCCTGAGAGAGGTCGTTCCCACACAG	
	3.2.2.19 PCR	3.2.2.20 F: GACCAGGGGGTTGGAATGAC	
		3.2.2.21 R: AGCTGAAGCAAAACAGTGCC	

3.2.3 Plasmid Generation

pHRS vector was purchased from PNA Bio Inc. The pHRS plasmid works as a surrogate reporter of CRISPR/Cas9 activity. It contains an expression cassette for mRFP, an oligonucleotide sequence containing a stop codon flanked by EcoRI and BamHI digestion sites, and a hygromycin selectable marker linked to GFP separated by a self-cleaving 2A peptide. In the unedited state, translation of reporter cassette stops after the mRFP and target region due to the presence of a stop codon. Upon cloning of oligonucleotide containing the target sequence of interest in the genome, CRISPR/Cas9 modification by the engineered nuclease induces a double-strand break in the target region, resulting in non-homologous end joining and introduction of insertion and/or deletion mutations in the plasmid. This frequently eliminates the stop codon by frame shifting the plasmid DNA, conferring translation of hygromycin resistance and GFP [267]. The same oligonucleotide guide sequences designed for the pX330 CRISPR/Cas9 plasmid were used for the pHRS reporter plasmid, with inclusion of respective PAM sequence for nuclease binding and activation. Reporter function was simulated *in silico* for frame shifting and loss of stop codon after indels are inserted into target region using Vector NTI Software (Life Technologies). Overhangs for EcoRI (AATTCT) were added to the 5' end of the plus strand, GA to the 3'end of the minus strand, as well as a G to the 3' end of the plus strand sequences. Additional residues necessary to maintain the reading frame of the plasmid were added as needed upon simulation using Vector NTI. Standard desalted oligos (refer to Table 2 for pHRS oligo sequences) were purchased from Integrated DNA Technologies. Each pair of complementary oligonucleotides for either pX330 or pHRS incorporation was phosphorylated and self-annealed for proper ligation (100 µM per single oligonucleotide) using T4 polynucleotide kinase (PNK) and T4 ligation buffer (New England BioLabs) according to

the manufacturer's protocol. Thermocycler settings were as follows: 37°C for 30 min, 95°C for 5 min, then ramping down to 25°C at 5°C/min.

The pHRS plasmid was digested with EcoR1-HF (New England Biolabs) and BamH1-HF (New England Biolabs) in CutSmart Buffer (New England Biolabs) for 30 min at 37°C. Gel purification was performed in 1% agarose gel using Wizard SV gel and PCR Clean-Up System (Promega) according to the manufacturer's protocol. Phosphorylated and annealed oligo duplexes (1:250 dilution) were then ligated into purified digested vector using T7 DNA ligase (New England BioLabs), incubated at ambient temperature for 30 min according to the manufacturer's protocol.

For the pX330 plasmid, settings for cloning of phosphorylated and annealed oligos into the backbone vector were optimized, and were performed as a single-step digestion ligation reaction as follows: pX330, 100 ng; oligo duplex, 1:250 dilution, 2 µL; Tango buffer (Thermo Scientific), 2µL; DTT 10 mM, 1 µL; ATP, FastDigest BbsI (Thermo Scientific), 1 µL, T7 DNA ligase (New England Biolabs), 0.5 µL and DEPC-treated H_2O, qsp 20 µL.. Thermocycler settings were as follows: 37°C for 5 min, 23°C for 5 min, cycling these two steps 6 times for a total run time of 1 h. In order to prevent unwanted recombination products, ligation reactions for both pHRS and pX330 vectors were treated with PlasmidSafe ATP-depended DNase (Epicentre) for 30 min at 37°C according to the manufacturer's protocol. Ligation products (2 µL) were transformed into One Shot® Stbl3™ Chemically Competent E. coli (Thermo Fischer Scientific) according to the manufacturer's protocol. Transformation products (25 µL or 100 µL) were seeded onto ampicillin (pX330) or kanamycin (pHRS) LB agar plates. Individual colonies were grown in LB broth solution with 1:1,000 ampicillin (100 mg/mL stock concentration) for pX330 or 1:1,000 kanamycin (50 mg/mL stock concentration) for pHRS.

Plasmid isolation and purification was performed using QIAprep spin Miniprep Kit (Qiagen) and QIAGEN Plasmid Maxi Kit (Qiagen) according to the manufacturer's protocol. Vector clones sequences were confirmed for oligo incorporation using Sanger Sequencing performed by the University of Pittsburgh Genomics Research Core using the hU6 and pCMV forward sequencing primers for pX330 and pHRS respectively. Oligo incorporation into vectors was confirmed using CLC Genomics Workbench (Qiagen). A representation of the plasmids used can be found in Figure 12.
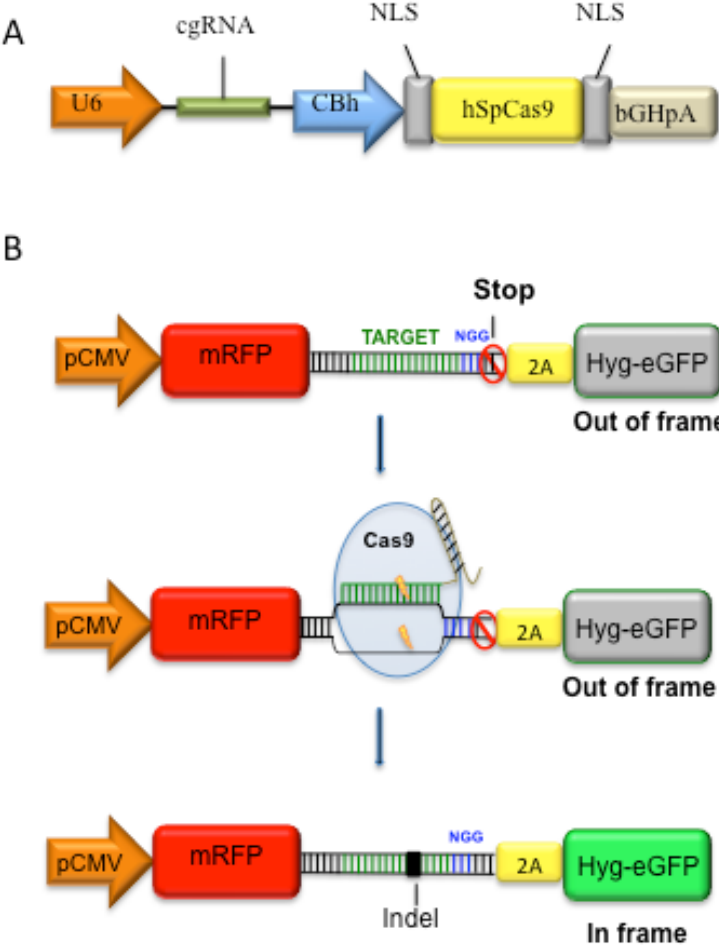
Figure 12

Figure 12: Plasmids used in this study.

A. pX330 CRISPR/Cas9 plasmid and B. pHRS surrogate reporter plasmid and its mechanism of action. Hyg-eGFP: hygromycin-eGFP.

70

3.2.4 Plasmid Delivery

Approximately 5 x 10^5 cells were seeded in 6-well plates with 2 µg of pX330 plasmid and immediately transfected with 2 µg of the corresponding pHRS plasmid per well using 4 µL of lipofectamine 3000 (Invitrogen), 10 µL of P3000 reagent and 1 mL of OptiMEM following the manufacturer's instructions. For concomitant delivery of pX330 and pHRS plasmids targeting the two different regions of *GLA*, 1 µg of each plasmid was used to transfect 5 x 10^5 cells, for a total of 4 µg of DNA. Transfection of empty pX330 and pHRS vectors was used as control. Growth medium was changed after 12 h and experiments were performed 48 to 72 h after transfection.

3.2.5 Fluorescence-Activated Cell Sorting

Approximately 1.5 x 10^6 cells co-transfected with pX330 and pHRS were trypsinized with TrypLE™ Select (Thermo Fischer Scientific) for 5 min, centrifuged at 500 x *g* for 3 min and re-suspended in 600 µL of PBS supplemented with 10% BFS. To achieve a single-cell suspension, cells were passed through 50-µm filcon filters (BD Biosciences). Single-cell suspensions were analyzed and sorted in a BD FACSAria II (BD Biosciences), with FACSDiva version 6.1.3 software. Default setup was applied for RFP and GFP fluorescence detection (For GFP: 488-nm blue laser, E PMT, 502 LP mirror, 430/30 BP filter; for RFP: 488-nm blue laser, D PMT, 556 LP mirror, 585/42 BP filter). RFP/GFP double-positive cells were collected into 96-well dishes for clonal populations and/or into 15 mL conical tubes, both containing specific growth medium. Gating for GFP and RFP fluorescence was performed using untransfected cells and cells transfected with empty pHRS and pX330 vectors as controls.

3.2.6 Hygromycin Treatment

A hygromycin selection dose-response curve in human immortalized podocytes and HK-2 cells, yielded 2 mg/mL as the optimal hygromycin concentration for rapid (48 h) toxicity to the majority of cells for both cell types. For hygromycin selection, 5×10^5 human immortalized podocytes or HK-2 cells were treated 48 h after co-transfection with pHRS and pX330 plasmids with 2 mg/mL of Hygromycin B (Invitrogen) in growth medium. After 48 h, the drug was removed and the remaining viable cells were cultured in growth medium until further characterization.

3.2.7 Genomic DNA extraction and PCR amplification

Genomic DNA from approximately 1×10^5 cells was extracted using QuickExtract DNA extraction solution (Epicentre) according to the manufacturer's protocol. Briefly, cells were pelleted in a microcentrifuge tube at 800 g for 3 min, washed once in 1X PBS, Dulbecco's Solution minus Mg^{2+} and Ca^{2+}, and lysed by vortexing for 15 s in 500 µL of DNA extraction solution. Lysates were then incubated at 65^oC for 6 min, vortexed for 15 s and then incubated at 98°C for 2 min and stored at -20^oC until further use. The genomic region flanking the CRISPR/Cas9 target sites were amplified by PCR using Phusion® High-Fidelity DNA Polymerase (New England BioLabs) using 5 µL of extracted genomic DNA as a template. A touchdown approach was applied for enhanced specificity and yield [268]. The following settings were applied: 30 s at 98°C, 15 cycles at [98°C for 10 s, 67°C for 30 s (reducing annealing temperature by 1°C each cycle), 72 °C for 30 s], followed by 25 cycles at [98 °C for 10 s, 52 °C for 30 s, 72°C for 30 s], and a final cycle of 72°C for 10 min. PCR products were

separated in a 2% agarose gel stained with SYBR® Safe DNA Gel Stain (Thermo Fischer Scientific) and visualized on a Molecular Imager® Gel Doc™ XR System (Bio-Rad Laboratories, Inc.). Images were processed using Image Lab™ 5.1 Software (Bio-Rad Laboratories, Inc.).

3.2.8 T7 Endonuclease I Assay

Amplicons were hybridized by denaturing and re-annealing to allow for homo- and heteroduplex formation. Briefly, 1.6 µg of PCR products were resuspended in a final volume of 10 µL in 1x Phusion High Fidelity PCR buffer (New England Biolabs) and duplicate samples amplified in a thermocycler using the following settings: 95°C for 10 min, then ramp down to 85°C, decreasing at 2.0^{o}C/s. After that, the temperature was dropped 10°C at a time at a rate of 0.3^{o}C/s, maintaining target temperatures for 1 min until reaching 25°C. Hybridized products do you just mean the final reactions? were stored at 4°C until further use. Hybridized products were then digested with T7 Endonuclease I (T7E1) (New England BioLabs) at 37°C for 15 min. Digested products along with undigested hybridized products were separated on a 2% agarose gel and scanned on a Molecular Imager® Gel Doc™ XR System (Bio-Rad Laboratories, Inc.). Images were processed using Image Lab™ 5.1 Software (Bio-Rad Laboratories, Inc.).

3.2.9 Immunofluorescence

For human immortalized podocytes, 2.5 x 10^4 cells were seeded on coverslips coated with 10% PureCol® type I bovine collagen solution (Advanced BioMatrix) in growth medium in 12 well cell culture dishes. After 24 h, coverslips were fixed with 10% neutral buffered formalin

solution (Sigma-Aldrich) for 15 min, quenched for 5 min in 50 mM NH$_4$Cl and 0.1M glycine in PBS and permeabilized with 0.1% Triton X-100 (Sigma-Aldrich) in quench solution for 8 min. The samples were then blocked for 1 h in 1% BSA (Sigma-Aldrich) and 0.1% saponin (Sigma-Aldrich) in PBS. Next, the coverslips were incubated with primary antibodies [anti-CD77 (Ab35768 rat monoclonal IgM, Abcam)] for 1 h then washed twice quickly with PBS followed by washing 3 times for 5 min in PBS containing 0.5% BSA (Sigma-Aldrich) and 0.05% saponin (Sigma-Aldrich) in a shaker. Coverslips were then incubated with secondary antibodies (Cy3 goat anti-rat IgM; Alexa Fluor 488 goat anti-rat IgM) for 30 min. All steps were performed at ambient temperature. The cover slips were mounted on slides with ProLong Gold Antifade Reagent with DAPI (Invitrogen). Images were captured using a Leica DM6000 B fluorescence upright microscope system (Leica Microsystems) and processed using Volocity 6.1 Software (PerkinElmer).

3.2.10 Enzyme Activity Assay

Alpha-galactosidase A activity was measured fluorimetrically in control and CRISPR/Cas9 modified (Fabry) immortalized human podocytes and HK-2 cells using 4-methylumbelliferyl-α-D-galactopyranoside (Sigma) as the substrate. Approximately 10^6 cells were pelleted in a microcentrifuge tube at 800 g for 3 min, washed once in PBS, Dulbecco's Solution minus Mg^{2+} and Ca^{2+}, and re-pelleted. Cells were then lysed by 3 cycles of freeze-thaw in 500 µL of citrate-phosphate buffer (50 mM citric acid monohydrate, 100 mM dibasic sodium phosphate-anhydrous, pH 4.8), vortexing for 15 s between freeze cycles. Protein concentration was measured using a BioPhotometer (Eppendorf) using the protein direct photometric measurement setting at 280 nm. Equal amounts of protein were used to measure enzyme activity. Lysates (50

µL) were incubated with 20 µL of substrate solution (5 mM 4-methylumbelliferyl-α-D-galactopyranoside (Sigma-Aldrich) and 100 mM N-acetylgalactosamine (Sigma-Aldrich) in DEPC treated water) for various times (1 h at 37°C or 6 h and 24 h at ambient temperature). To assess linearity of the assay, four reactions were set up by mixing 0, 5, 25, or 50 µL of lysate of control cells with of 50, 45, 25, or 0 µL of lysate that underwent boiling at 100°C for 10 min for enzyme inactivation. These reactions corresponded to 0, 10, 50, and 100% of enzyme activity in control cells, respectively. Two sets of reactions were incubated with substrate solution for 1 h at 37°C and 24 h at ambient temperature, respectively. Enzymatic activity was terminated by addition of 70 µL of 50 mM glycine ammonium hydroxide, pH 10.5. The fluorescence intensity of released 4-methyl-umbelliferone was quantified in a GloMax®-Multi+ Detection System with Instinct® Software at excitation 360-380nm/ emission 500nm.

3.3   RESULTS

3.3.1   CRISPR/Cas9 mediated editing of *GLA* in human immortalized podocytes and HK-2 cells

Progressive kidney dysfunction is a major clinical finding of the X-linked lysosomal storage disorder Fabry disease. [262] To model Fabry disease nephropathy *in vitro*, I created two genome edited renal cell lines: human immortalized podocytes and HK-2 cells, a human proximal epithelial cell line. While a variety of renal cell types can be affected in Fabry disease, involvement of podocytes and tubular epithelial cells is a typical and early finding of nephropathy in these patients. [261, 263]

Using bioinformatics tools, I selected two sgRNAs against the first and seventh exons of the human *GLA* gene and cloned them into the pX330 plasmid. The sequences of the oligonucleotides used in this study are listed in Table 2. I first delivered CRISPR/Cas9 pX330 plasmids targeting the *GLA* exon 7 or empty pX330 plasmids as control to human podocytes and HK-2 cells using lipid-mediated transfection. Next, I enriched for cells with CRISPR/Cas9-induced modifications by co-transfection with the surrogate reporter plasmid pHRS. This plasmid contains cassettes for mRFP expression, the same CRISPR/Cas9 genome target nucleotide sequence, (including the PAM for Cas9 recognition) and for an eGFP-hygromycin resistance fusion protein. This plasmid is designed so that mRFP is expressed constitutively whereas the eGFP and hygromycin genes are out-of-frame and preceded by a stop-codon and a self-cleaving 2A peptide. In the absence of plasmid editing, mRFP will be expressed but transfected cells will lack eGFP expression and hygromycin resistance. Double-stranded breaks at the target sequence of the plasmid by CRISPR/Cas9 and subsequent non-homologous end joining repair causes a frameshift, which enables eGFP expression and hygromycin resistance [267]. This provides two straightforward approaches (FACS and drug resistance) to enrich for gene-edited cell populations, as modification of this reporter plasmid mirrors genomic modification in the cells at least partially [267]. Forty-eight hours after co-transfection of plasmids into both immortalized podocytes and HK-2 cells, 4-10% of cells expressed mRFP, demonstrating moderate transfection efficiency of the reporter plasmid. A small proportion of the mRFP positive cells also were positive for eGFP fluorescence by FACS, indicating that frameshifting indel changes were incorporated into the reporter plasmid, inducing translation of eGFP. The efficiency of plasmid modification, characterized by eGFP expression, varied from 15 to 18%, corresponding to 0.8 to 1.6% of the starting population (data not shown).

For HK-2 cells, mRFP/eGFP double positive CRISPR/Cas9 *GLA* treated cells or mRFP positive for control cells were FACS sorted, collected, and clones expanded from single cells in 96-well dishes. As human immortalized podocytes are particularly sensitive to cell sorting and are difficult to grow from single cells, mRFP/eGFP double positive CRISPR/Cas9 *GLA* treated cells or RFP positive control cells were instead cloned by limiting dilution and plated in 15 cm dishes. Next, I assessed genomic level *GLA* modification in a mixed population of FAC sorted cells using the T7 Endonuclease 1 assay. Endonuclease I of phage T7 (T7E1) is a highly selective enzyme that introduces paired cleavages in Holliday junctions, which are four-way branched DNA structures that can be formed by double-strand break (DSB) repair [269]. The endonuclease T7 I assay was recently reported to be the preferred method to assess for genomic changes induced by engineered nucleases [270]. This paralleled my own experience that T7EI was more sensitive in showing editing in mixed cell populations. T7E1 assay of hybridized amplicons flanking the target region demonstrated cleavage of PCR products with bands of the expected product size. These bands were only present in CRISPR/Cas9 GLA treated cells, suggesting successful modification of *GLA* gene in both HK-2 and podocyte populations (Figure 13).

Of note, for one of the clonal podocyte populations of CRISPR/Cas9 GLA treated podocytes, initial analysis of PCR amplicons flanking target *GLA* region by gel electrophoresis revealed a large deletion, which was confirmed by Sanger sequencing. However, I observed a progressive drift back towards the unmodified amplicon over successive passages. This phenomenon was not observed in Hk-2 clonal cell populations, which, even after three months of continuous passage, have maintained the genomic modification and Fabry disease phenotype.

The initial mixed FACS population plus additional three clonal cell populations of podocytes, including an earlier passage of the clone that showed drifting, then underwent a second round of CRISPR/Cas9 treatment, this time with co-transfection of pX330 plasmids targeting both exons 1 and 7 and respective pHRS reporter plasmids. As pHRS plasmid induces expression of both GFP and hygromycin, I opted during the second round of CRISPR/Cas9 treatment to perform enrichment using hygromycin as described in Methods.

After the second round of CRISPR/Cas9 treatment in mixed populations of immortalized human podocytes, T7E1 assay of PCR amplifications flanking targeted regions of showed additional bands present only in the CRISPR/Cas9 *GLA* treated cells, again suggesting successful genome editing of both targeted regions. Interestingly, PCR analysis flanking the target region in exon 1 demonstrated the presence of amplicons significantly larger and smaller in size in all CRISPR/Cas9 *GLA* podocyte cell populations, suggesting generation of larger indels. PCR amplicons and T7E1 assay for HK-2 clone and podocyte mixed populations can be seen in Figure 13.
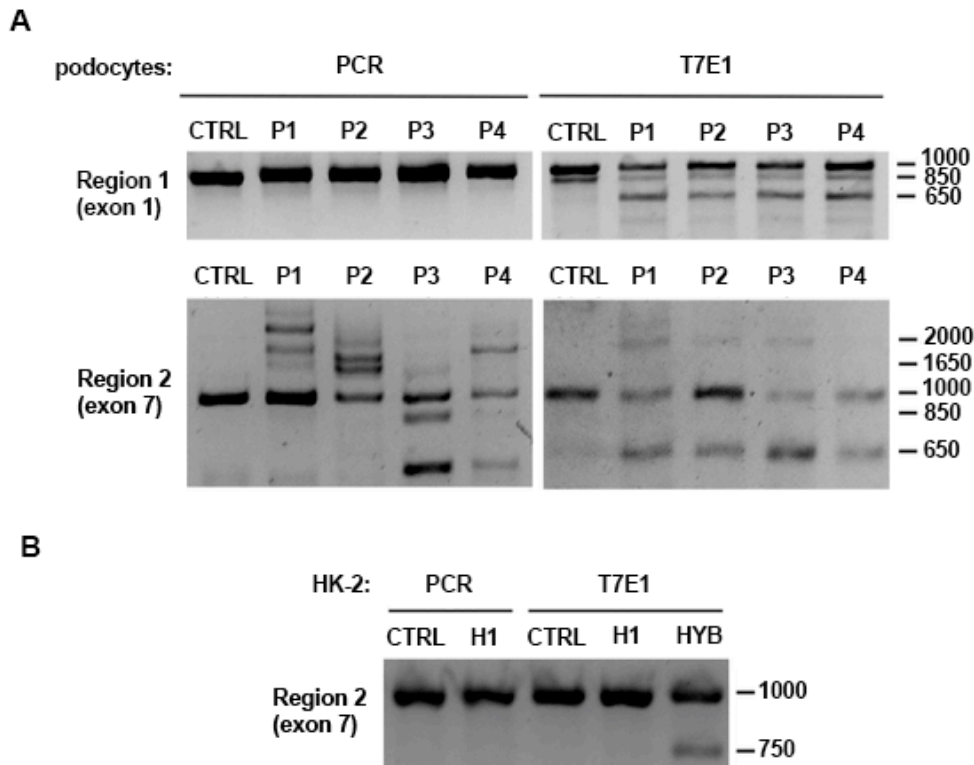
Figure 13: Amplicons and T7 endonuclease I assay of *GLA* gene region flanking the CRISPR/Cas98 genomic target in HK-2 cells and podocytes.

Panel A. PCR and T7E1 assay in control (CTRL) and CRISPR/Cas9 *GLA* podocyte cell populations (P1-P4). Panel B. PCR and T7E1 assay in control (CTRL) and HK-2 CRISPR/Cas9 *GLA* clone (H1). Hyb: hybridized amplicon heteroduplex.

These data are consistent with what Brandl et al. [271] observed when simultaneously targeting two different coding regions of *Rab38* in embryonic stem cells. They report that multiplex targeting for a same gene can result in larger deletions as well as non-canonical chromosomal rearrangements in at least one of the alleles.

3.3.2 Phenotypic characterization of CRISPR/Cas9 edited cells

Loss of function mutations in the *GLA* gene associated with Fabry disease result in α-gal A deficiency, with inability of the enzyme to metabolize neutral glycosphingolipids with α-D-galactosyl residues, mainly globotriaosylceramide (Gb3/CD77). To assess the phenotype of the generated kidney cell lines, enzyme activity and anti-CD77 staining were performed. We found no detectable α-gal A enzyme activity assay in CRISPR/Cas9 *GLA* edited HK-2 clonal cell and podocyte mixed cell populations (Figure 14), with preserved activity of α-mannosidase, a lysosomal hydrolase that cleaves mannoside residues of glycoproteins [272].
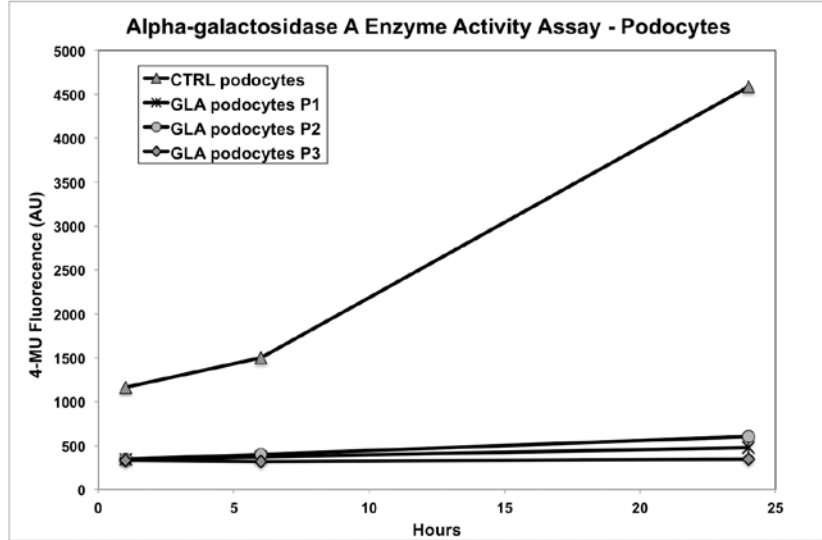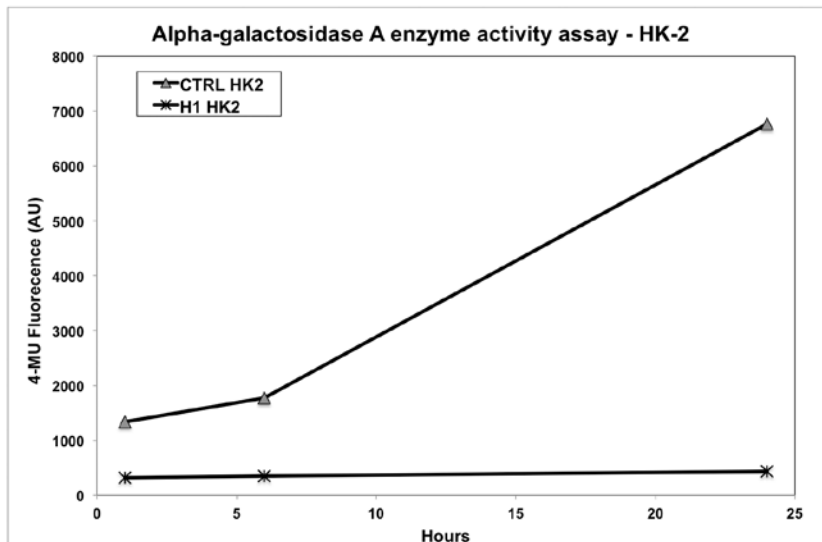
Figure 14: Decreased α-gal A enzyme activity in podocytes and HK-2 cells genome modified for Fabry disease.

Fluorometric enzyme activity assay for α-gal A using 4-MU substrate in human immortalized podocytes (A) and HK-2 cells (B) that undergone CRISPR/Cas9 treatment at the *GLA* gene.

Next, we examined Gb3 levels in CRISPR/Cas9 *GLA* edited cells. In Fabry disease, Gb3 is known to progressively accumulate in kidney cells, a process that can begin *in utero* and which results in tissue damage, often culminating in kidney failure. [273] Anti-CD77

immunofluorescence staining of both podocytes and HK-2 cells revealed higher levels of the

glycosphingolipid in CRISPR/Cas9 edited podocytes and HK-2 cells, confirming a substantial

increase in the substrate for alpha-galactosidase A in CRISPR/Cas9 *GLA* edited cells (Figure

15).
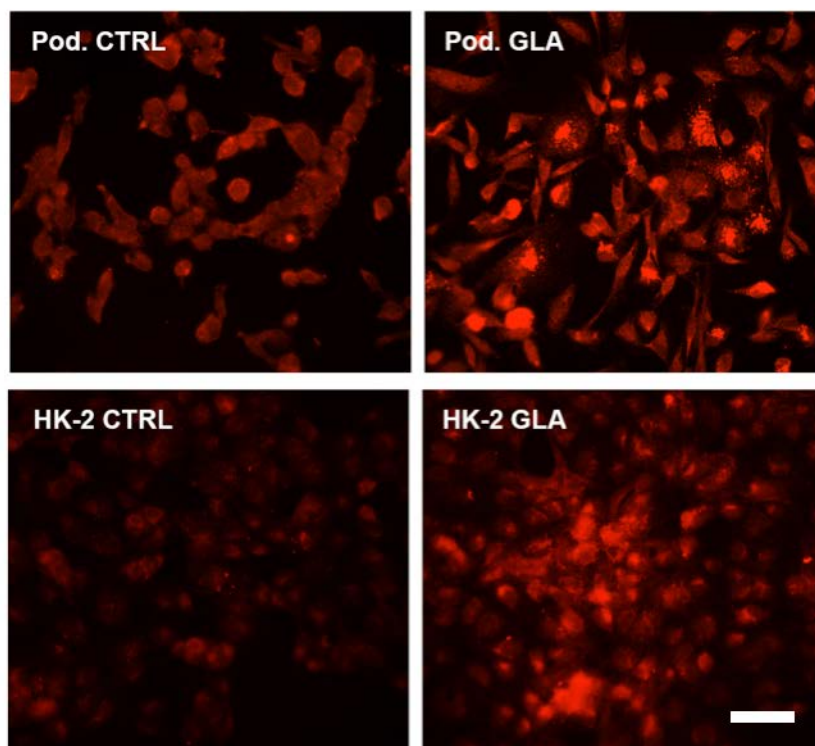
Figure 15: Globotriaosylceramide accumulation in podocytes and HK-2 cells genome modified for Fabry disease.

Immunofluorescence staining for globotriaosylceramide (Gb3) detected using anti-CD77 antibody in human immortalized podocytes (upper panel) and HK-2 cells (lower panel) that undergone CRISPR/Cas9 treatment at the *GLA* gene (right panels). Control podocytes and HK-2 cells are represented on the left. Scale bar: 20 μm.

Both of these biochemical methods indicate successful modeling of Fabry disease in

human podocytes and HK-2 cell lines through CRISPR/Cas9 editing, as the generated kidney

cells show both a deficiency in alpha-galactosidase A and accumulation of Gb3.

3.4 DISCUSSION

Understanding the cellular mechanisms underlying renal cell injury in Fabry disease is crucial for development of novel therapies, especially when the currently available enzyme replacement therapies only partially slows the progression of the nephropathy.

By applying CRISPR/Cas9 with the help of a surrogate reporter plasmid for enrichment, I have successfully developed kidney cell models of Fabry disease. *GLA* edited podocytes and HK-2 cells showed a dramatic reduction in α-gal A activity, coupled with an increase in Gb3, the main substrate of the enzyme. Both of these features are biochemical hallmarks of Fabry disease.

Post-transcriptional gene silencing techniques oftentimes do not enable a reduction in protein abundance that yields a phenotype. This is of particular concern in enzyme deficiencies such as Fabry disease, where the targeted protein has a prolonged half-life of 4 days [274] and where dramatic reduction of enzyme activity needs to be achieved to induce a phenotype. For instance, male patients with the condition present with α-gal A enzyme activities that typically range between 0 and 10% of normal [85].

Genome editing techniques are excellent alternatives for effectively modeling diseases when stable complete loss of function is desirable. CRISPR/Cas9 confers a superior alternative to TALENs and ZNFs due to its simplified design, easier prediction, potentially higher efficiency and lower cost. In addition, unlike their genome-editing counterparts, CRISPR/Cas9 can cleave methylated DNA, expanding editing capability. [275]

The majority of CRISPR-Cas9 editing efficiently generates loss-of-function alleles. [276] For autosomes in diploid cells, CRISPR/Cas9 induces DSB and consequently NHEJ independently in each allele, thus heterozygous changes are more likely than homozygous

modifications. [277] Therefore, modeling X-linked conditions such as Fabry disease in male cell lines has a higher probability of success.

However, some caveats regarding the use of CRISPR/Cas9 should be considered. As this is a relatively novel technique, guide design algorithms are constantly evolving, especially as we learn more about features that affect target efficiency such as sgRNA sequence and size, target GC content, exon location, presence of higher order chromosomal structures and accessibility to chromatin as well as Cas9-RNA interaction motifs. [276, 278, 279] The prediction algorithms currently available may apply different design and scoring systems, yielding different sgRNA recommendations with little or no overlap. This makes it challenging for researchers to proper select their sgRNAs. In addition, cell-type-specific and genomic-specific differences can be found in chromatin modification and conformation as well as accessibility to nucleases, resulting in variations in targeting efficiency that are difficult to predict. [278, 280]

Furthermore, recent studies have attempted to better understand CRISPR/Cas9 specificity using genomic approaches. [281, 282] As for other genome editing techniques, besides the intended gene of interest, other highly homologous coding and non-coding regions of the genome can also be targeted and cleaved by CRISPR/Cas9 with same efficiency as for intended targets, even in regions with a significant number of mismatches, leading to undesired off-target genome editing. [283] Several strategies in sgRNA and Cas9 design, modification and delivery have then been applied in an attempt to reduce off-target effects [284, 285] Bioinformatics algorithms predict off-target sites with varying accuracy based on sequence alignment against the reference genome, however, the magnitude of off-target effect varies greatly per site, regardless of numbers of mismatches. [278, 286] Thus, these tools need to be

more extensively assessed for efficacy and their results properly validated. In addition, off-target prediction can be particularly challenging when working with cell lines; cells in culture can undergo increasing number of genomic changes, including copy number variations, loss of heterozygosity and aneuploidies, making it difficult to anticipate the presence and consequences of off-targeting. [287, 288]

Obtaining efficient plasmid delivery with low cell toxicity is a challenge when working with several immortalized cell lines, and this was the case for our human immortalized podocytes. These cells required a longer recovery time after being sorted by FACS, even when transfected with empty vectors alone. In addition, we observed cell-type dependent drifting towards unmodified cells in CRISPR/Cas9 *GLA* treated immortalized human podocytes. This drifting was not observed in our HK-2 cell populations. Differences in the cell cloning approaches/requirements might have played a role in this phenomenon. For cells that can tolerate sorting by FACS and individual seeding in 96-well plates, this might represent a s uperior strategy for obtaining pure stable clonal cell populations. Furthermore, the drifting observed might indicate a significant survival or proliferation advantage of unmodified over *GLA* edited podocytes. These differences in cell viability and/or proliferation among *GLA* edited and control podocytes would not be surprising given that human podocytes are particularly sensitive to α-gal A deficiency.

3.5   CONCLUSION

Despite some limitations, cell models of disease can be extremely useful tools for understanding disease mechanisms and cell-type specific gene function. These models can be particularly

helpful in cases where disease cannot be properly replicated in other animals and can be easily applied for high throughput biomarker and drug discovery. CRISPR/Cas9 can induce efficient, stable, pathophysiologically relevant targeted genome modifications, which can be employed for hypothesis generating and testing in the study disease mechanisms *in vitro*.

4.0 HIGH THROUGHPUT PHOSPHORYLATION PROFILING OF A HUMAN PODOCYTE CELL MODEL OF FABRY DISEASE

4.1 INTRODUCTION

High-throughput approaches in cell biology allow for rapid unbiased generation of large amounts of data that can be used to understand a variety of cellular processes in health and disease as well as to generate and test novel hypotheses in disease pathophysiology, allowing for biomarker discovery and drug development.

Several techniques are currently used for high-throughput analyses of mRNA expression, including hybridization- and sequence-based approaches. Microarrays are based on principles of Northern or Southern blot analyses, in which mRNA or cDNA labeled with a fluorescent dye hybridizes to probes that are covalently spotted onto an inert surface (namely a glass slide or a microchip) [289]. Fluorescence for each spot is then measured and processed using a fluorescence laser scanner and computational tools. This value of measured fluorescence for each spot is directly proportional to the amount of bond fluorescently labeled mRNA/cDNA. While these techniques do not provide information on absolute abundance of a particular mRNA in a given sample, they do allow for comparative analysis of the expression level among genes or conditions (healthy control vs. disease). Microarray analysis results can then be applied in class comparison, class prediction or class discovery [290]. Microarrays are relatively

inexpensive and straightforward techniques, but they have some limitations. Analysis is limited to the probed targets in the specific microarray being used, thus can only be performed on known (and properly probed) mRNAs/cDNAs, limiting the discovery of novel transcripts or splicing forms. In addition, the presence of a background noise and the saturability of fluorescence signals limit the dynamic range of this technique for targets with very low or very high expression. Probes are also potentially susceptible to cross-hybridization, allowing for false positive results. Furthermore, the analysis depends on the quantitation of fluorescence signals in a scanned image of a slide/chip, which needs to be properly preprocessed and normalized, adding an extra level of complexity.

The sequence-based methods of RNA sequencing allow for detection and precise quantification of both common and rare transcripts, novel isoforms and gene fusions, all at the single base resolution and virtually no background noise [291]. While several different protocols can be employed depending on the platform used, they usually share the principle of reverse transcription of total RNA into a cDNA library, which is then fragmented and processed [292]. cDNA fragments are then read, assembled and mapped to a reference genome using computational pipelines. Estimation of expression of a transcript is then calculated as a function of the depth (i.e. number of read counts) normalized to length of the transcript, in the form of reads per kilobase of exon model per million mapped reads (RPKM) [293]. However, this technique also presents some important limitations. As with genome/exome deep-sequencing counterparts, RNA sequencing coverage varies across transcripts and ambiguity may hinder mRNA mapping, since short transcripts can often be matched to several regions of the reference genome [291]. Furthermore, considerable variation in expression level estimates can be seen when applying different RNA-seq methodologies [294].

Furthermore, the central dogma of molecular biology, which states that "DNA makes RNA and RNA makes protein", actually entails much more complexity than originally thought. While the human genome is comprised of approximately 21,000 genes, the human transcriptome contains more than 80,000 protein-coding transcripts, which are estimated to translate into 250,000 to 1 million proteins [295]. Non-coding RNAs, including microRNAs and small nucleolar RNAs, also play important roles in transcript modification and regulation, adding more to the complexity of biological systems. In addition, after translation, proteins can be reversibly or irreversibly modified, affecting the diversity and extension of their function [296]. Furthermore, the half-life of proteins also varies greatly, with several intrinsic and extrinsic factors contributing to protein degradation rate [297]. Thus, not surprisingly, mRNA expression does not always correlate with protein levels, just as not always protein abundance correlates with their function [298].

Protein modifications that modulate protein function after translation can occur through proteolytic cleavage or alterations to the side chains of amino acids, which include several enzymatic and non-enzymatic processes such as: adding of prosthetic groups (i.e. biotin, lipoate, panthotenate, pyridoxal phosphate and FAD), acetylation, acylation, alkylation, prenylation, glycosylation, sulfation, ribosylation, oxidation, hydroxylation, carboxylation, glycation, methylation, de- or transamidation, ubiquitination or phosphorylation [299].

Protein phosphorylation is the main post-translational modification by which signaling molecules modulate intracellular processes. This process takes place by the action of more than 2000 upstream kinases, which add a phosphate group to the side chains of serine, threonine or tyrosine residues, and is reversed by a smaller number of phosphatases [300]. Phosphorylation-dependent regulation of protein function can result in changes to protein activation,

89

transcriptional regulation, subcellular localization, protein and lipid interactions as well as degradation. In disease states, changes in phosphorylation status or abundance of key phosphoproteins result in aberrant activation or suppression of signaling.

High-resolution mass spectrometry (MS) based proteomics allows for quantitative analysis of protein abundance, post-translational modifications and interactions in a broad dynamic range and remains the method of choice for exploratory proteome discovery [301]. MS is based on the detection of ionized analytes converted into a gas phase, when they then go through a mass analyzer. Proteins can be processed for identification in their full-length (top-down) or from its peptides after digestion step (bottom-up). In either case, samples undergo several steps of enrichment and fractionation, which vary according to the biological question. Proteins or digested peptides then undergo separation and analysis. Each analyte has a specific mass over charge ratio (m/z), intensity, and retention time (RT), allowing for its precise detection, identification and quantification [302]. These techniques provide a very accurate and sensitive method for identification and quantitation of proteins in a sample. However proteomics methods are quite complex and involve multiple steps, which introduce sources of variability and hampers reproducibility of the results [303]. Functional analysis and interpretation of proteomic results can also be considerably challenging. While the discovery of novel post-translational modifications can provide novel insights regarding protein structure and function, validation of results using more established techniques such as Western blotting can be difficult due to lack of specific reagents.

Antibody microarrays serve as alternative tools for functional, semi-quantitative analysis of known physiologically relevant proteins. They also allow for analysis of particular post-translational modifications such as phosphorylation. [304] These immunoassay-based arrays

90

allow for multiplex detection and estimated quantification of hundreds of native and/or post-translationally modified proteins in complex biological samples. Commercially available antibody microarrays can be found in different formats. In the most common one, specific antibodies against the proteins of interest are immobilized onto a solid surface (e.g. glass slides) where the pre-processed sample is incubated and detection is performed using a fluorescent dye. [305]

Progressive loss of kidney function is a common serious complication of Fabry disease, an X-linked lysosomal storage disorder characterized by deficiency of alpha-galactosidase A (α-gal A) and glycosphingolipid accumulation. Podocyte injury is a major contributor to the glomerulopathy seen in these patients; foot process effacement can be seen even in subclinical disease and oftentimes worsens despite long-term enzyme replacement therapy. [263] Little is known about the intracellular events triggered by increased levels of glycosphingolipids and how they culminate in podocyte dysfunction in Fabry disease. Several proteomic-based studies have been performed in Fabry disease patients either in urine [306-310], serum [311], plasma [312] or peripheral blood mononuclear cells [313], however none of them specifically addressed disease-relevant podocyte-specific changes in signaling proteins.

Podocyte survival and function such as maintenance of the filtration barrier and of the glomerular basement membrane rely upon maintenance of cell homeostasis mediated by the action of several signaling molecules. Recent efforts have resulted in a comprehensive understanding of the transcriptome [314] as well as the phosphoproteome [315, 316] of podocytes. Exploring differences in abundance and phosphorylation of key proteins in the podocyte in the context of Fabry disease is crucial in improving our understanding of the pathophysiology of Fabry nephropathy.

I performed a phosphorylation profiling of immortalized human podocytes that were genome edited for Fabry disease and compared to control cells. Using a high-throughput antibody array containing 1318 antibodies covering a variety of signaling pathways crucial for cellular homeostasis, I measured the differential fold change for each total protein as well as their phosphorylation status per site in Fabry disease and control human immortalized podocytes. After mining data using R, I applied bioinformatics tools to select candidate phosphoproteins, as well as correspondent signaling pathways and gene networks. These analyses point to canonical pathways such as MAPK as being differentially activated in Fabry disease podocytes.

4.2   MATERIALS AND METHODS

4.2.1   Phospho-specific Antibody Microarray

Phospho-Explorer Antibody Arrays and Antibody Array Assay Kit were obtained from Full Moon Biosystems. Experiments were performed according to the manufacturer's protocol using solutions provided. Approximately $5x10^6$ control and *GLA* edited (Fabry disease) immortalized podocyte cells were pelleted by centrifugation at 500 *g* for 2 min at 4°C, washed 3 times with ice-cold PBS. Proteins were extracted by adding 200 μL of non-denaturing lysis buffer and lysis beads to the pellet, followed by 5 cycles of vortexing for 1 min and incubating on ice for 10 min. Lysates were centrifuged at 10,000 *g* for 5 min at 4°C and the supernatants were transferred to fresh tubes. Lysates (100 μL) were then purified using provided, previously hydrated affinity columns centrifuging at 750 *g* for 2 min. Purified lysates were frozen at -80°C

for 10 min and immediately centrifuged at 16,100 g for 15 min at 4°C. Lysate protein concentration was measured using UV absorbance spectroscopy at 280 nm using a NanoDrop Spectrophotometer (Thermo Scientific). Lysate quality control was verified by the presence of two well-separated peaks at 200-230 nm and 240-280 nm. Cell lysates (80 µg of protein resuspended in 75 µL of labeling buffer) were incubated with biotin solution (10 µg/uL in *N,N*-Dimethylformamide) for 2 h at ambient temperature, vortexing for 15 s every 10 min. Stop Reagent (35 µL) was then added biotinylated samples, which were then vortexed for 15 s, quickly spun and incubated at ambient temperature for 30 min, vortexing for 15 s every 5 min. Microarray slides were blocked with blocking solution (30 mL) for 45 min on an orbital shaker at 55 rpm at ambient temperature and then rinsed 10 times with ddH$_2$0 ddH$_2$0 in a 50 mL conical tube, shaking for 10 sec each time. Slides were then immersed in 6 mL of protein coupling solution mixed with biotinylated lysate and incubated for 2 h on an orbital shaker at 55 rpm at ambient temperature. Slides were then transferred to Petri dish containing 30 mL of wash solution and washed 3 times for 10 min on an orbital shaker at 55 rpm at ambient temperature, then rinsed 10 times with ddH$_2$0 in a 50 mL conical tube, shaking for 10 s each time. Next, slides were incubated in solution containing 30 µL of Cy3-Streptavidin (0.5 mg/mL, GE Healthcare) in 30 mL of detection buffer in an aluminum foil covered petri dish for 20 min on an orbital shaker at 35 rpm. Slides were then transferred to Petri dish containing 30 mL of wash solution and washed twice for 10 min and then once overnight rotating on an orbital shaker at 55 rpm at ambient temperature, then rinsed 10 times with ddH$_2$0 in a 50 mL conical tube, shaking for 10 s each time. Slides were dried by centrifugation, placing each slide in a 50 mL conical tube and centrifuging them at 1300 g for 10 min. Slides were scanned on a GenePix

4000B Microarray Scanner (Molecular Devices) at 500 PMT and fluorescence quantification information was extracted using GenePix Pro 6.0 Software (Molecular Devices).

4.2.2   Microarray Data Analysis

Data mining was performed using the R environment version 3.0 [317]. Median fluorescence signal at wavelength 532 minus the local background at wavelength 532 (F532-B532) for each feature (i.e. area of interest in image analysis) was used for calculations. For comparison of total protein abundance and phosphorylation between control and Fabry disease podocytes, fold changes of normalized median fluorescence values for each corresponding feature were calculated by dividing the value obtained for *GLA* edited podocyte lysates to the value obtaining for control cells. When value was lesser than 1, the inverse number multiplied to -1 was used. Fold change values greater than or equal to 1.2 (upregulation) or lesser than or equal to -1.2 (downregulation) were considered significant. Shapiro-Wilk test with α of 0.05 was used to test for normality. Values were represented as a log2 transformation.

4.2.3   Microarray Analysis Quality Control

A conservative approach was used throughout the quality control process to minimize false positive results. Only true values of fluorescence were used for further analysis. Measurements were considered true values when fluorescence signal for each spot was greater than 3 times the average of the median fluorescence signal of empty spots. When normalized fluorescence of replicates for a certain variable had values that overlapped between Fabry disease podocytes and control podocytes, a value of 1 was attributed to the fold change (i.e. no difference between

control and Fabry disease podocytes). As a noticeable proportion of variables showed coefficient of variation (CV) between replicates greater than 0.2, the fold changes were calculated by using values that showed minimal difference between Fabry disease and control podocytes. In total protein analysis, for proteins that were represented more than once (i.e. several total antibodies against the same protein), the most conservative number was used for analysis (i.e. the fold change value that was closest to 1). When fold change showed conflicting results among different epitopes representing the same protein (i.e. fold change results showing that same protein underwent both up and downregulation), these proteins were excluded from further analysis. Verification of expression of each individual protein in podocytes was performed using the Mouse Podocyte mRNA Database (available at http://helixweb.nih.gov/ESBL/Database/Podocyte_Transcriptome/index.htm) [318] and the NCBI Gene Expression Omnibus (GEO) Database [319, 320].

4.2.4 Enrichment Analysis

Site-specific information on protein regulation, upstream kinases and/or phosphatases and expected biological action were obtained using PhosphoSitePlus® (PSP) (Cell Signaling Technology®) [321]. Functional annotation, gene ontology functional classification, clustering and pathway analysis of significant data (fold change values greater than or equal to 1.2 or lesser than or equal to -1.2) were performed using Database for Annotation Visualization and Integrated Discovery (DAVID) Bioinformatics Resources 6.7 [National Institute of Allergy and Infectious Diseases (NIAID), National Institutes of Health] [322], considering all proteins tested in the array as the background population.

4.3   RESULTS

4.3.1   Phospho-Explorer Antibody Array of Fabry disease and control human immortalized podocytes

I generated a cell model of Fabry disease in human immortalized podocytes using CRISPR/Cas9 targeting exons 1 and 7 of the *GLA* gene, which is described in Chapter 3. These cells show absence of α-gal A activity and present increased levels of globotriaosylceramide (Gb3), the main substrate of α-gal A, which is known to accumulate in Fabry disease. I carried out an A280 absorbance assay to verify the quality of the lysates preparation. Both samples presented well-separated peaks at 200-230 and 240-280 nm,.

Using an exploratory approach to assess changes in abundance and phosphorylation of signaling molecules in Fabry disease nephropathy, I performed an antibody microarray in control and Fabry disease human immortalized podocytes. This array contains 1318 total and phosphorylation-specific antibodies antibodies against 414 different proteins and 686 phosphorylation sites in duplicate, allowing for high-throughput parallel analysis of abundance and phosphorylation of those proteins of interest in control and Fabry disease podocytes (refer to Figure 16 for schematic).
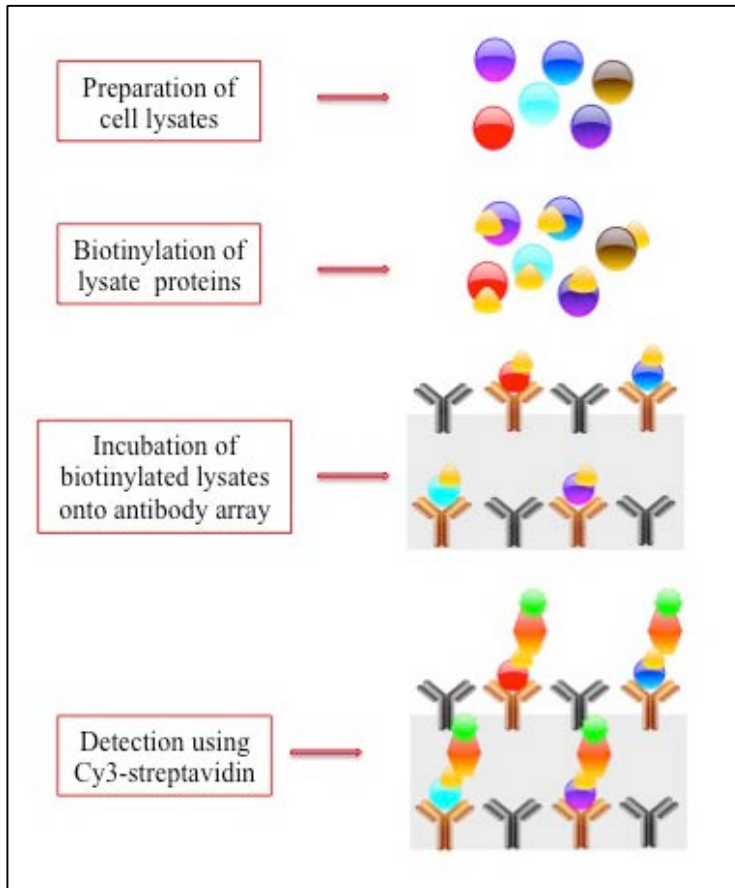
Figure 16: Schematic of the microarray experiment.

Cell lysates are incubated onto glass slides, which contain covalently bound total and phosphorylation-specific antibodies against the proteins of interest. Proteins are then biotinylated, followed by incubation with Cy3-streptavidin. Cy3 fluorescence is measured using a microarray fluorescence scanner.

I performed the microarray experiments in control and Fabry disease podocyte lysates, using biotin/Cy3-streptavidin for protein/primary antibody binding detection. Log2-transformed values of the median fluorescence intensity per pixel for each feature, applying a local background subtraction method, are represented in Figure 17.
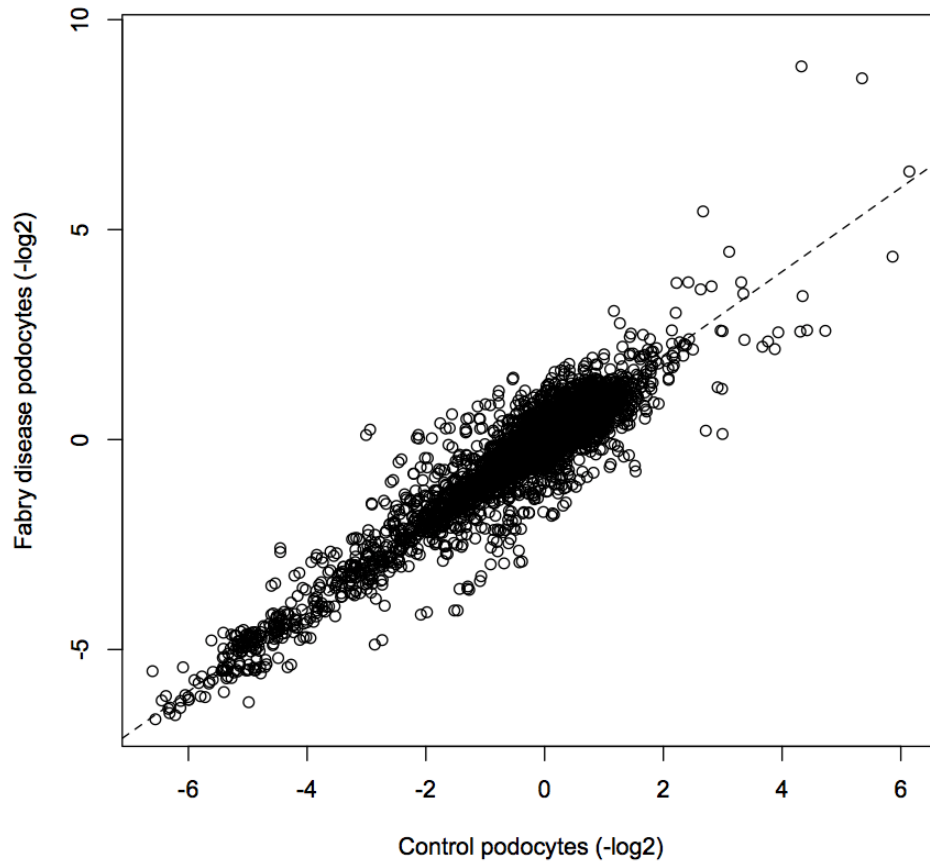
Figure 17: Scattered plot of microarray results.

Log2 transformed values of Cy3 median fluorescence intensity minus local background at wavelength 532 for each feature in the microarray for control (X axis) and Fabry disease podocytes (Y axis).

4.3.2 Total protein abundance analysis

The total abundance of signaling proteins impacts the status and extent of protein interactions leading to signaling cascades or networks. Class comparison or differential expression of proteins provides quantitative information on the analogy of the abundance of given proteins between two sets of samples. In differential expression analysis, fold change values of 1 imply no difference between samples when using non-transformed values, and the negative inverted fold change is calculated when the value attributed to the experimental sample is lesser than that of the control sample.

I first compared the total abundance of these signaling proteins between Fabry disease and control podocytes by calculating the fold change for each individual epitope. As significant variability was seen among several of the replicates, I chose to apply conservative approaches instead of measures of central tendency (i.e. mean, median). I selected for fold change calculations the two closest values between Fabry disease and control podocytes. Fold change values for all represented epitopes are illustrated in Figure 18.
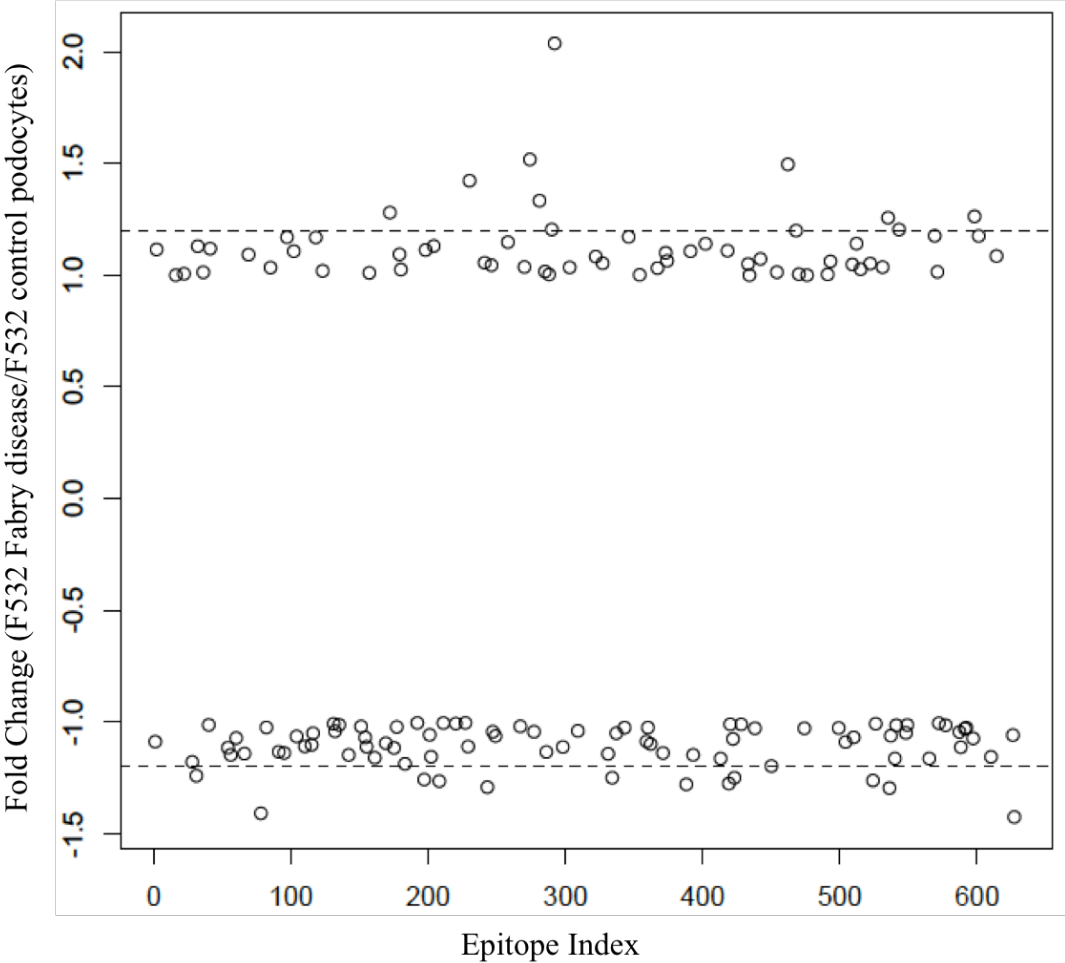
Figure 18: Fold change in fluorescence intensity for total protein abundance in Fabry disease podocytes compared to control podocytes.

Dashed lines correspond to the cutoffs of 1.2 and -1.2 fold changes.

I then selected candidate proteins based on a fold change threshold of greater than 1.2 or less than -1.2. For proteins covered multiple times through different epitopes, I eliminated those with conflicting results from further analysis. For those proteins that showed concordant values of fold change among epitopes, I again applied a conservative approach instead of a measure of central tendency for selecting the fold change value to be used, choosing the fold change values closest to 1.

This analysis demonstrated that 21 phosphoproteins in the array show differences in total protein abundance. Nine phosphoproteins showed increased total protein abundance in Fabry disease podocytes (Table 3), while 12 proteins had decreased levels in Fabry disease podocytes compared to control podocytes (Table 4).

Table 3: Phosphoproteins that showed increased total abundance in Fabry disease podocytes compared to control podocytes.

Protein (official full name)	Gene symbol	Fold change
Integrin, beta 1 (fibronectin receptor, beta polypeptide)	ITGB1	2.04
Paxillin	PXN	1.50
Gab2 (GRB2-associated binding protein 2)	GAB2	1.42
IR (Insulin receptor)	INSR	1.33
EGFR (Epidermal growth factor receptor)	EGFR	1.28
eIF4E (Eukaryotic translation initiation factor 4E)	EIF4E	1.26
Stathmin 1	STMN1	1.26
IkB-beta (Nuclear factor of kappa light polypeptide gene enhancer in B-cells inhibitor, beta)	NFKBIB	1.20
TGFBR1 (Transforming growth factor, beta receptor 1)	TGFBR1	1.20

Table 4: Phosphoproteins that showed decreased total abundance in Fabry disease podocytes compared to control podocytes.

Protein (official full name)	Gene symbol	Fold change
p53 (Tumor protein p53)	TP53	-1.42
BTK (Bruton agammaglobulinemia tyrosine kinase)	BTK	-1.41
Survivin (Baculoviral IAP repeat containing 5)	BIRC5	-1.29
HER2 (Erb-b2 receptor tyrosine kinase 2)	ERBB2	-1.29
NFkB-P65(V-rel avian reticuloendotheliosis viral oncogene homolog A)	RELA	-1.28
PAK4 (p21 protein (Cdc42/Rac)-activated kinase 4)	PAK4	-1.27
FKHR/FOXO1A (Forkhead box O1)	FOXO1	-1.26
Smad2 (SMAD family member 2)	SMAD2	-1.26
FAK (Protein tyrosine kinase 2)	PTK2	-1.26
PDGFR beta (Platelet-derived growth factor receptor, beta polypeptide)	PDGFRB	-1.25
MAP3K8/COT (Mitogen-activated protein kinase kinase kinase 8)	MAP3K8	-1.25
ASK1 (Mitogen-activated protein kinase kinase kinase 5)	MAP3K5	-1.24

4.3.3 Phosphorylation-specific analysis

Phosphorylation is the main form by which protein function is regulated and intracellular signaling is transduced. The availability of antibodies that recognize phosphorylated peptides, allowing for specific recognition of proteins in its post-translational modified phosphorylated state, opens opportunities to study intracellular signaling in the context of health and disease. To estimate differences in phosphorylation in signaling proteins between Fabry disease and control podocytes, I used a similar approach to that of total abundance analysis. Fold change in signal intensity values for phosphorylation-specific antibodies between Fabry disease and control podocytes are seen in Figure 19. Again, a threshold of +/- 0.2 was set to assess significant differences in phosphorylation.
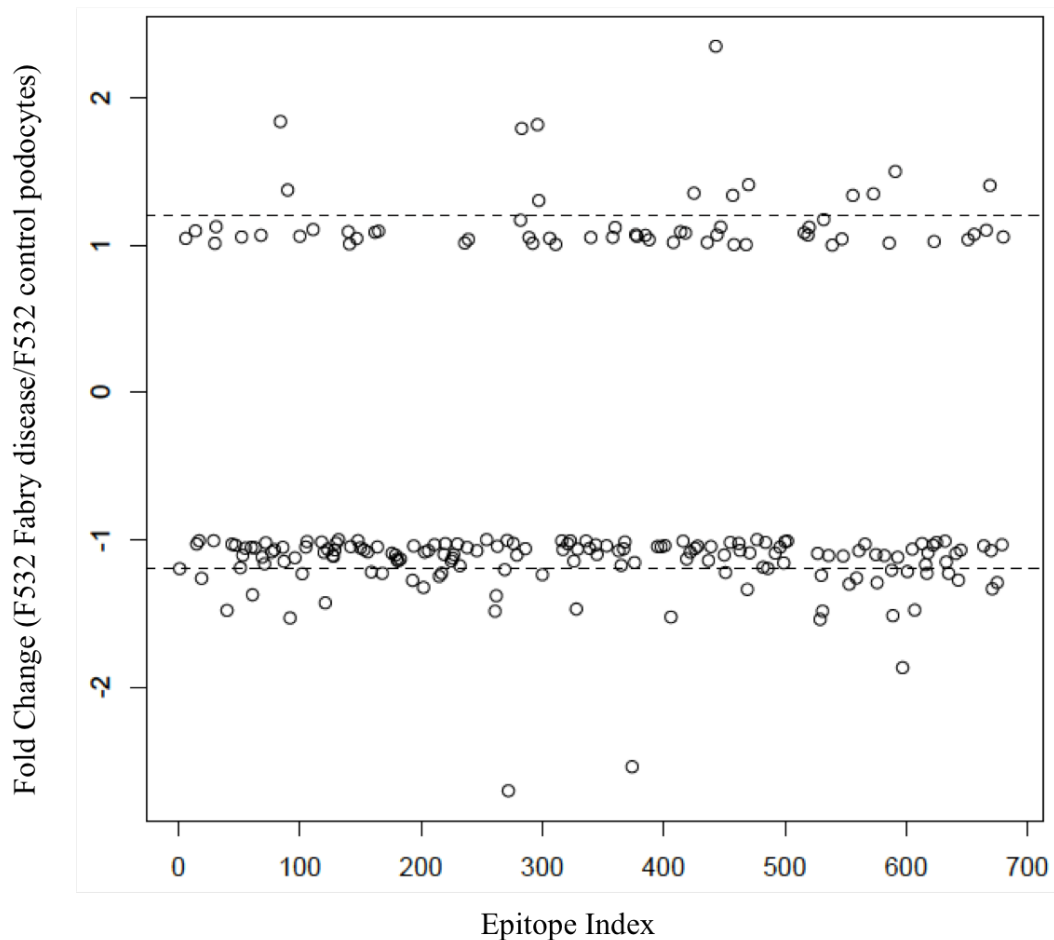
Figure 19: Fold change in fluorescence intensity of phosphorylation sites in phosphoproteins in Fabry disease podocytes compared to control podocytes.

Dashed lines correspond to the cutoffs of 1.2 and -1.2 fold changes.

A total of 43 proteins showed differences in phosphorylation in 51 specific sites. Increased phosphorylation was noted in13 phosphorylation sites of 12 different proteins (Table 5) and decreased phosphorylation was observed in 38 sites of 33 different signaling proteins (Table 6). Some proteins showed both an increase and decrease in phosphorylation for different sites.

Table 5: Phosphorylation sites and respective phosphoproteins that showed increased fluorescence in Fabry disease podocytes compared to control podocytes.

Protein (Official full name)	Phosphorylation site	Gene symbol	Fold change
P90RSK (Ribosomal protein S6 kinase, 90 kDa, polypeptide 1)	Phospho-Thr359/Ser363	RPS6KA1	2.88
HSP27 (Heat shock 27kDa protein 1)	Phospho-Ser82	HSPB1	2.64
CBL (Cbl proto-oncogene, E3 ubiquitin protein ligase)	Phospho-Tyr700	CBL	2.45
Table 5 Continued r of kappa light polypeptide gene enhancer in B-cells, kinase beta)	Phospho-Tyr188	IKBKB	1.82
Synuclein, alpha	Phospho-Tyr133	SNCA	1.50
PKC delta (Protein kinase C, delta)	Phospho-Ser645	PRKCD	1.41
p38 MAPK (Mitogen-activated protein kinase 14)	Phospho-Tyr182	MAPK14	1.40
CD3Z (CD247 molecule)	Phospho-Tyr142	CD247	1.37
NFkB-p65 (V-rel avian reticuloendotheliosis viral oncogene homolog A)	Phospho-Ser536	RELA	1.35
SMAD family member 3	Phospho-Ser204	SMAD3	1.35
PDGFR beta (Platelet-derived growth factor receptor, beta polypeptide)	Phospho-Tyr751	PDGFRB	1.34
STAT5A (Signal transducer and activator of transcription 5A)	Phospho-Ser725	STAT5A	1.34
IKK-beta (Inhibitor of kappa light polypeptide gene enhancer in B-cells, kinase beta)	Phospho-Tyr199	IKBKB	1.30

Table 6: Phosphorylation sites and respective phosphoproteins that showed decreased fluorescence in Fabry disease podocytes compared to control podocytes.

Protein (official full name)	Phosphorylation site	Gene symbol	Fold change
HER2 (Erb-b2 receptor tyrosine kinase 2)	Phospho-Tyr877	ERBB2	-2.71
MEK1 (Mitogen-activated protein kinase kinase 1)	Phospho-Ser217	MAP2K1	-2.54
TYK2 (Tyrosine kinase 2)	Phospho-Tyr1054	TYK2	-1.87
Rb (Retinoblastoma 1)	Phospho-Ser807	RB1	-1.54
CD45 (Protein tyrosine phosphatase, receptor type, C)	Phospho-Ser1007	PTPRC	-1.53
Mst1/Mst2 (Serine/threonine kinase 4)	(Phospho-Thr183	STK4/STK3	-1.53
Synaptotagmin I	Phospho-Thr202	SYT1	-1.52
HDAC1 (Histone deacetylase 1)	Phospho-Ser421	HDAC1	-1.49
Rb (Retinoblastoma 1)	Phospho-Thr821	RB1	-1.49
ATP citrate lyase	Phospho-Ser454	ACLY	-1.48
Tau (Microtubule-associated protein tau)	Phospho-Thr212	MAPT	-1.48
JAK1 (Janus kinase 1)	Phospho-Tyr1022	JAK1	-1.47

Table 6 Continued

KCNIP3 (Kv channel interacting protein 3, calsenilin)	Phospho-Ser63	KCNIP3	-1.43
HDAC2 (Histone deacetylase 2)	Phospho-Ser394	HDAC2	-1.38
BAD (BCL2-associated agonist of cell death)	Phospho-Ser134	BAD	-1.37
PKC beta (Protein kinase C, beta)	Phospho-Ser661	PRKCB	-1.34
p44/42 MAPK (Mitogen-activated protein kinase 3)	Phospho-Thr202	MAPK3	-1.33
Ephrin-B1/B2/B3	Phospho-Tyr324	EFNB1/2/3	-1.32
STAT3 (Signal transducer and activator of transcription 3 (acute-phase response factor))	Phospho-Ser727	STAT3	-1.3
p53 (Tumor protein p53)	Phospho-Ser315	TP53	-1.29
Smad3 (SMAD family member 3)	Phospho-Ser425	SMAD3	-1.29
c-Ab (ABL proto-oncogene 1, non-receptor tyrosine kinase)	Phospho-Tyr412	ABL1	-1.28
EPHA2/3/4 (EPH receptor A2/3/4)	Phospho-Tyr588/596	EPHA2	-1.28
AKT1 (V-akt murine thymoma viral oncogene homolog 1)	Phospho-Thr308	AKT1	-1.26
STAT5B (Signal transducer and activator of transcription 5B)	Phospho-Ser731	STAT5B	-1.26
FAK (Protein tyrosine kinase 2)	Phospho-Tyr407	PTK2	-1.25
IL-10R-alpha (Interleukin 10 receptor, alpha)	Phospho-Tyr496	IL10RA	-1.24
Rb (Retinoblastoma 1)	Phospho-Ser811	RB1	-1.24
CDK2 (Cyclin-dependent kinase 2)	Phospho-Thr160	CDK2	-1.23
DAB1 (Dab, reelin signal transducer, homolog 1)	Phospho-Tyr232	DAB1	-1.23
Protein tyrosine kinase 2	Phospho-Tyr861	PTK2	-1.23
Tyrosine hydroxylase	Phospho-Ser31	TH	-1.23
WEE1 G2 checkpoint kinase	Phospho-Ser642	WEE1	-1.23
Cyclin B1	Phospho-Ser126	CCNB1	-1.22
PAK2 (p21 protein (Cdc42/Rac)-activated kinase 2)	Phospho-Ser192	PAK2	-1.22
Tau (Microtubule-associated protein tau)	Phospho-Ser356	MAPT	-1.22
Synaptotagmin I	Phospho-Ser309	SYT1	-1.21
HER2 (Erb-b2 receptor tyrosine kinase 2)	Phospho-Thr686	ERBB2	-1.2

Protein (official full name)	Phosphorylation site	Gene symbol	Fold change
HER2 (Erb-b2 receptor tyrosine kinase 2)	Phospho-Tyr877	ERBB2	-2.71
MEK1 (Mitogen-activated protein kinase kinase 1)	Phospho-Ser217	MAP2K1	-2.54
TYK2 (Tyrosine kinase 2)	Phospho-Tyr1054	TYK2	-1.87
Rb (Retinoblastoma 1)	Phospho-Ser807	RB1	-1.54
CD45 (Protein tyrosine phosphatase, receptor type, C)	Phospho-Ser1007	PTPRC	-1.53
Mst1/Mst2 (Serine/threonine kinase 4)	(Phospho-Thr183	STK4/STK3	-1.53

Table 6 Continued

Synaptotagmin I	Phospho-Thr202	SYT1	-1.52
HDAC1 (Histone deacetylase 1)	Phospho-Ser421	HDAC1	-1.49
Rb (Retinoblastoma 1)	Phospho-Thr821	RB1	-1.49
ATP citrate lyase	Phospho-Ser454	ACLY	-1.48
Tau (Microtubule-associated protein tau)	Phospho-Thr212	MAPT	-1.48
JAK1 (Janus kinase 1)	Phospho-Tyr1022	JAK1	-1.47
KCNIP3 (Kv channel interacting protein 3, calsenilin)	Phospho-Ser63	KCNIP3	-1.43
HDAC2 (Histone deacetylase 2)	Phospho-Ser394	HDAC2	-1.38
BAD (BCL2-associated agonist of cell death)	Phospho-Ser134	BAD	-1.37
PKC beta (Protein kinase C, beta)	Phospho-Ser661	PRKCB	-1.34
p44/42 MAPK (Mitogen-activated protein kinase 3)	Phospho-Thr202	MAPK3	-1.33
Ephrin-B1/B2/B3	Phospho-Tyr324	EFNB1/2/3	-1.32
STAT3 (Signal transducer and activator of transcription 3 (acute-phase response factor))	Phospho-Ser727	STAT3	-1.3
p53 (Tumor protein p53)	Phospho-Ser315	TP53	-1.29
Smad3 (SMAD family member 3)	Phospho-Ser425	SMAD3	-1.29
c-Ab (ABL proto-oncogene 1, non-receptor tyrosine kinase)	Phospho-Tyr412	ABL1	-1.28
EPHA2/3/4 (EPH receptor A2/3/4)	Phospho-Tyr588/596	EPHA2	-1.28
AKT1 (V-akt murine thymoma viral oncogene homolog 1)	Phospho-Thr308	AKT1	-1.26
STAT5B (Signal transducer and activator of transcription 5B)	Phospho-Ser731	STAT5B	-1.26
FAK (Protein tyrosine kinase 2)	Phospho-Tyr407	PTK2	-1.25
IL-10R-alpha (Interleukin 10 receptor, alpha)	Phospho-Tyr496	IL10RA	-1.24
Rb (Retinoblastoma 1)	Phospho-Ser811	RB1	-1.24
CDK2 (Cyclin-dependent kinase 2)	Phospho-Thr160	CDK2	-1.23
DAB1 (Dab, reelin signal	Phospho-	DA	-

Table 6 Continued

transducer, homolog 1)	Tyr232	B1	1.23	
Protein tyrosine kinase 2	Phospho-Tyr861	PT K2	1.23	-
Tyrosine hydroxylase	Phospho-Ser31	TH	1.23	-
WEE1 G2 checkpoint kinase	Phospho-Ser642	WE E1	1.23	-
Cyclin B1	Phospho-Ser126	CC NB1	1.22	-
PAK2 (p21 protein (Cdc42/Rac)-activated kinase 2)	Phospho-Ser192	PA K2	1.22	-
Tau (Microtubule-associated protein tau)	Phospho-Ser356	MA PT	1.22	-
Synaptotagmin I	Phospho-Ser309	SY T1	1.21	-
HER2 (Erb-b2 receptor tyrosine kinase 2)	Phospho-Thr686	ER BB2	-1.2	

4.3.4 Gene Set Enrichment Analysis

I next performed a gene ontology enrichment analysis of positive array findings, which comprised proteins with at least 20 percent difference in either abundance or phosphorylation among Fabry disease and control podocytes. The gene ontology (GO) consortium is a collaborative effort to add uniformity and consistency to gene annotation. Functional descriptions and intracellular location of gene products and cellular processes that are implicated are described using a predefined vocabulary [323]. Table 7shows the top 5 hits in enrichment analysis based on GO terms for Fabry disease podocytes compared to control podocytes. These genes show only modest fold enrichment to the background gene population on the array.

Table 7: Gene set enrichment analysis.

GO identifier	Term	Fold Enrichment	Bonferroni	Benjamini	FDR
GO:0051173	positive regulation of nitrogen compound metabolic process	1.88	0.99	0.99	5.39
GO:0045597	positive regulation of cell differentiation	2.28	1.00	1.00	11.02
GO:0051726	regulation of cell cycle	1.92	1.00	0.98	11.69
GO:0040008	regulation of growth	2.22	1.00	0.97	13.72
GO:004593	positive regulation of nucleobase, nucleoside, nucleotide and nucleic acid metabolic process	1.82	1.00	0.95	14.97

Clustering analysis of the candidate proteins at DAVID, including all 59 proteins that showed differences in either total abundance or phosphorylation and taking into account all proteins in the array as the background gene population, revealed a total of 73 enrichment clusters. To note, none of these clusters reached an enrichment score of 1.3 or higher, which is equivalent to a non-log scale of 0.05. A representation of the cluster that achieved the highest enrichment can be found on Figure 20.

Figure 20: Clustering annotation.

Green squares represent fields where a corresponding protein-GO term association has been previously reported.

4.3.5 Expression of candidate proteins in podocytes

Repositories of gene expression data facilitate the storage and sharing of transcriptome information. Many peer-reviewed journals as well as funding sources currently require principal investigators to make their raw gene expression data publicly available, allowing for independent researchers to combine information from several previous studies and to generate and test novel hypotheses. The National Center for Biotechnology (NCBI) gene expression omnibus (GEO) is the largest gene expression resource publicly available [319, 320].

Hence, I searched publicly available transcriptome databases for expression information of candidate proteins in podocytes. Surprisingly, four of the 21 proteins that showed differences

in total abundance as well as 13 of the 51 proteins with differential phosphorylation pattern could not be located in the RNA sequencing expression database of mouse podocytes performed by Kann et al. [318] and available on the Renal Epithelial Transcriptome and Proteome Databases website (http://helixweb.nih.gov/ESBL/Database). Moreover, none of those proteins could be identified in the transcriptomic (Affymetrix Mouse Gene 1.0 ST microarray) and proteomic (SILAC) data on freshly isolated mouse podocytes recently published by Boerries et al. [314] A comprehensive list of these proteins can be found in Table 8.

Interestingly, inquiry for these same dataset of candidate proteins on the GEO repository, limiting the search to studies performed in podocytes, revealed that all candidate proteins were identified as expressed in the transcriptome of the conditionally immortalized human podocyte cell line generated by Saleem et al. [324] according to expression profiling performed by Da Sacco et al [325] using the Affymetrix Human Gene 1.0 ST microarray (NCBI GEO database accession GSE49439).

Table 8: Candidate proteins not found to be expressed in mouse podocytes.

Name	Gene symbol	Microarray category
Cyclin B1	CCNB1	Total protein
CD3Z/CD247 molecule	CD247	Total protein
Baculoviral IAP repeat containing 5	BIRC5	Total protein
Tumor protein p53	TP53	Total protein and phosphorylated form
Cyclin B1	CCNB1	Phosphorylated form
CD247 molecule	CD247	Phosphorylated form
Dab, reelin signal transducer, homolog 1 (Drosophila)	DAB1	Phosphorylated form
Interleukin 10 receptor, alpha	IL10RA	Phosphorylated form
Kv channel interacting protein 3, calsenilin	KCNIP3	Phosphorylated form
Protein kinase C, beta	PRKCB	Phosphorylated form
Protein tyrosine phosphatase, receptor type, C	PTPRC	Phosphorylated form
Ribosomal protein S6 kinase, 90 kDa, polypeptide 1	RPS6KA1	Phosphorylated form
Synuclein, alpha	SNCA	Phosphorylated form
Signal transducer and activator of transcription 5A	STAT5A	Phosphorylated form
Synaptotagmin I	SYT1	Phosphorylated form
Tyrosine hydroxylase	TH	Phosphorylated form

From Kann et al. [318]

4.3.6   Pathway enrichment analysis

Pathway analysis of all the phosphoproteins represented in the array was carried out using the Kyoto Encyclopedia of Genes and Genomes (KEGG) function of the Database for Annotation Visualization and Integrated Discovery (DAVID) Bioinformatics Resources. This analysis reveals enrichment for 65 different signaling pathways, covering a variety of intracellular processes crucial for cell function. [326, 327]

KEGG pathway analysis of candidate proteins reveals 11 pathways being over-represented among those with significant fold changes between Fabry disease and control podocytes (Table 9). An illustration of proteins differentially expressed in the context of the MAPK pathway is seen in Figure 21.

Table 9: KEGG canonical pathways most represented in number of genes among the candidate proteins.

KEGG Pathway ID	Description	Count	P value	Fold Enrichment	Bonferroni	Benjamini	FDR
hsa05200	Pathways in cancer	29	0.00013	1.80	0.0098	0.0098	0.13
hsa05220	Chronic myeloid leukemia	17	0.00024	2.41	0.0185	0.0093	0.25
hsa05212	Pancreatic cancer	15	0.00073	2.41	0.0550	0.0187	0.76
hsa05223	Non-small cell lung cancer	10	0.01998	2.20	0.7929	0.3254	19.23
hsa04010	MAPK signaling pathway	19	0.04409	1.49	0.9703	0.5051	37.93
hsa05210	Colorectal cancer	11	0.05134	1.82	0.9836	0.4960	42.73
hsa04660	T cell receptor signaling pathway	13	0.06122	1.64	0.9928	0.5053	48.74
hsa05215	Prostate cancer	13	0.06122	1.64	0.9928	0.5053	48.74
hsa05221	Acute myeloid leukemia	9	0.06919	1.91	0.9963	0.5030	53.16
hsa04370	VEGF signaling pathway	9	0.06919	1.91	0.9963	0.5030	53.16
hsa04012	ErbB signaling pathway	14	0.07944	1.54	0.9984	0.5120	58.34
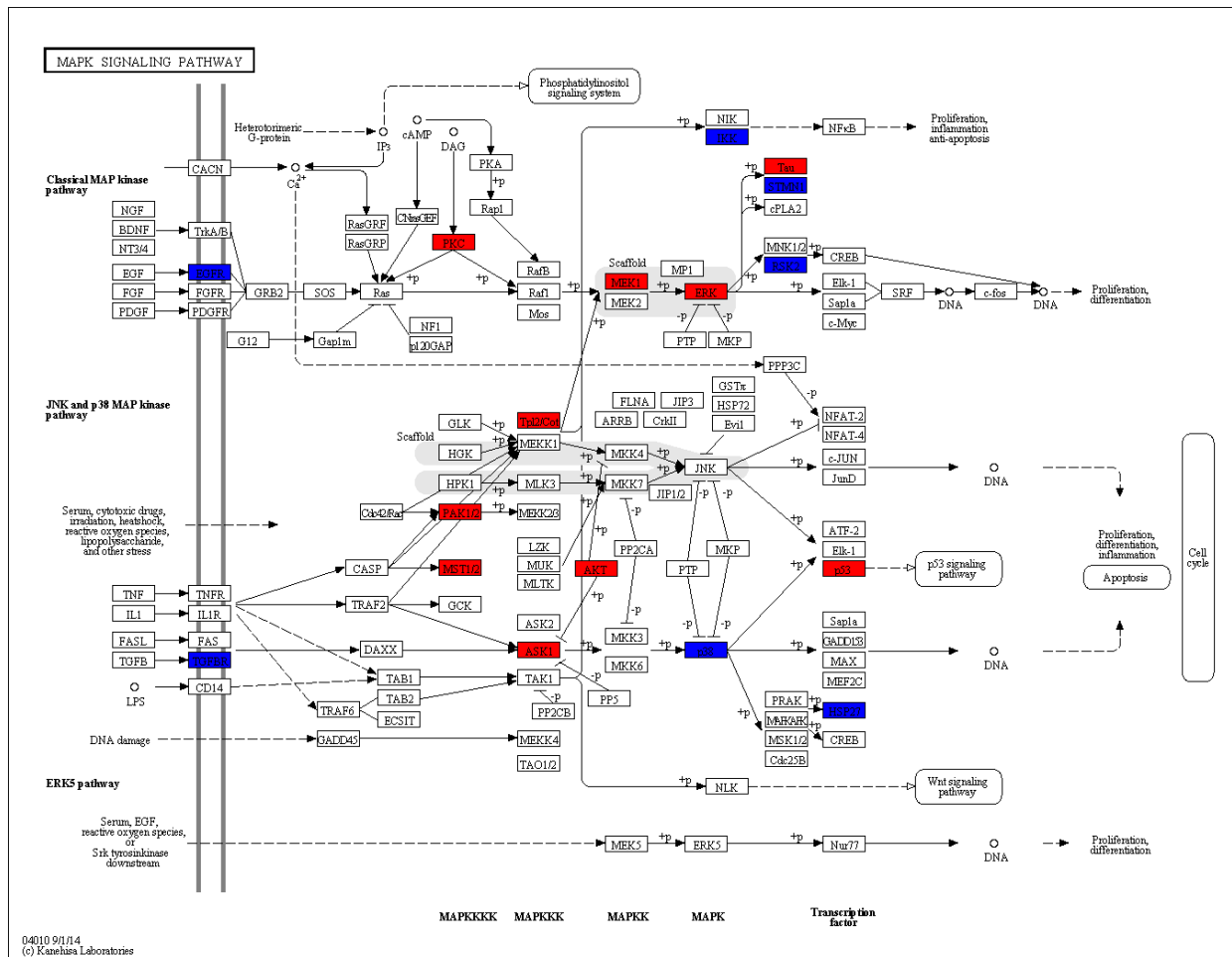
Figure 21: Candidate proteins in the context of the MAPK signaling pathway.

Proteins in red showed decreased and protein in blue showed increased abundance and/or phosphorylation in Fabry disease and control podocytes.

4.4   DISCUSSION

Assessing changes in homeostasis of signaling proteins, from differences in expression to changes in activation, self and hetero-association, stabilization or degradation are crucial to a better understanding of the intracellular mechanisms in health and disease. Using a high throughput approach that takes into account post-phosphorylation, I obtained parallel

information on the abundance and phosphorylation of hundreds of signaling proteins in Fabry disease podocytes. The 59 phosphoproteins that showed at least a 20 percent difference in either total abundance or phosphorylation between Fabry disease and control podocytes (i.e. positive array findings) are considered "candidate proteins" to validate further. Gene ontology and clustering analysis of these proteins showed a slight enrichment for proteins involved in cell growth and differentiation and cell death in Fabry disease podocytes, which correlates well with the fact that I observe differences in proliferation and/or cell death in these Fabry disease podocytes when compared to control podocytes.

The antibody microarray used in this study is enriched for 65 different signaling pathways that are relevant to human disease, several of which have been implicated in the pathogenesis of other glomerular diseases. Pathway analysis revealed that MAPK and VEGF pathways as well as nine other different signaling pathways as being significantly enriched or overrepresented among our candidate proteins. The MAPK pathway seems to play a critical role in kidney development [328-330]. Through its interplay with the NFkB pathway, MAPK pathway is also implicated in the pathophysiology of steroid responsive glomerulopathies. [331]

Other physiologically relevant signaling pathways that did not show statistically significant enrichment when compared to the background proteins tested in the array but that are considerably represented among the candidate proteins are also worth exploring further. For instance, the PI3K/Akt/mTOR pathway had a substantial number of candidate proteins represented (14 proteins, data not shown). The PI3K pathway is also crucial in kidney development [332]. Accordingly, podocyte injury with proteinuria is a relatively common "second-hit" complication of the use of sirolimus (rapamycin) and everolimus, clinically used

mTOR inhibitors, in patients with underlying kidney disease and/or previous history of use of immunosuppressant drugs. [333, 334]

Previous work by Lee et al. [335] in Fabry disease mice suggested that VEGF and TGF-beta signaling might contribute to Fabry disease nephropathy. VEGF pathway showed statistically significant enrichment, and several components of the TGF-beta pathway also showed differences in protein abundance and phosphorylation. Perturbed TGF-beta signaling has also been implicated in the pathogenesis of renal fibrosis leading to focal segmental and global glomerulosclerosis seen in several chronic glomerular diseases, including Fabry disease. [336, 337] Deregulated TGF-beta signaling is also thought to be a major contributor to podocyte epithelial mesenchymal transition (EMT). [338]

Quantitative proteomics remains the method of choice for protein discovery in complex biological samples. [339] Nonetheless, targeted strategies using antibody microarrays achieve semi-quantitative information on a large number of proteins of interest with known regulatory mechanisms, which facilitate validation and interpretation of the results.

Microarray analysis involves four main steps: (i) sample preparation and microarray experiment, (ii) image analysis and fluorescence signal acquisition, (iii) data normalization and quality control, and (iv) higher level analysis and functional interpretation of results. The first two steps are subject to sources of unwanted signal variation that may interfere with interpretation of the results. In addition, proper normalization procedures and application of quality control measurements helps account for technical variations. Normalization methods vary broadly and should be tailored to each specific set of experiments. Choosing the most conservative approaches for normalization and quality control allows for elimination of artifacts or false positive results, which is preferable since it reduces uncertainties.

Our study presents some limitations to consider. Human immortalized podocytes maintained in culture fail to present some of the morphological and functional features seen in a podocyte *in vivo,* such as interdigitating foot processes, as well as expression of slit diaphragm podocyte-specific proteins such as nephrin, which are crucial for podocyte function. Even though all proper controls were applied, as both control and Fabry disease cells used in the study have undergone lipofectamine treatment as well as the same number of passages, some of the changes in signaling that are observed *in vitro* may not be relevant for human disease *in vivo*. Unfortunately, none of the podocyte-specific proteins was covered in our microarray. To the best of our knowledge, none of the commercially available antibody microarrays allows for analysis of those podocyte-specific proteins. Another key point is that none of the components of the Coordinated Lysosomal Expression and Regulation (CLEAR) gene network was represented in this study. Certainly some of these proteins would be expected to have different activation pattern in Fabry disease podocytes, which could not be detected using our approach.

A database search in previously published transcriptome literature demonstrated that some of our candidate proteins were only found to be expressed in human cultured podocytes and not present in FACS sorted mouse podocytes. Several factors can explain these differences: (i) podocytes are post-mitotic highly differentiated cells. When exposed to an artificial environment in culture, where they proliferate at a much greater rate, it is not uncommon for podocytes to undergo substantial changes in morphology and expression of podocyte-specific markers [340], thus, it would not surprising if the expression profile of signaling proteins is altered *in vitro* compared to *in vivo*. (ii) These differences can arise from species-specific differences in expression of signaling proteins between mouse and human podocytes. Renal pathophysiology of mice is considerably different from that of humans. Healthy mice present

some proteinuria as baseline, which is not seen in humans [341] and their kidneys are quite resistant to Gb3 buildup. As previously mentioned, neither the Gla KO mice alone nor when interbred with mice expressing transgenic Gb3 synthase to significantly increase Gb3 accumulation present renal dysfunction to the extent of what is seen in humans [104]. (iii) The experiments were performed by different groups, using different methodologies (i.e. RNA-seq vs. DNA microarrays), which could result in differences in transcript detection. The yield of human podocytes from biopsy specimens is very low, hampering cell-type specific *in vivo* studies of gene expression. However, as the next generation sequencing technologies advance to single cell "omics" studies [342], this type of analysis might be feasible in the future.

Another factor to consider is that some of the differences in signaling that were revealed through the microarray analysis could potentially have actually derived from the CRISPR/Cas9 treatment itself. For instance, double-stranded DNA breaks induced by Cas9 trigger the activation of the DNA repair machinery, especially of those proteins involved in non-homologous end-joining (NHEJ) pathway, which includes DNA-dependent protein kinase catalytic subunit (DNA-PKcs), Artemis, Polymerases λ and μ, XRCC4 and ligase IV. [343] Some of these DNA repair proteins are also involved in other signaling pathways, notably those related to cell cycle. [344] Nevertheless, changes in signaling that are due to DNA repair activation would be unlikely to be seen in the cell population lysed for the microarray experiment, as they expanded from approximately 100,000 cells when they undergone CRISPR/Cas9 treatment to 5 million cells before the microarray was performed.

The accuracy and sensitivity of the antibody microarray analysis rely upon affinity and specificity of the probed antibodies, and antibodies are inherently prone to unpredicted, sample-specific interferences, yielding false positive or negative results [345]. Some probed antibodies

are also known to lack of specificity, since they cannot distinguish between some proteins that are highly similar in structure (i.e. Ephrin B1/B2/B3, EPHA 2/3/4). As those proteins do not completely overlap in their function and regulation, other approaches should be used in these instances to differentiate the individual contribution of a specific protein. Another factor to consider is when performing class comparison with proteins that show low signal intensity in the microarray, either due to low abundance of that protein in the biological sample or due to low antibody affinity. An inherent bias on those cases is that fold change values will have a much larger variance when comparing with proteins that show higher signal intensity. [346] Another limitation of this microarray is that due to a limited number of spots or features that can be probed in a single slide, a large number of variables are tested with a limited number of technical replicates. In the specific case of our microarray, each epitope was probed only twice. A considerable number of these technical replicates presented a higher than optimal coefficient of variation (CV). In addition, several proteins were covered multiple times through different epitopes, while others were represented only through a single epitope, thus our analysis was also biased through a differential power to detect any differences in abundance of individual proteins.

Proper functional interpretation of phosphoproteomics or phospho-antibody microarray results can be very challenging. While bioinformatics tools are evolving at exponential rates, the vast majority of used in enrichment analysis do not account for post-translational modifications and their effect on protein function as well as any differential regulatory effects exerted by each individual component of a given pathway or gene network. In addition, as our understanding of protein function and protein interactions also expands, new connections or relationships among well-established canonical pathways are discovered, and boundaries of individual pathways

start blurring [347]. Furthermore, fold change representation of proteins takes the assumption that the effect of the abundance of a given protein is multiplicative and independent from one another; however, in general, the biological effects of changes in protein abundance are largely unknown, and could well be additive or exponential and also dependent on the changes seen in other interacting proteins within a cascade or network.

4.5   CONCLUSION

In brief, antibody microarrays can be an excellent exploratory resource to generate and test hypothesis about disease pathogenesis. I performed a phosphoantibody microarray to assess differences in abundance and phosphorylation of signaling proteins in Fabry disease podocytes. Our analysis unfolded several candidate proteins and canonical pathways that could potentially be implicated in the pathophysiology of Fabry nephropathy.

4.6   FUTURE DIRECTIONS

Candidate proteins should be validated using established immunoassays such as Western blotting or indirect immunofluorescence, preferably in several control and Fabry disease CRISPR/Cas9-treated podocyte populations. Rescue experiments using heterologous expression of α-gal A and/or recombinant enzyme would ensure that the changes observed in protein abundance or phosphorylation are not a result of off-target effects of the genome editing

technique and are responsive to recombinant enzyme treatment. *In tissue* validation using Fabry disease and wild-type mice glomeruli would provide stronger evidence of these findings. Yet, negative validation results in mice should be interpreted with caution. While Fabry disease mice show biochemical features of the disease, they do not present classic signs of Fabry nephropathy. [101] Ideally, histopathology analysis of these proteins in kidney biopsy samples of Fabry disease patients in various stages of the disease and matched controls would provide some temporal information on the cascade of intracellular events leading to renal failure in these patients.

APPENDIX A: ABBREVIATONS

α-gal A   Alpha-galactosidase A

CLEAR   Coordinated Lysosomal Expression and Regulation

CKD   Chronic Kidney Disease

CRISPR/Cas9 Clustered Regularly Interspaced Short Palindromic Repeats and associated
            nuclease 9

CV   Coefficient of variation

DPPIV   Dipeptidylpeptidase IV

DAVID   Database for Annotation, Visualization and Integrated Discovery

DSB   Double-strand break

EEA1   Early endosomal antigen 1

EMT   Epithelial-mesenchymal transition

ERT   Enzyme replacement therapy

FACS   Fluorescence-activated cell sorting

Gb3   Globotriaosylceramide

GEO   Gene Expression Omnibus

GO   Gene ontology

GPI   Glycosylphosphatidylinositol

HA   Hemagglutinin

KEGG	Kyoto Encyclopedia of Genes and Genomes
LAMP-2	Lysosomal membrane associated protein 2
LSD	Lysosomal storage disorder
MDCK	Madin-Darby canine kidney
N&B	Number and brightness
NHEJ	Non-homologous end joining
RT-PCR	Reverse transcription polymerase chain reaction
qRT-PCR	Real-time quantitative reverse-transcription polymerase chain reaction
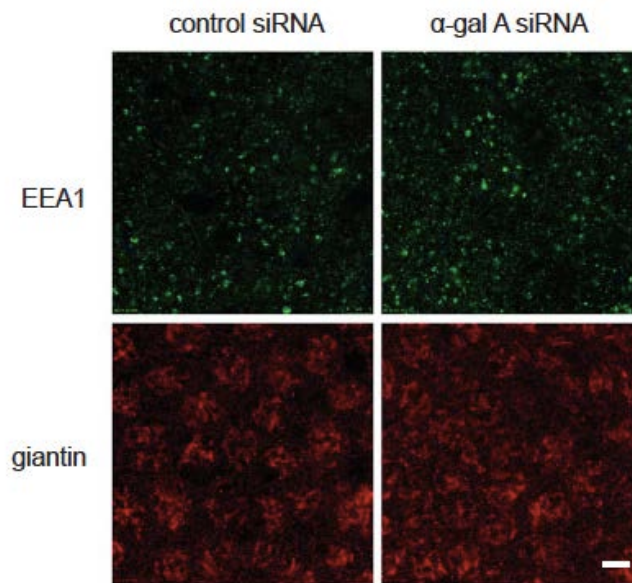
Supplementary Figure 1: Morphology and distribution of early endosomes and the Golgi complex are unaffected by α-gal A siRNA silencing.

Indirect immunofluorescence staining for the early endosome marker EEA1 and the Golgi complex marker giantin in MDCK cells transfected with control or α-gal A siRNA. Scale bar: 10 µm.
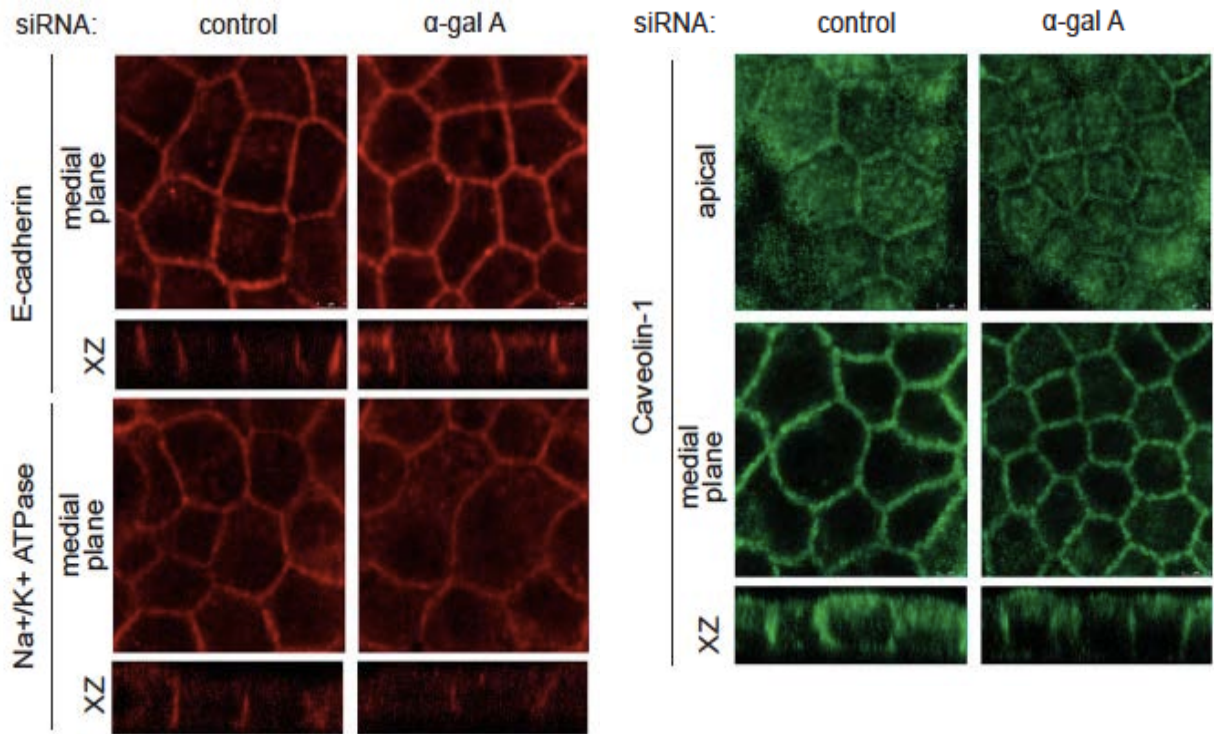
Supplementary Figure 2: Steady-state distribution of raft-associated and raft-independent basolateral cargoes is not perturbed by α-gal A siRNA silencing.

Indirect immunofluorescence staining of the raft-independent cell adhesion protein E-cadherin (upper panels), the raft associated pump Na^+/K^+ ATPase (middle panels) and the raft associated scaffolding protein caveolin-1 (lower panels) in cells transfected with control siRNA (left) and α-gal A siRNA (right) for four days. Images taken at the level of the apical surface and at a medial plane are shown for each protein, and xz reconstructions are shown below. Scale bar: 5 µm
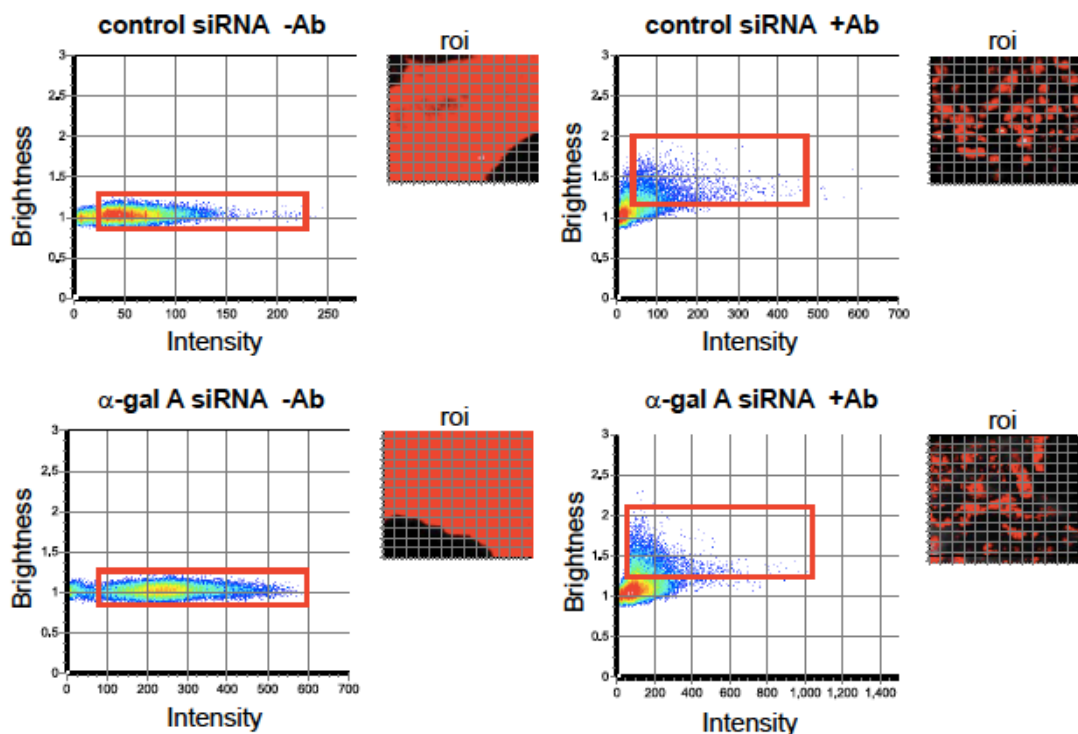
Supplementary Figure 3: Representative brightness vs. intensity histograms of GFP-GPI in untreated and antibody-clustered control and α-gal A silenced cells.

Histograms (Brightness vs. Intensity) for control and α-gal A siRNA treated MDCK cells expressing GFP-GPI in the absence (-Ab) or presence (+Ab) of anti-GFP antibody. Individual points represent data from a single pixel within the region of interest (roi) shown adjacent to each plot. The y-axis values correspond to increasing brightness (i.e., a higher average oligomeric size of fluorescent particles in the pixel) while increasing x-axis values correspond to higher signal intensities within each pixel (i.e., higher levels of fluorescence intensity in that pixel). For example, a pixel containing large numbers of monomers would map to the intersection of a small y-axis value and large x-axis value. Conversely, a pixel containing a small number of larger oligomers would map to a larger y-axis value and a low value on the x-axis. Brightness values in these histograms are raw values of the sum of the molecular brightness and the detector noise and, in this plot, are not normalized to GFP. Subtraction of one from the B value gives ε (counts/dwell time/molecule). Multiplication of ε by the dwell time used for acquisition and divided by the average molecular brightness for GFP provides the normalized brightness as reported in Figure 5, which enables direct quantitation of oligomeric size (e.g., monomer, dimer, etc.). In the representative examples shown here, pixels bounded by the red rectangular box are mapped onto the adjacent roi image. Note that selected pixels map evenly across the entire imaged area of the cell (i.e., there are no brightness "hot-spots"). In contrast, numerous brighter pixels are evident in histograms of cells incubated with anti-GFP antibody, and these brighter pixels map to large clusters in the roi.

124

BIBLIOGRAPHY

1. Go, A.S., et al., *Chronic kidney disease and the risks of death, cardiovascular events, and hospitalization.* N Engl J Med, 2004. **351**(13): p. 1296-305.
2. System, U.S.R.D. *USRDS 2014 Annual Data Report: Atlas of End-Stage Renal Disease in the United States.* 2014.
3. *Healthy People 2020: Chronic Kidney Disease.* 2010-2014; Available from: http://www.healthypeople.gov/2020/topics-objectives/topic/chronic-kidney-disease.
4. Wagner, M., et al., *Kidney function as an underestimated factor for reduced health related quality of life in patients with Fabry disease.* BMC Nephrol, 2014. **15**(1): p. 188.
5. Wanner, C., et al., *Prognostic indicators of renal disease progression in adults with Fabry disease: natural history data from the Fabry Registry.* Clin J Am Soc Nephrol, 2010. **5**(12): p. 2220-8.
6. Inoue, T., et al., *Newborn screening for Fabry disease in Japan: prevalence and genotypes of Fabry disease in a pilot study.* J Hum Genet, 2013. **58**(8): p. 548-52.
7. Hwu, W.L., et al., *Newborn screening for Fabry disease in Taiwan reveals a high incidence of the later-onset GLA mutation c.936+919G>A (IVS4+919G>A).* Hum Mutat, 2009. **30**(10): p. 1397-405.
8. Spada, M., et al., *High incidence of later-onset fabry disease revealed by newborn screening.* Am J Hum Genet, 2006. **79**(1): p. 31-40.
9. Hopkins, P.V., et al., *Lysosomal storage disorder screening implementation: findings from the first six months of full population pilot testing in Missouri.* J Pediatr, 2015. **166**(1): p. 172-7.
10. Scott, C.R., et al., *Identification of infants at risk for developing Fabry, Pompe, or mucopolysaccharidosis-I from newborn blood spots by tandem mass spectrometry.* J Pediatr, 2013. **163**(2): p. 498-503.
11. Bennett, M.J., *Newborn screening for metabolic diseases: saving children's lives and improving outcomes.* Clin Biochem, 2014. **47**(9): p. 693-4.
12. Rombach, S.M., et al., *Cost-effectiveness of enzyme replacement therapy for Fabry disease.* Orphanet J Rare Dis, 2013. **8**: p. 29.
13. Germain, D.P., et al., *Ten-year outcome of enzyme replacement therapy with agalsidase beta in patients with Fabry disease.* J Med Genet, 2015.
14. McWalter, K. and A. Gaviglio, *Introduction to the Special Issue: Public Health Genetics and Genomics.* J Genet Couns, 2015.
15. Desnick, R.J., Y.A. Ioannou, and C.M. Eng, eds. *alpha-galactosidase A deficiency: Fabry disease.* 8th ed. The Metabolic and Molecular Bases of Inherited Disease, ed. C.R. Scriver, et al. 2001, McGraw-Hill: New York. 3733-3774.
16. Anderson, W., *A case of angiokeratoma.* Br J Dermatol, 1898. **10**: p. 113.

17.   Fabry, J., *Ein Beitrag Zur Kenntnis der Purpura haemorrhagica nodularis.* Arch Dermatol Syph, 1898. **43**: p. 187-200.

18.   Meikle, P.J., et al., *Prevalence of lysosomal storage disorders.* JAMA, 1999. **281**(3): p. 249-54.

19.   Poupetova, H., et al., *The birth prevalence of lysosomal storage disorders in the Czech Republic: comparison with data in different populations.* J Inherit Metab Dis, 2010. **33**(4): p. 387-96.

20.   Kleinert, J., et al., *Anderson-Fabry disease: a case-finding study among male kidney transplant recipients in Austria.* Transpl Int, 2009. **22**(3): p. 287-92.

21.   Gaspar, P., et al., *Frequency of Fabry disease in male and female haemodialysis patients in Spain.* BMC Med Genet, 2010. **11**: p. 19.

22.   Wallin, E.F., M.R. Clatworthy, and N.R. Pritchard, *Fabry disease: results of the first UK hemodialysis screening study.* Clin Nephrol, 2011. **75**(6): p. 506-10.

23.   Okur, I., et al., *Screening for Fabry disease in patients undergoing dialysis for chronic renal failure in Turkey: identification of new case with novel mutation.* Gene, 2013. **527**(1): p. 42-7.

24.   Herrera, J. and C.S. Miranda, *Prevalence of Fabry's disease within hemodialysis patients in Spain.* Clin Nephrol, 2014. **81**(2): p. 112-20.

25.   Shi, Q., et al., *Prevalence of Fabry disease in stroke patients--a systematic review and meta-analysis.* J Stroke Cerebrovasc Dis, 2014. **23**(5): p. 985-92.

26.   Terryn, W., et al., *Prevalence of Fabry disease in a predominantly hypertensive population with left ventricular hypertrophy.* Int J Cardiol, 2013. **167**(6): p. 2555-60.

27.   Garman, S.C. and D.N. Garboczi, *The molecular defect leading to Fabry disease: structure of human alpha-galactosidase.* J Mol Biol, 2004. **337**(2): p. 319-35.

28.   Daitx, V.V., et al., *Comparing the alpha-galactosidase A biochemical properties from healthy individuals and Fabry disease patients.* Clin Chim Acta, 2015. **445**: p. 60-64.

29.   Lemansky, P., et al., *Synthesis and processing of alpha-galactosidase A in human fibroblasts. Evidence for different mutations in Fabry disease.* J Biol Chem, 1987. **262**(5): p. 2062-5.

30.   Bekri, S., *Importance of glycosylation in enzyme replacement therapy*, in *Fabry Disease: Perspectives from 5 Years of FOS*, A. Mehta, M. Beck, and G. Sunder-Plassmann, Editors. 2006: Oxford.

31.   Wang, A.M., D.F. Bishop, and R.J. Desnick, *Human alpha-N-acetylgalactosaminidase-molecular cloning, nucleotide sequence, and expression of a full-length cDNA. Homology with human alpha-galactosidase A suggests evolution from a common ancestral gene.* J Biol Chem, 1990. **265**(35): p. 21859-66.

32.   Clark, N.E. and S.C. Garman, *The 1.9 a structure of human alpha-N-acetylgalactosaminidase: The molecular basis of Schindler and Kanzaki diseases.* J Mol Biol, 2009. **393**(2): p. 435-47.

33.   Keusch, J.J., et al., *Cloning of Gb3 synthase, the key enzyme in globo-series glycosphingolipid synthesis, predicts a family of alpha 1, 4-glycosyltransferases conserved in plants, insects, and mammals.* J Biol Chem, 2000. **275**(33): p. 25315-21.

34.   Lannert, H., et al., *Functional organization of the Golgi apparatus in glycosphingolipid biosynthesis. Lactosylceramide and subsequent glycosphingolipids are formed in the lumen of the late Golgi.* The Journal of biological chemistry, 1998. **273**(5): p. 2939-46.

35. Nutikka, A. and C. Lingwood, *Generation of receptor-active, globotriaosyl ceramide/cholesterol lipid 'rafts' in vitro : A new assay to define factors affecting glycosphingolipid receptor activity.* Glycoconjugate journal, 2004. **20**(1): p. 33-8.

36. Dawson, G., A.W. Kruski, and A.M. Scanu, *Distribution of glycosphingolipids in the serum lipoproteins of normal human subjects and patients with hypo- and hyperlipidemias.* J Lipid Res, 1976. **17**(2): p. 125-31.

37. Miyazaki, C., et al., *Altered phospholipid molecular species and glycolipid composition in brain, liver and fibroblasts of Zellweger syndrome.* Neurosci Lett, 2013. **552**: p. 71-5.

38. Fellous, M., et al., *A monoclonal antibody against a Burkitt lymphoma associated antigen has an anti-Pk red blood cell specificity.* Br J Haematol, 1985. **60**(3): p. 559-65.

39. Stimmer, L., et al., *Human breast cancer and lymph node metastases express Gb3 and can be targeted by STxB-vectorized chemotherapeutic compounds.* BMC Cancer, 2014. **14**: p. 916.

40. Garner, B., et al., *Increased glycosphingolipid levels in serum and aortae of apolipoprotein E gene knockout mice.* J Lipid Res, 2002. **43**(2): p. 205-14.

41. Memon, R.A., et al., *Regulation of glycosphingolipid metabolism in liver during the acute phase response.* J Biol Chem, 1999. **274**(28): p. 19707-13.

42. Memon, R.A., et al., *Regulation of sphingolipid and glycosphingolipid metabolism in extrahepatic tissues by endotoxin.* J Lipid Res, 2001. **42**(3): p. 452-9.

43. Fantini, J., et al., *Role of glycosphingolipid microdomains in CD4-dependent HIV-1 fusion.* Glycoconj J, 2000. **17**(3 -4): p. 199-204.

44. Behnam-Motlagh, P., et al., *Verotoxin-1 treatment or manipulation of its receptor globotriaosylceramide (gb3) for reversal of multidrug resistance to cancer chemotherapy.* Toxins (Basel), 2010. **2**(10): p. 2467-77.

45. Stapleton, A.E., et al., *The globoseries glycosphingolipid sialosyl galactosyl globoside is found in urinary tract tissues and is a preferred binding receptor In vitro for uropathogenic Escherichia coli expressing pap-encoded adhesins.* Infect Immun, 1998. **66**(8): p. 3856-61.

46. Gehrmann, M., et al., *Tumor-specific Hsp70 plasma membrane localization is enabled by the glycosphingolipid Gb3.* PLoS One, 2008. **3**(4): p. e1925.

47. De Los Rios, P., et al., *Hsp70 chaperones accelerate protein translocation and the unfolding of stable protein aggregates by entropic pulling.* Proc Natl Acad Sci U S A, 2006. **103**(16): p. 6166-71.

48. Desselle, A., et al., *Anti-Gb3 monoclonal antibody inhibits angiogenesis and tumor development.* PLoS One, 2012. **7**(11): p. e45423.

49. Dupont, F.O., et al., *A metabolomic study reveals novel plasma lyso-Gb3 analogs as Fabry disease biomarkers.* Curr Med Chem, 2013. **20**(2): p. 280-8.

50. Auray-Blais, C., et al., *Urinary globotriaosylsphingosine-related biomarkers for Fabry disease targeted by metabolomics.* Anal Chem, 2012. **84**(6): p. 2745-53.

51. Aerts, J.M., et al., *Elevated globotriaosylsphingosine is a hallmark of Fabry disease.* Proc Natl Acad Sci U S A, 2008. **105**(8): p. 2812-7.

52. Niemann, M., et al., *Gene mutations versus clinically relevant phenotypes: lyso-Gb3 defines Fabry disease.* Circ Cardiovasc Genet, 2014. **7**(1): p. 8-16.

53. Togawa, T., et al., *Tissue and plasma globotriaosylsphingosine could be a biomarker for assessing enzyme replacement therapy for Fabry disease.* Biochem Biophys Res Commun, 2010. **399**(4): p. 716-20.

54. Choi, L., et al., *The Fabry disease-associated lipid Lyso-Gb3 enhances voltage-gated calcium currents in sensory neurons and causes pain.* Neurosci Lett, 2015.

55. Sanchez-Nino, M.D., et al., *Globotriaosylsphingosine actions on human glomerular podocytes: implications for Fabry nephropathy.* Nephrol Dial Transplant, 2011. **26**(6): p. 1797-802.

56. Bishop, D.F., R. Kornreich, and R.J. Desnick, *Structural organization of the human alpha-galactosidase A gene: further evidence for the absence of a 3' untranslated region.* Proc Natl Acad Sci U S A, 1988. **85**(11): p. 3903-7.

57. Ferreira, S., C. Reguenga, and J.P. Oliveira, *The Modulatory Effects of the Polymorphisms in GLA 5'-Untranslated Region Upon Gene Expression Are Cell-Type Specific.* JIMD Rep, 2015.

58. Garman, S.C. and D.N. Garboczi, *Structural basis of Fabry disease.* Mol Genet Metab, 2002. **77**(1-2): p. 3-11.

59. Stenson, P.D., et al., *Human Gene Mutation Database (HGMD): 2003 update.* Hum Mutat, 2003. **21**(6): p. 577-81.

60. Schaefer, E., A. Mehta, and A. Gal, *Genotype and phenotype in Fabry disease: analysis of the Fabry Outcome Survey.* Acta Paediatr Suppl, 2005. **94**(447): p. 87-92; discussion 79.

61. MacDermot, K.D., A. Holmes, and A.H. Miners, *Natural history of Fabry disease in affected males and obligate carrier females.* J Inherit Metab Dis, 2001. **24 Suppl 2**: p. 13-4; discussion 11-2.

62. Deegan, P.B., et al., *Natural history of Fabry disease in females in the Fabry Outcome Survey.* J Med Genet, 2006. **43**(4): p. 347-52.

63. Elstein, D., et al., *X-inactivation in Fabry disease.* Gene, 2012. **505**(2): p. 266-8.

64. van den Berg, I.M., et al., *X chromosome inactivation is initiated in human preimplantation embryos.* Am J Hum Genet, 2009. **84**(6): p. 771-9.

65. Ries, M., et al., *The early clinical phenotype of Fabry disease: a study on 35 European children and adolescents.* Eur J Pediatr, 2003. **162**(11): p. 767-72.

66. Tondel, C., et al., *Agalsidase benefits renal histology in young patients with Fabry disease.* J Am Soc Nephrol, 2013. **24**(1): p. 137-48.

67. Tondel, C., et al., *Renal biopsy findings in children and adolescents with Fabry disease and minimal albuminuria.* Am J Kidney Dis, 2008. **51**(5): p. 767-76.

68. Waldek, S., et al., *Life expectancy and cause of death in males and females with Fabry disease: findings from the Fabry Registry.* Genet Med, 2009. **11**(11): p. 790-6.

69. Patel, M.R., et al., *Cardiovascular events in patients with fabry disease natural history data from the fabry registry.* J Am Coll Cardiol, 2011. **57**(9): p. 1093-9.

70. Nappi, C., et al., *First experience of simultaneous PET/MRI for the early detection of cardiac involvement in patients with Anderson-Fabry disease.* Eur J Nucl Med Mol Imaging, 2015.

71. Linhart, A., et al., *Cardiac manifestations of Anderson-Fabry disease: results from the international Fabry outcome survey.* Eur Heart J, 2007. **28**(10): p. 1228-35.

72. Kolodny, E., et al., *Cerebrovascular involvement in fabry disease: current status of knowledge.* Stroke, 2015. **46**(1): p. 302-13.

73. Tuttolomondo, A., et al., *Neurological complications of Anderson-Fabry disease.* Curr Pharm Des, 2013. **19**(33): p. 6014-30.

74.   Beck, M., *The Mainz Severity Score Index (MSSI): development and validation of a system for scoring the signs and symptoms of Fabry disease.* Acta Paediatr Suppl, 2006. **95**(451): p. 43-6.

75.   Hughes, D.A., et al., *Age adjusting severity scores for Anderson-Fabry disease.* Mol Genet Metab, 2010. **101**(2-3): p. 219-27.

76.   Giannini, E.H., et al., *A validated disease severity scoring system for Fabry disease.* Mol Genet Metab, 2010. **99**(3): p. 283-90.

77.   Hughes, D.A., et al., *Fabry International Prognostic Index: a predictive severity score for Anderson-Fabry disease.* J Med Genet, 2012. **49**(3): p. 212-20.

78.   Lukas, J., et al., *Functional characterisation of alpha-galactosidase a mutations as a basis for a new classification system in fabry disease.* PLoS Genet, 2013. **9**(8): p. e1003632.

79.   Germain, D.P., *Fabry disease.* Orphanet J Rare Dis, 2010. **5**: p. 30.

80.   Desnick, R.J., et al., *Fabry disease: molecular diagnosis of hemizygotes and heterozygotes.* Enzyme, 1987. **38**(1-4): p. 54-64.

81.   Pasqualim, G., et al., *Fabry disease: a new approach for the screening of females in high-risk groups.* Clin Biochem, 2014. **47**(7-8): p. 657-62.

82.   Eng, C.M. and R.J. Desnick, *Molecular basis of Fabry disease: mutations and polymorphisms in the human alpha-galactosidase A gene.* Hum Mutat, 1994. **3**(2): p. 103-11.

83.   van der Tol, L., et al., *Uncertain diagnosis of fabry disease in patients with neuropathic pain, angiokeratoma or cornea verticillata: consensus on the approach to diagnosis and follow-up.* JIMD Rep, 2014. **17**: p. 83-90.

84.   Smid, B.E., et al., *Uncertain diagnosis of Fabry disease: Consensus recommendation on diagnosis in adults with left ventricular hypertrophy and genetic variants of unknown significance.* Int J Cardiol, 2014. **177**(2): p. 400-8.

85.   Ishii, S., et al., *Mutant alpha-galactosidase A enzymes identified in Fabry disease patients with residual enzyme activity: biochemical characterization and restoration of normal intracellular processing by 1-deoxygalactonojirimycin.* Biochem J, 2007. **406**(2): p. 285-95.

86.   Bottcher, T., et al., *Fabry disease - underestimated in the differential diagnosis of multiple sclerosis?* PLoS One, 2013. **8**(8): p. e71894.

87.   Mancuso, M., et al., *Common Genetic Conditions of Ischemic Stroke to Keep in Mind.* Curr Mol Med, 2014.

88.   Rota, E., et al., *Missing link: could the elusive Wartenberg's neuritis be a peripheral nerve variant of Fabry's disease?* Neurol India, 2014. **62**(2): p. 219-21.

89.   Biegstraaten, M., et al., *Fabry disease: a rare cause of neuropathic pain.* Curr Pain Headache Rep, 2013. **17**(10): p. 365.

90.   Martinez, P., M. Aggio, and P. Rozenfeld, *High incidence of autoantibodies in Fabry disease patients.* J Inherit Metab Dis, 2007. **30**(3): p. 365-9.

91.   Rubio, C.A., et al., *Fabry disease simulating Crohn's ileitis.* Anticancer Res, 2014. **34**(5): p. 2437-41.

92.   Dean, S.M. and J. Starr, *An unusual case of familial lymphedema.* Ann Vasc Surg, 2014. **28**(5): p. 1314 e1-3.

93.   Zizzo, C., et al., *Misdiagnosis of familial Mediterranean fever in patients with Anderson-Fabry disease.* Clin Genet, 2013. **83**(6): p. 576-81.

94. Horner, M.E., et al., *The spectrum of oculocutaneous disease: Part I. Infectious, inflammatory, and genetic causes of oculocutaneous disease.* J Am Acad Dermatol, 2014. **70**(5): p. 795 e1-25.

95. Eng, C.M., et al., *Fabry disease: guidelines for the evaluation and management of multi-organ system involvement.* Genet Med, 2006. **8**(9): p. 539-48.

96. Martins, A.M., *Introduction to Brazilian Guidelines to Diagnosis, Treatment,and Monitoring for Gaucher Disease, Fabry Disease, Mucopolysaccharidosis I, and Pompe Disease.* J Pediatr, 2009. **155**(4 Suppl): p. S9.

97. Martins, A.M., et al., *Guidelines to diagnosis and monitoring of Fabry disease and review of treatment experiences.* J Pediatr, 2009. **155**(4 Suppl): p. S19-31.

98. Kes, V.B., et al., *Guidelines for diagnosis, therapy and follow up of Anderson-Fabry disease.* Acta Clin Croat, 2013. **52**(3): p. 395-405.

99. Laney, D.A., et al., *Fabry disease practice guidelines: recommendations of the National Society of Genetic Counselors.* J Genet Couns, 2013. **22**(5): p. 555-64.

100. Weidemann, F., et al., *Long-term outcome of enzyme-replacement therapy in advanced Fabry disease: evidence for disease progression towards serious complications.* J Intern Med, 2013. **274**(4): p. 331-41.

101. Ohshima, T., et al., *alpha-Galactosidase A deficient mice: a model of Fabry disease.* Proc Natl Acad Sci U S A, 1997. **94**(6): p. 2540-4.

102. Valbuena, C., et al., *Kidney histologic alterations in alpha-Galactosidase-deficient mice.* Virchows Arch, 2011. **458**(4): p. 477-86.

103. Shimmoto, M., et al., *Generation and characterization of transgenic mice expressing a human mutant alpha-galactosidase with an R301Q substitution causing a variant form of Fabry disease.* FEBS Lett, 1997. **417**(1): p. 89-91.

104. Ishii, S., et al., *Transgenic mouse expressing human mutant alpha-galactosidase A in an endogenous enzyme deficient background: a biochemical animal model for studying active-site specific chaperone therapy for Fabry disease.* Biochim Biophys Acta, 2004. **1690**(3): p. 250-7.

105. Taguchi, A., et al., *A symptomatic Fabry disease mouse model generated by inducing globotriaosylceramide synthesis.* Biochem J, 2013. **456**(3): p. 373-83.

106. Inagaki, M., et al., *Lysosomal glycosphingolipid storage in chloroquine-induced alpha-galactosidase-deficient human endothelial cells with transformation by simian virus 40: in vitro model of Fabry disease.* Acta Neuropathol, 1993. **85**(3): p. 272-9.

107. Shu, L., et al., *An in vitro model of Fabry disease.* J Am Soc Nephrol, 2005. **16**(9): p. 2636-45.

108. Shen, J.S., et al., *Establishment and characterization of Fabry disease endothelial cells with an extended lifespan.* Mol Genet Metab, 2007. **92**(1-2): p. 137-44.

109. Itier, J.M., et al., *Effective clearance of GL-3 in a human iPSC-derived cardiomyocyte model of Fabry disease.* J Inherit Metab Dis, 2014. **37**(6): p. 1013-22.

110. Kawagoe, S., et al., *Morphological features of iPS cells generated from Fabry disease skin fibroblasts using Sendai virus vector (SeVdp).* Mol Genet Metab, 2013. **109**(4): p. 386-9.

111. Thomaidis, T., et al., *Downregulation of alpha-galactosidase A upregulates CD77: functional impact for Fabry nephropathy.* Kidney Int, 2009. **75**(4): p. 399-407.

112. Liebau, M.C., et al., *Dysregulated autophagy contributes to podocyte damage in Fabry's disease.* PLoS One, 2013. **8**(5): p. e63506.

113. de Duve, C., *The lysosome turns fifty.* Nat Cell Biol, 2005. **7**(9): p. 847-9.
114. Schroder, B.A., et al., *The proteome of lysosomes.* Proteomics, 2010. **10**(22): p. 4053-76.
115. Yoshimori, T., et al., *Bafilomycin A1, a specific inhibitor of vacuolar-type H(+)-ATPase, inhibits acidification and protein degradation in lysosomes of cultured cells.* J Biol Chem, 1991. **266**(26): p. 17707-12.
116. Brozzi, A., et al., *hLGDB: a database of human lysosomal genes and their regulation.* Database (Oxford), 2013. **2013**: p. bat024.
117. Alberts B, J.A., Lewis J, et al., *Transport from the Trans Golgi Network to Lysosomes.*, in *Molecular Biology of the Cell.* 2002, Garland Science: New York.
118. Bellettato, C.M. and M. Scarpa, *Pathophysiology of neuropathic lysosomal storage disorders.* J Inherit Metab Dis, 2010. **33**(4): p. 347-62.
119. Luzio, J.P., et al., *The biogenesis of lysosomes and lysosome-related organelles.* Cold Spring Harb Perspect Biol, 2014. **6**(9): p. a016840.
120. Saftig, P. and J. Klumperman, *Lysosome biogenesis and lysosomal membrane proteins: trafficking meets function.* Nat Rev Mol Cell Biol, 2009. **10**(9): p. 623-35.
121. Parkinson-Lawrence, E.J., et al., *Lysosomal storage disease: revealing lysosomal function and physiology.* Physiology (Bethesda), 2010. **25**(2): p. 102-15.
122. Sardiello, M., et al., *A gene network regulating lysosomal biogenesis and function.* Science, 2009. **325**(5939): p. 473-7.
123. Xu, H. and D. Ren, *Lysosomal physiology.* Annu Rev Physiol, 2015. **77**: p. 57-80.
124. Yu, L., et al., *Termination of autophagy and reformation of lysosomes regulated by mTOR.* Nature, 2010. **465**(7300): p. 942-6.
125. Roczniak-Ferguson, A., et al., *The transcription factor TFEB links mTORC1 signaling to transcriptional control of lysosome homeostasis.* Sci Signal, 2012. **5**(228): p. ra42.
126. Hult, M., et al., *Epidemiology of lysosomal storage diseases in Sweden.* Acta Paediatr, 2014. **103**(12): p. 1258-63.
127. Kaplan, P., et al., *Revised recommendations for the management of Gaucher disease in children.* Eur J Pediatr, 2013. **172**(4): p. 447-58.
128. Ferreira, J.C., et al., *Carrier testing for Ashkenazi Jewish disorders in the prenatal setting: navigating the genetic maze.* Am J Obstet Gynecol, 2014. **211**(3): p. 197-204.
129. Ballabio, A. and V. Gieselmann, *Lysosomal disorders: from storage to cellular damage.* Biochim Biophys Acta, 2009. **1793**(4): p. 684-96.
130. Platt, F.M., *Sphingolipid lysosomal storage disorders.* Nature, 2014. **510**(7503): p. 68-75.
131. Kacew, S., *Cationic amphiphilic drug-induced renal cortical lysosomal phospholipidosis: an in vivo comparative study with gentamicin and chlorphentermine.* Toxicol Appl Pharmacol, 1987. **91**(3): p. 469-76.
132. Halliwell, W.H., *Cationic amphiphilic drug-induced phospholipidosis.* Toxicol Pathol, 1997. **25**(1): p. 53-60.
133. Bracamonte, E.R., et al., *Iatrogenic phospholipidosis mimicking Fabry disease.* Am J Kidney Dis, 2006. **48**(5): p. 844-50.
134. Wasielica-Poslednik, J., et al., *Confocal laser-scanning microscopy allows differentiation between Fabry disease and amiodarone-induced keratopathy.* Graefes Arch Clin Exp Ophthalmol, 2011. **249**(11): p. 1689-96.
135. Lingwood, D. and K. Simons, *Lipid rafts as a membrane-organizing principle.* Science, 2010. **327**(5961): p. 46-50.

136. Melkonian, K.A., et al., *Characterization of proteins in detergent-resistant membrane complexes from Madin-Darby canine kidney epithelial cells.* Biochemistry, 1995. **34**(49): p. 16161-70.

137. Delacour, D., et al., *Galectin-4 and sulfatides in apical membrane trafficking in enterocyte-like cells.* The Journal of cell biology, 2005. **169**(3): p. 491-501.

138. Damm, E.M., et al., *Clathrin- and caveolin-1-independent endocytosis: entry of simian virus 40 into cells devoid of caveolae.* The Journal of cell biology, 2005. **168**(3): p. 477-88.

139. Oh, P., D.P. McIntosh, and J.E. Schnitzer, *Dynamin at the neck of caveolae mediates their budding to form transport vesicles by GTP-driven fission from the plasma membrane of endothelium.* The Journal of cell biology, 1998. **141**(1): p. 101-14.

140. Poole, K., et al., *The effect of raft lipid depletion on microvilli formation in MDCK cells, visualized by atomic force microscopy.* FEBS letters, 2004. **565**(1-3): p. 53-8.

141. Bonifacino, J.S. and R. Rojas, *Retrograde transport from endosomes to the trans-Golgi network.* Nature reviews. Molecular cell biology, 2006. **7**(8): p. 568-79.

142. Parton, R.G. and A.A. Richards, *Lipid rafts and caveolae as portals for endocytosis: new insights and common mechanisms.* Traffic, 2003. **4**(11): p. 724-38.

143. Mayor, S., S. Sabharanjak, and F.R. Maxfield, *Cholesterol-dependent retention of GPI-anchored proteins in endosomes.* The EMBO journal, 1998. **17**(16): p. 4626-38.

144. Chatterjee, S., et al., *GPI anchoring leads to sphingolipid-dependent retention of endocytosed proteins in the recycling endosomal compartment.* The EMBO journal, 2001. **20**(7): p. 1583-92.

145. Simons, K. and D. Toomre, *Lipid rafts and signal transduction.* Nature reviews. Molecular cell biology, 2000. **1**(1): p. 31-9.

146. Roepstorff, K., et al., *Sequestration of epidermal growth factor receptors in non-caveolar lipid rafts inhibits ligand binding.* The Journal of biological chemistry, 2002. **277**(21): p. 18954-60.

147. Coffin, W.F., 3rd, T.R. Geiger, and J.M. Martin, *Transmembrane domains 1 and 2 of the latent membrane protein 1 of Epstein-Barr virus contain a lipid raft targeting signal and play a critical role in cytostasis.* Journal of virology, 2003. **77**(6): p. 3749-58.

148. Kulma, M., K. Kwiatkowska, and A. Sobota, *Raft coalescence and FcgammaRIIA activation upon sphingomyelin clustering induced by lysenin.* Cellular signalling, 2012. **24**(8): p. 1641-7.

149. Dhungana, S., et al., *Quantitative proteomics analysis of macrophage rafts reveals compartmentalized activation of the proteasome and of proteasome-mediated ERK activation in response to lipopolysaccharide.* Mol Cell Proteomics, 2009. **8**(1): p. 201-13.

150. Inder, K.L., M. Davis, and M.M. Hill, *Ripples in the pond--using a systems approach to decipher the cellular functions of membrane microdomains.* Mol Biosyst, 2013. **9**(3): p. 330-8.

151. Lemaire-Ewing, S., L. Lagrost, and D. Neel, *Lipid rafts: a signalling platform linking lipoprotein metabolism to atherogenesis.* Atherosclerosis, 2012. **221**(2): p. 303-10.

152. Ehehalt, R., et al., *Amyloidogenic processing of the Alzheimer beta-amyloid precursor protein depends on lipid rafts.* The Journal of cell biology, 2003. **160**(1): p. 113-23.

153. Bowie, R.V., et al., *Lipid rafts are disrupted in mildly inflamed intestinal microenvironments without overt disruption of the epithelial barrier.* American journal of physiology. Gastrointestinal and liver physiology, 2012. **302**(8): p. G781-93.

154. Kosicek, M., et al., *Cholesterol accumulation in Niemann Pick type C (NPC) model cells causes a shift in APP localization to lipid rafts.* Biochemical and biophysical research communications, 2010. **393**(3): p. 404-9.

155. Fuller, M., *Sphingolipids: the nexus between Gaucher disease and insulin resistance.* Lipids in health and disease, 2010. **9**: p. 113.

156. te Vruchte, D., et al., *Glycosphingolipid storage leads to the enhanced degradation of the B cell receptor in Sandhoff disease mice.* J Inherit Metab Dis, 2010. **33**(3): p. 261-70.

157. Dawson, G., et al., *Abnormal gangliosides are localized in lipid rafts in Sanfilippo (MPS3a) mouse brain.* Neurochemical research, 2012. **37**(6): p. 1372-80.

158. Chen, C.S., et al., *Broad screening test for sphingolipid-storage diseases.* Lancet, 1999. **354**(9182): p. 901-5.

159. Maalouf, K., et al., *A modified lipid composition in Fabry disease leads to an intracellular block of the detergent-resistant membrane-associated dipeptidyl peptidase IV.* J Inherit Metab Dis, 2010. **33**(4): p. 445-9.

160. Toto, R.D., *Microalbuminuria: definition, detection, and clinical significance.* J Clin Hypertens (Greenwich), 2004. **6**(11 Suppl 3): p. 2-7.

161. Carroll, M.F. and J.L. Temte, *Proteinuria in adults: a diagnostic approach.* Am Fam Physician, 2000. **62**(6): p. 1333-40.

162. Greka, A. and P. Mundel, *Cell biology and pathology of podocytes.* Annu Rev Physiol, 2012. **74**: p. 299-323.

163. Roselli, S., et al., *Podocin localizes in the kidney to the slit diaphragm area.* Am J Pathol, 2002. **160**(1): p. 131-9.

164. Kawachi, H., et al., *Slit diaphragm dysfunction in proteinuric states: identification of novel therapeutic targets for nephrotic syndrome.* Clin Exp Nephrol, 2009. **13**(4): p. 275-80.

165. Venkatareddy, M., et al., *Nephrin regulates lamellipodia formation by assembling a protein complex that includes Ship2, filamin and lamellipodin.* PLoS One, 2011. **6**(12): p. e28710.

166. Saleem, M.A., et al., *The molecular and functional phenotype of glomerular podocytes reveals key features of contractile smooth muscle cells.* Am J Physiol Renal Physiol, 2008. **295**(4): p. F959-70.

167. Liu, Y., et al., *IQGAP1 regulates actin cytoskeleton organization in podocytes through interaction with nephrin.* Cell Signal, 2015. **27**(4): p. 867-77.

168. Perisic, L., et al., *Schip1 Is a Novel Podocyte Foot Process Protein that Mediates Actin Cytoskeleton Rearrangements and Forms a Complex with Nherf2 and Ezrin.* PLoS One, 2015. **10**(3): p. e0122067.

169. Lal, M.A., et al., *Rhophilin-1 is a key regulator of the podocyte cytoskeleton and is essential for glomerular filtration.* J Am Soc Nephrol, 2015. **26**(3): p. 647-62.

170. Welsh, G.I. and M.A. Saleem, *The podocyte cytoskeleton--key to a functioning glomerulus in health and disease.* Nat Rev Nephrol, 2012. **8**(1): p. 14-21.

171. van den Berg, J.G., et al., *Podocyte foot process effacement is not correlated with the level of proteinuria in human glomerulopathies.* Kidney Int, 2004. **66**(5): p. 1901-6.

172. Levental, I., M. Grzybek, and K. Simons, *Greasing their way: lipid modifications determine protein association with membrane rafts.* Biochemistry, 2010. **49**(30): p. 6305-16.

173. Coskun, U., et al., *Regulation of human EGF receptor by lipids.* Proceedings of the National Academy of Sciences of the United States of America, 2011. **108**(22): p. 9044-8.

174. Shvets, E., et al., *Dynamic caveolae exclude bulk membrane proteins and are required for sorting of excess glycosphingolipids.* Nat Commun, 2015. **6**: p. 6867.

175. Lipardi, C., L. Nitsch, and C. Zurzolo, *Detergent-insoluble GPI-anchored proteins are apically sorted in fischer rat thyroid cells, but interference with cholesterol or sphingolipids differentially affects detergent insolubility and apical sorting.* Molecular biology of the cell, 2000. **11**(2): p. 531-42.

176. Paladino, S., et al., *Oligomerization is a specific requirement for apical sorting of glycosyl-phosphatidylinositol-anchored proteins but not for non-raft-associated apical proteins.* Traffic, 2007. **8**(3): p. 251-8.

177. Groves, J.T. and J. Kuriyan, *Molecular mechanisms in signal transduction at the membrane.* Nature structural & molecular biology, 2010. **17**(6): p. 659-65.

178. Hsu, P.D., E.S. Lander, and F. Zhang, *Development and applications of CRISPR-Cas9 for genome engineering.* Cell, 2014. **157**(6): p. 1262-78.

179. Chuang, P.Y. and J.C. He, *Signaling in regulation of podocyte phenotypes.* Nephron Physiol, 2009. **111**(2): p. p9-15.

180. Yoshimitsu, M., et al., *Identification of novel mutations in the alpha-galactosidase A gene in patients with Fabry disease: pitfalls of mutation analyses in patients with low alpha-galactosidase A activity.* J Cardiol, 2011. **57**(3): p. 345-53.

181. Eng, C.M., et al., *Fabry disease: baseline medical characteristics of a cohort of 1765 males and females in the Fabry Registry.* J Inherit Metab Dis, 2007. **30**(2): p. 184-92.

182. Ortiz, A., et al., *End-stage renal disease in patients with Fabry disease: natural history data from the Fabry Registry.* Nephrology, dialysis, transplantation : official publication of the European Dialysis and Transplant Association - European Renal Association, 2010. **25**(3): p. 769-75.

183. Pintos-Morell, G. and M. Beck, *Fabry disease in children and the effects of enzyme replacement treatment.* Eur J Pediatr, 2009. **168**(11): p. 1355-63.

184. Hopkin, R.J., et al., *Characterization of Fabry disease in 352 pediatric patients in the Fabry Registry.* Pediatr Res, 2008. **64**(5): p. 550-5.

185. Tondel, C., et al., *Agalsidase benefits renal histology in young patients with Fabry disease.* Journal of the American Society of Nephrology : JASN, 2013. **24**(1): p. 137-48.

186. Fogo, A.B., et al., *Scoring system for renal pathology in Fabry disease: report of the International Study Group of Fabry Nephropathy (ISGFN).* Nephrol Dial Transplant, 2010. **25**(7): p. 2168-77.

187. Watt, T., et al., *Agalsidase beta treatment is associated with improved quality of life in patients with Fabry disease: findings from the Fabry Registry.* Genet Med, 2010. **12**(11): p. 703-12.

188. Wilcox, W.R., et al., *Long-term safety and efficacy of enzyme replacement therapy for Fabry disease.* Am J Hum Genet, 2004. **75**(1): p. 65-74.

189. Hughes, D.A., et al., *A randomised, double-blind, placebo-controlled, crossover study to assess the efficacy and safety of three dosing schedules of agalsidase alfa enzyme replacement therapy for Fabry disease.* Molecular genetics and metabolism, 2013.

190. Weidemann, F., et al., *Long-term outcome of enzyme-replacement therapy in advanced Fabry disease: evidence for disease progression towards serious complications.* Journal of internal medicine, 2013.

191. Feriozzi, S., et al., *The effectiveness of long-term agalsidase alfa therapy in the treatment of Fabry nephropathy.* Clin J Am Soc Nephrol, 2012. **7**(1): p. 60-9.

192. Warnock, D.G., et al., *Renal outcomes of agalsidase beta treatment for Fabry disease: role of proteinuria and timing of treatment initiation.* Nephrol Dial Transplant, 2011.

193. Melkonian, K.A., et al., *Role of lipid modifications in targeting proteins to detergent-resistant membrane rafts. Many raft proteins are acylated, while few are prenylated.* The Journal of biological chemistry, 1999. **274**(6): p. 3910-7.

194. Owen, D.M., et al., *The lipid raft hypothesis revisited--new insights on raft composition and function from super-resolution fluorescence microscopy.* BioEssays : news and reviews in molecular, cellular and developmental biology, 2012. **34**(9): p. 739-47.

195. Wang, R., et al., *Lipid raft regulates the initial spreading of melanoma A375 cells by modulating beta1 integrin clustering.* The international journal of biochemistry & cell biology, 2013.

196. Fullekrug, J. and K. Simons, *Lipid rafts and apical membrane traffic.* Annals of the New York Academy of Sciences, 2004. **1014**: p. 164-9.

197. Weisz, O.A. and E. Rodriguez-Boulan, *Apical trafficking in epithelial cells: signals, clusters and motors.* J Cell Sci, 2009. **122**(Pt 23): p. 4253-66.

198. Schuck, S. and K. Simons, *Polarized sorting in epithelial cells: raft clustering and the biogenesis of the apical membrane.* Journal of cell science, 2004. **117**(Pt 25): p. 5955-64.

199. Paladino, S., et al., *Protein oligomerization modulates raft partitioning and apical sorting of GPI-anchored proteins.* The Journal of cell biology, 2004. **167**(4): p. 699-709.

200. Galmes, R., et al., *Oligomerization is required for normal endocytosis/transcytosis of a GPI-anchored protein in polarized hepatic cells.* Journal of cell science, 2013.

201. Shi, D., et al., *Smoothened oligomerization/higher order clustering in lipid rafts is essential for high hedgehog activity transduction.* The Journal of biological chemistry, 2013. **288**(18): p. 12605-14.

202. Langeveld, M., et al., *Type I Gaucher disease, a glycosphingolipid storage disorder, is associated with insulin resistance.* The Journal of clinical endocrinology and metabolism, 2008. **93**(3): p. 845-51.

203. Rusyn, E., et al., *CLN3p impacts galactosylceramide transport, raft morphology, and lipid content.* Pediatric research, 2008. **63**(6): p. 625-31.

204. White, A.B., et al., *Persistence of psychosine in brain lipid rafts is a limiting factor in the therapeutic recovery of a mouse model for Krabbe disease.* J Neurosci Res, 2011. **89**(3): p. 352-64.

205. Simons, K. and W.L. Vaz, *Model systems, lipid rafts, and cell membranes.* Annual review of biophysics and biomolecular structure, 2004. **33**: p. 269-95.

206. Digman, M.A., et al., *Mapping the number of molecules and brightness in the laser scanning microscope.* Biophysical journal, 2008. **94**(6): p. 2320-32.

207. Crosby, K.C., et al., *Quantitative analysis of self-association and mobility of annexin a4 at the plasma membrane.* Biophysical journal, 2013. **104**(9): p. 1875-85.

208. Hellriegel, C., et al., *Number and brightness image analysis reveals ATF-induced dimerization kinetics of uPAR in the cell membrane.* FASEB journal : official publication of the Federation of American Societies for Experimental Biology, 2011. **25**(9): p. 2883-97.

209. Herrick-Davis, K., et al., *Oligomer size of the serotonin 5-hydroxytryptamine 2C (5-HT2C) receptor revealed by fluorescence correlation spectroscopy with photon counting histogram analysis: evidence for homodimers without monomers or tetramers.* The Journal of biological chemistry, 2012. **287**(28): p. 23604-14.

210. Henkel, J.R., et al., *Selective perturbation of apical membrane traffic by expression of influenza M2, an acid-activated ion channel, in polarized madin-darby canine kidney cells.* Mol Biol Cell, 1998. **9**(9): p. 2477-90.

211. Youker, R.T., et al., *Multiple motifs regulate apical sorting of p75 via a mechanism that involves dimerization and higher-order oligomerization.* Molecular biology of the cell, 2013. **24**(12): p. 1996-2007.

212. Namdar, M., et al., *Globotriaosylsphingosine accumulation and not alpha-galactosidase-A deficiency causes endothelial dysfunction in Fabry disease.* PLoS One, 2012. **7**(4): p. e36373.

213. Medin, J.A., et al., *Correction in trans for Fabry disease: expression, secretion and uptake of alpha-galactosidase A in patient-derived cells driven by a high-titer recombinant retroviral vector.* Proceedings of the National Academy of Sciences of the United States of America, 1996. **93**(15): p. 7917-22.

214. Askari, H., et al., *Cellular and tissue localization of globotriaosylceramide in Fabry disease.* Virchows Arch, 2007. **451**(4): p. 823-34.

215. Yam, G.H., et al., *Pharmacological chaperone corrects lysosomal storage in Fabry disease caused by trafficking-incompetent variants.* American journal of physiology. Cell physiology, 2006. **290**(4): p. C1076-82.

216. Alroy, J., S. Sabnis, and J.B. Kopp, *Renal pathology in Fabry disease.* J Am Soc Nephrol, 2002. **13 Suppl 2**: p. S134-8.

217. Ikonen, E., *Roles of lipid rafts in membrane transport.* Current opinion in cell biology, 2001. **13**(4): p. 470-7.

218. Glebov, O.O. and B.J. Nichols, *Distribution of lipid raft markers in live cells.* Biochemical Society transactions, 2004. **32**(Pt 5): p. 673-5.

219. Nohe, A., et al., *Dynamics of GPI-anchored proteins on the surface of living cells.* Nanomedicine : nanotechnology, biology, and medicine, 2006. **2**(1): p. 1-7.

220. Suzuki, K.G., et al., *GPI-anchored receptor clusters transiently recruit Lyn and G alpha for temporary cluster immobilization and Lyn activation: single-molecule tracking study 1.* The Journal of cell biology, 2007. **177**(4): p. 717-30.

221. Legewie, S., et al., *Recurrent design patterns in the feedback regulation of the mammalian signalling network.* Molecular systems biology, 2008. **4**: p. 190.

222. Suzuki, K.G., et al., *Transient GPI-anchored protein homodimers are units for raft organization and function.* Nature chemical biology, 2012. **8**(9): p. 774-83.

223. Friedrichson, T. and T.V. Kurzchalia, *Microdomains of GPI-anchored proteins in living cells revealed by crosslinking.* Nature, 1998. **394**(6695): p. 802-5.

224. Hofman, E.G., et al., *EGF induces coalescence of different lipid rafts.* Journal of cell science, 2008. **121**(Pt 15): p. 2519-28.

225. Horejsi, V., et al., *Signal transduction in leucocytes via GPI-anchored proteins: an experimental artefact or an aspect of immunoreceptor function?* Immunology letters, 1998. **63**(2): p. 63-73.

226. Potter, B.A., et al., *Specific N-glycans direct apical delivery of transmembrane, but not soluble or glycosylphosphatidylinositol-anchored forms of endolyn in Madin-Darby canine kidney cells.* Mol Biol Cell, 2004. **15**(3): p. 1407-16.

227. Simons, K. and R. Ehehalt, *Cholesterol, lipid rafts, and disease.* The Journal of clinical investigation, 2002. **110**(5): p. 597-603.

228. Cheng, P.C., et al., *Translocation of the B cell antigen receptor into lipid rafts reveals a novel step in signaling.* Journal of immunology, 2001. **166**(6): p. 3693-701.

229. Hern, J.A., et al., *Formation and dissociation of M1 muscarinic receptor dimers seen by total internal reflection fluorescence imaging of single molecules.* Proceedings of the National Academy of Sciences of the United States of America, 2010. **107**(6): p. 2693-8.

230. Kasai, R.S., et al., *Full characterization of GPCR monomer-dimer dynamic equilibrium by single molecule imaging.* The Journal of cell biology, 2011. **192**(3): p. 463-80.

231. Calebiro, D., et al., *Single-molecule analysis of fluorescently labeled G-protein-coupled receptors reveals complexes with distinct dynamics and organization.* Proceedings of the National Academy of Sciences of the United States of America, 2013. **110**(2): p. 743-8.

232. Suzuki, K.G., et al., *Dynamic recruitment of phospholipase C gamma at transiently immobilized GPI-anchored receptor clusters induces IP3-Ca2+ signaling: single-molecule tracking study 2.* The Journal of cell biology, 2007. **177**(4): p. 731-42.

233. Finger, E.C., et al., *Endocytosis of the type III transforming growth factor-beta (TGF-beta) receptor through the clathrin-independent/lipid raft pathway regulates TGF-beta signaling and receptor down-regulation.* The Journal of biological chemistry, 2008. **283**(50): p. 34808-18.

234. Di Guglielmo, G.M., et al., *Distinct endocytic pathways regulate TGF-beta receptor signalling and turnover.* Nature cell biology, 2003. **5**(5): p. 410-21.

235. Sanchez-Nino, M.D., et al., *Globotriaosylsphingosine actions on human glomerular podocytes: implications for Fabry nephropathy.* Nephrology, dialysis, transplantation : official publication of the European Dialysis and Transplant Association - European Renal Association, 2011. **26**(6): p. 1797-802.

236. Houdebine, L.M., *Transgenic animal models in biomedical research.* Methods Mol Biol, 2007. **360**: p. 163-202.

237. Batzoglou, S., et al., *Human and mouse gene structure: comparative analysis and application to exon prediction.* Genome Res, 2000. **10**(7): p. 950-8.

238. Fire, A., et al., *Potent and specific genetic interference by double-stranded RNA in Caenorhabditis elegans.* Nature, 1998. **391**(6669): p. 806-11.

239. Li, Z. and T.M. Rana, *Molecular mechanisms of RNA-triggered gene silencing machineries.* Acc Chem Res, 2012. **45**(7): p. 1122-31.

240. Bartlett, D.W. and M.E. Davis, *Insights into the kinetics of siRNA-mediated gene silencing from live-cell and live-animal bioluminescent imaging.* Nucleic Acids Res, 2006. **34**(1): p. 322-33.

241. Whitehead, K.A., R. Langer, and D.G. Anderson, *Knocking down barriers: advances in siRNA delivery.* Nat Rev Drug Discov, 2009. **8**(2): p. 129-38.

242. Summerton, J. and D. Weller, *Morpholino antisense oligomers: design, preparation, and properties.* Antisense Nucleic Acid Drug Dev, 1997. **7**(3): p. 187-95.

243. Corey, D.R. and J.M. Abrams, *Morpholino antisense oligonucleotides: tools for investigating vertebrate development.* Genome Biol, 2001. **2**(5): p. REVIEWS1015.

244. Bedell, V.M., S.E. Westcot, and S.C. Ekker, *Lessons from morpholino-based screening in zebrafish.* Brief Funct Genomics, 2011. **10**(4): p. 181-8.

245. Sakuma, T. and K. Woltjen, *Nuclease-mediated genome editing: At the front-line of functional genomics technology.* Dev Growth Differ, 2014. **56**(1): p. 2-13.

246. Shibata, A. and P.A. Jeggo, *DNA double-strand break repair in a cellular context.* Clin Oncol (R Coll Radiol), 2014. **26**(5): p. 243-9.

247. Durai, S., et al., *Zinc finger nucleases: custom-designed molecular scissors for genome engineering of plant and mammalian cells.* Nucleic Acids Res, 2005. **33**(18): p. 5978-90.

248. Kim, Y., J. Kweon, and J.S. Kim, *TALENs and ZFNs are associated with different mutation signatures.* Nat Methods, 2013. **10**(3): p. 185.

249. Barrangou, R. and L.A. Marraffini, *CRISPR-Cas systems: Prokaryotes upgrade to adaptive immunity.* Mol Cell, 2014. **54**(2): p. 234-44.

250. Mali, P., et al., *RNA-guided human genome engineering via Cas9.* Science, 2013. **339**(6121): p. 823-6.

251. Cong, L., et al., *Multiplex genome engineering using CRISPR/Cas systems.* Science, 2013. **339**(6121): p. 819-23.

252. Jinek, M., et al., *Structures of Cas9 endonucleases reveal RNA-mediated conformational activation.* Science, 2014. **343**(6176): p. 1247997.

253. Jinek, M., et al., *A programmable dual-RNA-guided DNA endonuclease in adaptive bacterial immunity.* Science, 2012. **337**(6096): p. 816-21.

254. Gasiunas, G., et al., *Cas9-crRNA ribonucleoprotein complex mediates specific DNA cleavage for adaptive immunity in bacteria.* Proc Natl Acad Sci U S A, 2012. **109**(39): p. E2579-86.

255. Ran, F.A., et al., *Genome engineering using the CRISPR-Cas9 system.* Nat Protoc, 2013. **8**(11): p. 2281-308.

256. Ramalingam, S., N. Annaluru, and S. Chandrasegaran, *A CRISPR way to engineer the human genome.* Genome Biol, 2013. **14**(2): p. 107.

257. Shabbeer, J., et al., *Fabry disease: identification of 50 novel alpha-galactosidase A mutations causing the classic phenotype and three-dimensional structural analysis of 29 missense mutations.* Hum Genomics, 2006. **2**(5): p. 297-309.

258. Rodriguez-Mari, A., M.J. Coll, and A. Chabas, *Molecular analysis in Fabry disease in Spain: fifteen novel GLA mutations and identification of a homozygous female.* Hum Mutat, 2003. **22**(3): p. 258.

259. Sessa, A., et al., *Chronic renal failure, dialysis, and renal transplantation in Anderson-Fabry disease.* Semin Nephrol, 2004. **24**(5): p. 532-6.

260. Najafian, B., et al., *Progressive podocyte injury and globotriaosylceramide (GL-3) accumulation in young patients with Fabry disease.* Kidney Int, 2011. **79**(6): p. 663-70.

261. Prabakaran, T., et al., *Long-term enzyme replacement therapy is associated with reduced proteinuria and preserved proximal tubular function in women with Fabry disease.* Nephrol Dial Transplant, 2014. **29**(3): p. 619-25.

262. Ortiz, A., et al., *End-stage renal disease in patients with Fabry disease: natural history data from the Fabry Registry.* Nephrol Dial Transplant, 2010. **25**(3): p. 769-75.

263. Tondel, C., et al., *Foot process effacement is an early marker of nephropathy in young classic Fabry patients without albuminuria.* Nephron, 2015. **129**(1): p. 16-21.

264. Ryan, M.J., et al., *HK-2: an immortalized proximal tubule epithelial cell line from normal adult human kidney.* Kidney Int, 1994. **45**(1): p. 48-57.

265. Delarue, F., et al., *Stable cell line of T-SV40 immortalized human glomerular visceral epithelial cells.* Kidney Int, 1991. **40**(5): p. 906-12.

266. Heigwer, F., G. Kerr, and M. Boutros, *E-CRISP: fast CRISPR target site identification.* Nat Methods, 2014. **11**(2): p. 122-3.

267. Ramakrishna, S., et al., *Surrogate reporter-based enrichment of cells containing RNA-guided Cas9 nuclease-induced mutations.* Nat Commun, 2014. **5**: p. 3378.

268. Korbie, D.J. and J.S. Mattick, *Touchdown PCR for increased specificity and sensitivity in PCR amplification.* Nat Protoc, 2008. **3**(9): p. 1452-6.

269. Declais, A.C. and D.M. Lilley, *New insight into the recognition of branched DNA structure by junction-resolving enzymes.* Curr Opin Struct Biol, 2008. **18**(1): p. 86-95.

270. Vouillot, L., A. Thelie, and N. Pollet, *Comparison of T7E1 and Surveyor Mismatch Cleavage Assays to Detect Mutations Triggered by Engineered Nucleases.* G3 (Bethesda), 2015. **5**(3): p. 407-15.

271. Brandl, C., et al., *Creation of targeted genomic deletions using TALEN or CRISPR/Cas nuclease pairs in one-cell mouse embryos.* FEBS Open Bio, 2015. **5**: p. 26-35.

272. Borgwardt, L., A.M. Lund, and C.I. Dali, *Alpha-mannosidosis - a review of genetic, clinical findings and options of treatment.* Pediatr Endocrinol Rev, 2014. **12 Suppl 1**: p. 185-91.

273. Valbuena, C., et al., *Immunohistochemical diagnosis of Fabry nephropathy and localisation of globotriaosylceramide deposits in paraffin-embedded kidney tissue sections.* Virchows Arch, 2012. **460**(2): p. 211-21.

274. Mayes, J.S., et al., *Endocytosis of lysosomal alpha-galactosidase A by cultured fibroblasts from patients with Fabry disease.* Am J Hum Genet, 1982. **34**(4): p. 602-10.

275. Hsu, P.D., et al., *DNA targeting specificity of RNA-guided Cas9 nucleases.* Nat Biotechnol, 2013. **31**(9): p. 827-32.

276. Wang, T., et al., *Genetic screens in human cells using the CRISPR-Cas9 system.* Science, 2014. **343**(6166): p. 80-4.

277. Shalem, O., N.E. Sanjana, and F. Zhang, *High-throughput functional genomics using CRISPR-Cas9.* Nat Rev Genet, 2015.

278. Tsai, S.Q., et al., *GUIDE-seq enables genome-wide profiling of off-target cleavage by CRISPR-Cas nucleases.* Nat Biotechnol, 2015. **33**(2): p. 187-97.

279. Sexton, T. and G. Cavalli, *The Role of Chromosome Domains in Shaping the Functional Genome.* Cell, 2015. **160**(6): p. 1049-1059.

280. Arvey, A., et al., *Sequence and chromatin determinants of cell-type-specific transcription factor binding.* Genome Res, 2012. **22**(9): p. 1723-34.

281. O'Geen, H., et al., *A genome-wide analysis of Cas9 binding specificity using ChIP-seq and targeted sequence capture.* Nucleic Acids Res, 2015. **43**(6): p. 3389-404.

282. Kim, D., et al., *Digenome-seq: genome-wide profiling of CRISPR-Cas9 off-target effects in human cells.* Nat Methods, 2015. **12**(3): p. 237-43.

283. Fu, Y., et al., *High-frequency off-target mutagenesis induced by CRISPR-Cas nucleases in human cells.* Nat Biotechnol, 2013. **31**(9): p. 822-6.

284. Cho, S.W., et al., *Analysis of off-target effects of CRISPR/Cas-derived RNA-guided endonucleases and nickases.* Genome Res, 2014. **24**(1): p. 132-41.

285. Fu, Y., et al., *Improving CRISPR-Cas nuclease specificity using truncated guide RNAs.* Nat Biotechnol, 2014. **32**(3): p. 279-84.

286. Carroll, D., *Staying on target with CRISPR-Cas.* Nat Biotechnol, 2013. **31**(9): p. 807-9.

287. Li, A., et al., *Genomic changes and gene expression profiles reveal that established glioma cell lines are poorly representative of primary human gliomas.* Mol Cancer Res, 2008. **6**(1): p. 21-30.

288. Roemeling-van Rhijn, M., et al., *Culture expansion induces non-tumorigenic aneuploidy in adipose tissue-derived mesenchymal stromal cells.* Cytotherapy, 2013. **15**(11): p. 1352-61.

289. Trevino, V., F. Falciani, and H.A. Barrera-Saldana, *DNA microarrays: a powerful genomic tool for biomedical and clinical research.* Mol Med, 2007. **13**(9-10): p. 527-41.

290. Tarca, A.L., R. Romero, and S. Draghici, *Analysis of microarray experiments of gene expression profiling.* Am J Obstet Gynecol, 2006. **195**(2): p. 373-88.

291. Wang, Z., M. Gerstein, and M. Snyder, *RNA-Seq: a revolutionary tool for transcriptomics.* Nat Rev Genet, 2009. **10**(1): p. 57-63.

292. de Klerk, E., J.T. den Dunnen, and P.A. t Hoen, *RNA sequencing: from tag-based profiling to resolving complete transcript structure.* Cell Mol Life Sci, 2014. **71**(18): p. 3537-51.

293. Mortazavi, A., et al., *Mapping and quantifying mammalian transcriptomes by RNA-Seq.* Nat Methods, 2008. **5**(7): p. 621-8.

294. Steijger, T., et al., *Assessment of transcript reconstruction methods for RNA-seq.* Nat Methods, 2013. **10**(12): p. 1177-84.

295. de Klerk, E. and P.A. t Hoen, *Alternative mRNA transcription, processing, and translation: insights from RNA sequencing.* Trends Genet, 2015. **31**(3): p. 128-39.

296. Wang, Y.C., S.E. Peterson, and J.F. Loring, *Protein post-translational modifications and regulation of pluripotency in human stem cells.* Cell Res, 2014. **24**(2): p. 143-60.

297. Belle, A., et al., *Quantification of protein half-lives in the budding yeast proteome.* Proc Natl Acad Sci U S A, 2006. **103**(35): p. 13004-9.

298. Gry, M., et al., *Correlations between RNA and protein expression profiles in 23 human cell lines.* BMC Genomics, 2009. **10**: p. 365.

299. Knorre, D.G., N.V. Kudryashova, and T.S. Godovikova, *Chemical and functional aspects of posttranslational modification of proteins.* Acta Naturae, 2009. **1**(3): p. 29-51.

300. Mandell, J.W., *Phosphorylation state-specific antibodies: applications in investigative and diagnostic pathology.* Am J Pathol, 2003. **163**(5): p. 1687-98.

301. Meissner, F. and M. Mann, *Quantitative shotgun proteomics: considerations for a high-quality workflow in immunology.* Nat Immunol, 2014. **15**(2): p. 112-7.

302. Scherl, A., *Clinical protein mass spectrometry.* Methods, 2015.

303. Tabb, D.L., et al., *Repeatability and reproducibility in proteomic identifications by liquid chromatography-tandem mass spectrometry.* J Proteome Res, 2010. **9**(2): p. 761-76.

304. Kopf, E. and D. Zharhary, *Antibody arrays--an emerging tool in cancer proteomics.* Int J Biochem Cell Biol, 2007. **39**(7-8): p. 1305-17.

305.   Sutandy, F.X., et al., *Overview of protein microarrays.* Curr Protoc Protein Sci, 2013. **Chapter 27**: p. Unit 27 1.

306.   Matafora, V., et al., *Early markers of Fabry disease revealed by proteomics.* Mol Biosyst, 2015.

307.   Manwaring, V., et al., *The identification of new biomarkers for identifying and monitoring kidney disease and their translation into a rapid mass spectrometry-based test: evidence of presymptomatic kidney disease in pediatric Fabry and type-I diabetic patients.* J Proteome Res, 2013. **12**(5): p. 2013-21.

308.   Kistler, A.D., et al., *A distinct urinary biomarker pattern characteristic of female Fabry patients that mirrors response to enzyme replacement therapy.* PLoS One, 2011. **6**(6): p. e20534.

309.   Cuccurullo, M., et al., *Fabry disease: perspectives of urinary proteomics.* J Nephrol, 2010. **23 Suppl 16**: p. S199-212.

310.   Vojtova, L., et al., *Study of urinary proteomes in Anderson-Fabry disease.* Ren Fail, 2010. **32**(10): p. 1202-9.

311.   Moore, D.F., et al., *Proteomics of specific treatment-related alterations in Fabry disease: a strategy to identify biological abnormalities.* Proc Natl Acad Sci U S A, 2007. **104**(8): p. 2873-8.

312.   Hollander, Z., et al., *Gender-specific plasma proteomic biomarkers in patients with Anderson-Fabry disease.* Eur J Heart Fail, 2015. **17**(3): p. 291-300.

313.   Cigna, D., et al., *Alteration of proteomic profiles in PBMC isolated from patients with Fabry disease: preliminary findings.* Mol Biosyst, 2013. **9**(6): p. 1162-8.

314.   Boerries, M., et al., *Molecular fingerprinting of the podocyte reveals novel gene and protein regulatory networks.* Kidney Int, 2013. **83**(6): p. 1052-64.

315.   Rinschen, M.M., et al., *Phosphoproteomic analysis reveals regulatory mechanisms at the kidney filtration barrier.* J Am Soc Nephrol, 2014. **25**(7): p. 1509-22.

316.   Rinschen, M.M., et al., *Comparative phosphoproteomic analysis of mammalian glomeruli reveals conserved podocin C-terminal phosphorylation as a determinant of slit diaphragm complex architecture.* Proteomics, 2015. **15**(7): p. 1326-31.

317.   Team, R.D.C., *R: A language and environment for statistical computing.* R Foundation for Statistical Computing. 2008, Vienna, Austria.

318.   Kann, M., et al., *Genome-Wide Analysis of Wilms' Tumor 1-Controlled Gene Expression in Podocytes Reveals Key Regulatory Mechanisms.* J Am Soc Nephrol, 2015.

319.   Edgar, R., M. Domrachev, and A.E. Lash, *Gene Expression Omnibus: NCBI gene expression and hybridization array data repository.* Nucleic Acids Res, 2002. **30**(1): p. 207-10.

320.   Barrett, T., et al., *NCBI GEO: archive for functional genomics data sets--update.* Nucleic Acids Res, 2013. **41**(Database issue): p. D991-5.

321.   Hornbeck, P.V., et al., *PhosphoSitePlus: a comprehensive resource for investigating the structure and function of experimentally determined post-translational modifications in man and mouse.* Nucleic Acids Res, 2012. **40**(Database issue): p. D261-70.

322.   Huang da, W., B.T. Sherman, and R.A. Lempicki, *Systematic and integrative analysis of large gene lists using DAVID bioinformatics resources.* Nat Protoc, 2009. **4**(1): p. 44-57.

323.   Ashburner, M., et al., *Gene ontology: tool for the unification of biology. The Gene Ontology Consortium.* Nat Genet, 2000. **25**(1): p. 25-9.

324. Saleem, M.A., et al., *A conditionally immortalized human podocyte cell line demonstrating nephrin and podocin expression.* J Am Soc Nephrol, 2002. **13**(3): p. 630-8.

325. Da Sacco, S., et al., *A novel source of cultured podocytes.* PLoS One, 2013. **8**(12): p. e81812.

326. Goto, S., et al., *Organizing and computing metabolic pathway data in terms of binary relations.* Pac Symp Biocomput, 1997: p. 175-86.

327. Nakao, M., et al., *Genome-scale Gene Expression Analysis and Pathway Reconstruction in KEGG.* Genome Inform Ser Workshop Genome Inform, 1999. **10**: p. 94-103.

328. Omori, S., et al., *Expression of mitogen-activated protein kinase family in rat renal development.* Kidney Int, 2000. **58**(1): p. 27-37.

329. Balbi, A.P., et al., *Roles of mitogen-activated protein kinases and angiotensin II in renal development.* Braz J Med Biol Res, 2009. **42**(1): p. 38-43.

330. Yim, H.E., et al., *Aldosterone regulates cellular turnover and mitogen-activated protein kinase family expression in the neonatal rat kidney.* J Cell Physiol, 2009. **219**(3): p. 724-33.

331. de Haij, S., M.R. Daha, and C. van Kooten, *Mechanism of steroid action in renal epithelial cells.* Kidney Int, 2004. **65**(5): p. 1577-88.

332. Lindstrom, N.O., N.O. Carragher, and P. Hohenstein, *The PI3K Pathway Balances Self-Renewal and Differentiation of Nephron Progenitor Cells through beta-Catenin Signaling.* Stem Cell Reports, 2015. **4**(4): p. 551-60.

333. Kaplan, B., Y. Qazi, and J.R. Wellen, *Strategies for the management of adverse events associated with mTOR inhibitors.* Transplant Rev (Orlando), 2014. **28**(3): p. 126-33.

334. Guney, M., et al., *Proteinuria associated with mTOR inhibitors after kidney transplant.* Exp Clin Transplant, 2014. **12**(6): p. 539-42.

335. Lee, M.H., et al., *Possible role of transforming growth factor-beta1 and vascular endothelial growth factor in Fabry disease nephropathy.* Int J Mol Med, 2012. **30**(6): p. 1275-80.

336. Svarstad, E., et al., *Focal and segmental glomerular sclerosis (FSGS) in a man and a woman with Fabry's disease.* Clin Nephrol, 2005. **63**(5): p. 394-401.

337. Meng, X.M., et al., *TGF-beta/Smad signaling in renal fibrosis.* Front Physiol, 2015. **6**: p. 82.

338. Lee, H.S., *Mechanisms and consequences of TGF-ss overexpression by podocytes in progressive podocyte disease.* Cell Tissue Res, 2012. **347**(1): p. 129-40.

339. Ahmad, Y. and A.I. Lamond, *A perspective on proteomics in cell biology.* Trends Cell Biol, 2014. **24**(4): p. 257-64.

340. Mundel, P., J. Reiser, and W. Kriz, *Induction of differentiation in cultured rat and human podocytes.* J Am Soc Nephrol, 1997. **8**(5): p. 697-705.

341. Thung, P.J., *Physiological proteinuria in mice.* Acta Physiol Pharmacol Neerl, 1962. **10**: p. 248-61.

342. Macaulay, I.C., et al., *G&T-seq: parallel sequencing of single-cell genomes and transcriptomes.* Nat Methods, 2015.

343. Taleei, R. and H. Nikjoo, *The non-homologous end-joining (NHEJ) pathway for the repair of DNA double-strand breaks: I. A mathematical model.* Radiat Res, 2013. **179**(5): p. 530-9.

344. Medunjanin, S., et al., *DNA-dependent protein kinase (DNA-PK) permits vascular smooth muscle cell proliferation through phosphorylation of the orphan nuclear receptor NOR1.* Cardiovasc Res, 2015.

345. Tate, J. and G. Ward, *Interferences in immunoassay.* Clin Biochem Rev, 2004. **25**(2): p. 105-20.

346. Cui, X. and G.A. Churchill, *Statistical tests for differential expression in cDNA microarray experiments.* Genome Biol, 2003. **4**(4): p. 210.

347. Ponzoni, I., et al., *Pathway network inference from gene expression data.* BMC Syst Biol, 2014. **8 Suppl 2**: p. S7.